

**Luminescence dating of Middle and Late
Pleistocene ice-marginal and alluvial depositional
systems in northern Germany**

Von der Naturwissenschaftlichen Fakultät der
Gottfried Wilhelm Leibniz Universität Hannover

zur Erlangung des Grades
Doktorin der Naturwissenschaften (Dr. rer. nat.)

genehmigte Dissertation

von

M.Sc. Julia Roskosch

geboren am 10. März 1983 in Datteln

Referentin: Prof. Dr. Jutta Winsemann

Korreferent: Prof. Dr. Manfred Frechen

Tag der Promotion: 15. Juni 2015

Für Papa (†1997) und Mama

Abstract	7
Zusammenfassung	8
Chapter 1 Introduction	9
1.1 The Pleistocene glaciations	12
1.2 Study area	13
1.2.1 The Münsterland Embayment	14
1.2.2 The Leine valley	15
1.2.3 The Weser valley	16
1.3 Methods	17
1.3.1 Field work	17
1.3.2 Shear wave seismic profiles	17
1.3.3 Three-dimensional subsurface modeling (GOCAD®)	18
1.3.4 Luminescence dating	18
1.3.4.1 The basic principles of luminescence dating	18
1.3.4.2 Luminescence dosimeters – their advantages and disadvantages	20
1.3.4.3 Dose rate determination	20
1.3.4.4 Equivalent dose determination	21
1.3.4.5 Incomplete bleaching	22
1.4 Outline of the thesis – Publications and their contents	23
References	24
Chapter 2 Publication 1: Luminescence dating of an Upper Pleistocene alluvial fan and aeolian sandsheet complex: The Senne in the Münsterland Embayment, NW Germany	33
by Julia Roskosch, Sumiko Tsukamoto, Janine Meinsen, Manfred Frechen, Jutta Winsemann (2012), Quaternary Geochronology 10, 94-101, DOI: 10.1016/j.quageo.2012.02.012.	
Online supplementary data to publication 1	55

Chapter 3	Publication 2: Luminescence dating of ice-marginal deposits in northern Germany: evidence for glaciations during the Middle Pleistocene (MIS 12 to MIS 6)	65
	by Julia Roskosch, Jutta Winsemann, Ulrich Polom, Christian Brandes, Sumiko Tsukamoto, Axel Weitkamp, Werner A. Bartholomäus, Dierk Henningsen, Manfred Frechen (2015), <i>Boreas</i> 44, 103-126, DOI: 10.1111/bor.12083.	
	Online supplementary data to publication 2	111
Chapter 4	Publication 3: Luminescence dating of fluvial deposits from the Weser valley, Germany: a comparison with independent age control	119
	by Julia Roskosch, Sumiko Tsukamoto, Manfred Frechen, <i>Geochronometria</i> (in review).	
Chapter 5	Summarising discussion	141
	5.1 Geochronological discussion	143
	5.2 Geological implications	146
Chapter 6	Conclusions	151
	References	154
Chapter 7	Acknowledgements/Danksagung	161
	Curriculum vitae	165
	List of publications	167

Abstract

During the past century, the Middle and Late Pleistocene glaciation history in northern Germany has mostly been reconstructed on the basis of geomorphological and lithostratigraphical approaches, pointing to three major ice advances during the Elsterian, Saalian and Weichselian. However, the exact chronology of these ice advances remained unclear due to the absence of numerical dating methods covering the relevant geological time span. The overall aim of this thesis is to establish a reliable high-resolution geochronological framework for the Middle and Late Pleistocene deposits of northern Germany by means of luminescence dating techniques. Luminescence dating provides the age of the last bleaching and thus depositional event of the dated feldspar and quartz minerals. The study areas are located in the Münsterland Embayment and the Leine and Weser valleys, representing fluvial and ice-marginal depositional systems which were previously situated within, close to and even beyond the former ice-margins, and/or large proglacial lakes. Luminescence dating of sediments derived from these depositional environments is considered to be challenging because the natural luminescence signal may have been insufficiently reset (bleached) prior to deposition, leading to a possible age overestimation.

Methodological results show that using a pulsed infrared stimulated luminescence (IRSL) protocol with infrared (IR) stimulation at 50°C (IR₅₀) gave reliable and robust feldspar ages, which did not necessarily need fading correction. An age agreement of IR₅₀ and quartz ages pointed to good bleaching conditions prior to deposition and led to the assumption that the effect of age overestimation due to insufficient bleaching is likely to be very small. In case of supporting independent age control (e.g. uranium-thorium ages) of sediments from the exact same sedimentary succession, the applied dating method(s) can be considered reliable and accurate. From a geochronological point of view, the determined luminescence ages obtained from the Senne area of the Münsterland Embayment were able to reconstruct small-scale climate variations. Yet, luminescence dating techniques were not precise enough to resolve smaller-scaled (millennial-scale) variations. For the first time, at least two separate ice advances could be proved for the Elsterian glaciation, correlating with Marine Isotope Stages (MIS) 12 and MIS 10, and two separate ice advances were identified for the Saalian glaciation during MIS 8 and MIS 6. One of the main findings is the reconstruction of a possible MIS 8 ice advance which has not yet been numerically dated in northern Germany.

Keywords: *Luminescence dating, Middle and Late Pleistocene, northern Germany*

Zusammenfassung

Die pleistozäne Vereisungsgeschichte Norddeutschlands mit ihren drei großen Eisvorstöße während der Elster-, Saale- und Weichsel-Kaltzeiten wurde im vergangenen Jahrhundert hauptsächlich auf Basis geomorphologischer und lithostratigraphischer Untersuchungen rekonstruiert. Dabei blieb bisher allerdings die zeitliche Einordnung dieser Eisvorstöße aufgrund mangelnder, zeitlich entsprechend weit zurückreichender Datierungstechniken ungenau. Das Ziel dieser Studie ist daher, die Erstellung eines verlässlichen hoch auflösenden geochronologischen Rahmens mittel- und jungpleistozäner Ablagerungen in Norddeutschland auf Basis der numerischen Datierungsmethode der Lumineszenz. Diese liefert als Ergebnis das letzte Belichtungs- und damit Ablagerungsalter der datierten Feldspat- und Quarz-Mineraie. Die Untersuchungsgebiete befinden sich in der Münsterländer Bucht sowie im Leine- und Wesertal und damit im Bereich fluvialer Systeme sowie ehemaliger mittelpleistozäner Eisränder und/oder großer Eisstauseen. Die Lumineszenzdatierung der Sedimente dieser Ablagerungssysteme ist insofern herausfordernd, da das natürliche Lumineszenzsignal vor der letzten Ablagerung möglicherweise nicht gänzlich vom Sonnenlicht zurückgesetzt (gebleicht) worden ist, so dass eine Altersüberbestimmung wahrscheinlich sein kann.

Die methodischen Ergebnisse zeigen, dass mit Hilfe eines gepulsten, Infrarot-stimulierten Lumineszenz (IRSL)-Messprotokolls und einem gepulsten, bei 50°C gemessene IRSL-Signal (IR_{50}) verlässliche und robuste Feldspat-Alter erzielt werden können, die z.T. nicht einmal mehr einer *fading*-Korrektur bedürfen. Die Altersübereinstimmung beim Vergleich von IR_{50} - und Quarz-Altern zeigt zudem, dass eine Altersüberbestimmung basierend auf unzureichender Bleichung nicht wahrscheinlich ist. Liegt zusätzlich eine unabhängige Alterskontrolle (z.B. Uran-Thorium-Alter) von Sedimenten aus demselben Ablagerungssystem vor, die das chronologische Ergebnis unterstützt, so spiegelt dies die gute Verlässlichkeit und hohe Präzision der angewandten Datierungsmethode(n) wider. Aus geochronologischer Sicht zeigen die generierten Lumineszenzalter der Senne-Ablagerungen (Münsterländer Bucht), dass kleinmaßstäbliche Klimaschwankungen sehr wohl rekonstruiert werden können, wenn auch die Datierungsgrenze in diesem Fall im Bereich von wenigen 1000 a zu finden ist. Für die Elster-Kaltzeit konnten erstmals mindestens zwei separate Eisvorstöße während der Marinen Isotopenstadien (MIS) 12 und MIS 10 und für die Saale-Kaltzeit ebenfalls zwei Vergletscherungsphasen während MIS 8 und MIS 6 nachgewiesen werden. Eine wesentliche Erkenntnis ist hierbei der mögliche Nachweis des MIS 8-Eisvorstoßes, der so bislang in Norddeutschland noch nicht numerisch datiert wurde.

Schlagnvorte: *Lumineszenzdatierung, Mittel- und Jungpleistozän, Norddeutschland*

Chapter 1

Introduction

The Pleistocene of northern Central Europe was characterised by several major glacial phases which all had a profound impact on the overall landscape evolution. Yet, the reconstruction of the Middle and Late Pleistocene glaciations by defining the exact number, extent and chronology of these glacial phases has long been discussed on the basis of geomorphology and lithostratigraphy. Sedimentological studies of sedimentary successions within, close to and even beyond the former ice-margins were conscientiously carried out and provided useful insights into the depositional environments. However, the reason for the great variety of different depositional models is very simple: the greatest challenge has always been to provide a reliable and robust chronology by using appropriate dating methods. Relative dating methods such as palaeomagnetism, palynology or tephrochronology may cover the corresponding geological time span, but these methods simply determine the relative order of past depositional events. For instance, radiocarbon (^{14}C) dating, as part of the numerical dating methods, gives an absolute age, but only reaches back to about 50 ka and requires organic matter, which may not always be available within the studied sedimentary successions. Luminescence dating methods, however, make use of omnipresent feldspar and quartz minerals of aeolian, waterlain (lacustrine, fluvial, alluvial) or glacial (glacifluvial, glaciallacustrine) sediments and allow for the direct determination of the last depositional event. Final ages cover an age range from a few years to several hundred thousand years (e.g., Yoshida et al., 2000; Preusser et al., 2008), reaching back to the Middle Pleistocene and thus being the ideal numerical dating technique for the sediments under investigation of this thesis.

The greatest challenge in luminescence dating is assigned to the effect of insufficient bleaching of the dated minerals. This effect occurs when the sampled sediment was exposed to insufficient and inadequate light during transport, leading to an incomplete resetting (bleaching) of the luminescence signal and thus to an age overestimation. As the degree of bleaching depends on the depositional environment, it is considered a particular challenge for sediments derived from a glacial and/or waterlain depositional environment because light exposure may be strongly hampered here (e.g., Preusser et al., 2008). The dated sediments of this thesis were derived from such challenging depositional systems in northwestern Germany. The studied areas of the Münsterland Embayment, the Leine and Weser valleys were all located adjacent to the former Middle Pleistocene ice-margins and/or in the vicinity of former proglacial lakes, which formed in front of the advancing ice sheets. The main topic for discussion for all three studied areas has long been assigned to the depositional history due to the lack of reliable and robust numerical ages, reflecting the last depositional event.

The overall aim of this thesis is to set up a geochronological framework for the studied sedimentary successions in northwestern Germany and to evaluate and, if necessary, revise previously established depositional models and interpretations. This is achieved by performing both optically stimulated luminescence (OSL) and infrared stimulated luminescence (IRSL) dating techniques on potassium-rich feldspar and quartz minerals of aeolian, waterlain, and glacial successions, which are considered to be excellent high-resolution terrestrial archives bearing evidences of former glaciations. The results of this thesis will contribute to a better understanding of the glaciation history of northwestern Germany during the Middle and Late Pleistocene, and for the first time allow for correlation with other well-dated regions in northern Central Europe.

1.1 The Pleistocene glaciations

Northern Central Europe has been affected by repeated ice advances during the Pleistocene (**Fig. 1**; e.g., Litt et al., 2007; Ehlers et al., 2011; Houmark-Nielsen, 2011; Laban and van der Meer, 2011; Marks, 2011). While the most complete record of Middle and Late Pleistocene glaciations has been found in the North Sea basin and was reconstructed from several seismic studies, giving evidence of seven ice advances during this geological time span (e.g., Huuse and Lykke-Andersen, 2000; Sejrup et al., 2005; Lutz et al., 2009; Stewart and Lonergan, 2011), the terrestrial record of northern Central Europe revealed only three major glaciations based on predominantly lithostratigraphic, geomorphological and palynological analysis. These glaciations were characterised by the glacial periods of the Elsterian, Saalian and Weichselian, and by the interglacial periods of the Holsteinian and Eemian (Litt et al., 2007).

In northern and eastern Germany, the Elsterian ice sheet advanced from a northern/northeastern direction (Eissmann, 2002; Ehlers et al., 2011) as is indicated by the orientation of the subglacial tunnel valleys in this part of Germany (Stackebrandt, 2009). From the lithostratigraphic record, two ice advances have been reconstructed (e.g., Eissmann, 2002; Litt et al., 2007; Ehlers et al., 2011), that approximately reached the same maximum position (**Fig. 1**; Eissmann, 2002; Litt et al., 2007). Intercalated interglacial sediments were not reported (Eissmann, 2002). However, correlation with the Marine Isotope Stages (MIS) is difficult because it is still unclear whether the Elsterian glaciation occurred during MIS 12 (e.g., Toucanne et al., 2009b; Ehlers et al., 2011) or MIS 10 (e.g., Geyh and Müller, 2005; Litt et al., 2007; Lee et al., 2012). The succeeding Holsteinian interglacial is assigned to MIS 9 (Geyh and Müller, 2005; Sierralta et al., 2011) and is characterised by interglacial deposits, which are often found well-preserved in underfilled tunnel valleys and overdeepened glacial basins (Eissmann, 2002;

Lang et al., 2012). The Saalian Complex is correlated with MIS 8 to MIS 6. While there are no indications for an early Saalian MIS 8 glaciation in northern Germany, glacial sediments from the late Saalian MIS 6 Drenthe and Warthe ice advances are widespread (e.g., Litt et al., 2007; Ehlers et al., 2011) and characterised by subglacial tills which are separated by glacial-lacustrine and glacial-fluvial deposits. Interglacial sediments are unknown (Litt et al., 2007). In northern Germany, altogether three Saalian ice advances occurred from the north and northeast (Caspers et al., 1995; Eissmann, 2002; Litt et al., 2007; Ehlers et al., 2011). Two of them occurred during the Saalian Drenthe glaciation and one during the Saalian Warthe glaciation about 20 ka later (Lambeck et al., 2006; Litt et al., 2007; Busschers et al., 2008; Krbetschek et al., 2008). However, the maximum extent of the Saalian ice sheets is assigned to the Saalian Drenthe glaciation (Litt et al., 2007; Ehlers et al., 2011), reaching to approximately the same position as the Elsterian glaciation (Ehlers et al., 2011). During the Saalian Drenthe glaciation, large and deep proglacial lakes temporarily formed at the margin of the ice sheets (e.g. Thome, 1983; Klostermann, 1992; Eissmann, 2002; Winsemann et al., 2007, 2009, 2011a). Lithological evidence is given by the occurrence of coarse-grained ice-marginal deposits, fine-grained lake-bottom sediments, and ice-rafted debris (e.g., Winsemann et al., 2009; Meinsen et al., 2011). Catastrophic drainage of these proglacial lakes, caused by (rapid) ice retreat and the opening of overspill ways, is considered to have led to characteristic erosional and depositional features, such as the formation of plunge pools, channels, valleys, and streamlined hills (e.g., Winsemann et al., 2009; Meinsen et al., 2011).

The following Saalian Warthe (late MIS 6) glaciation had a much lesser extent when compared to the older glaciations (**Fig. 1**). The subsequent MIS 5e is assigned to the Eemian interglacial (Litt et al., 2008). The occurrence of glacial deposits overlying the Eemian sediments allowed for the reconstruction of the maximum extent of the Weichselian MIS 2 glaciation (Litt et al., 2007; Ehlers et al., 2011), which is characterised by up to three Weichselian ice sheets that occurred in northeastern and eastern Germany (Ehlers et al., 2011). All three studied areas were located within, close to or adjacent to the Middle Pleistocene ice margins (**Fig. 1**).

1.2 Study area

The three studied areas are located in northwestern Germany (**Fig. 1**), south of the North German Lowlands, and structurally belong to the complex Central European Basin System (CEBS). After the Variscan orogeny, the formation of the CEBS started in the Late Carboniferous to Early Permian and was marked by the development of a continental rift system that

was characterised by major north-south trending normal faults (Littke et al., 2005; Gast and Gundlach, 2006). During the Mesozoic, faulting was subsequently replaced by subsidence, and the altered tectonic regime led to the evolution of several sub-basins (Littke et al., 2005). During the Late Cretaceous to Early Pleistocene, a distinct inversion phase occurred (Kley and Voigt, 2008), which is considered to have been the last major tectonic phase in northwestern Germany.



Fig. 1: Map of northern Central Europe, showing the maximum extents of the Pleistocene ice-margins and the locations of the study areas. These are from west to east: the Münsterland Embayment, Weser valley, Leine valley (modified after Ehlers et al., 2011).

1.2.1 The Münsterland Embayment

Structurally, the Münsterland Embayment in northwestern Germany is a syncline that formed during the Late Cretaceous (Drozdowski, 1995; Grobe und Machel, 2002). It is characterised by a northeast-southwest trending folded Palaeozoic basement which is unconformably over-

lain by Mesozoic rocks as well as Pleistocene and Holocene deposits (e.g., Lotze, 1951; Seraphim, 1979b; Klostermann, 1992, 1995; Skupin et al., 1993). To the north and east, the Münsterland Embayment is bounded by the up to 400 m high Teutoburger Wald Mountains, to the south, it is bounded by the up to 850 m high Rhenish Massif.

The Münsterland Embayment experienced ice-coverage only during the Saalian Drenthe glaciation, as is indicated by meltwater deposits and overlying tills (e.g., Seraphim, 1979a; Klostermann, 1992; Skupin et al., 1993; **Fig. 1**). During this glaciation, ice blockage of the eastern part of the Münsterland Embayment and of the upper Weser valley resulted in the formation of glacial Lake Münsterland (Thome, 1998; Herget, 2002; Skupin, 2002; Meinsen et al., 2011) and glacial Lake Weser (Thome, 1983; Klostermann, 1992; Winsemann et al., 2009, 2011a, b; Meinsen et al., 2011). When the Saalian Drenthe ice-lobe retreated, glacial Lake Münsterland probably almost entirely drained towards the southwest (cf. Thome, 1983; Meinsen et al., 2011). At the same time, two catastrophic lake-level falls of glacial Lake Weser occurred, which were caused by rapid ice-lobe retreat, and led to the drainage of glacial Lake Weser into the Münsterland Embayment (Winsemann et al., 2011b). In the Münsterland Embayment, this can be documented by the occurrence of erosional and depositional features such as plunge pools, channels, valleys, and streamlined hills (Meinsen et al., 2011). The ice sheets of the Elsterian as well as the Saalian Warthe and Weichselian were either blocked by the Teutoburger Wald Mountains or did not reach the Münsterland Embayment at all (Ehlers et al., 2011; **Fig. 1**).

The Senne area is located at the southern slope of the Teutoburger Wald Mountains. Its sedimentary succession covers an area of about 250 km² and comprises up to averagely 30 m thick sand-gravel alternations. The Senne is subdivided into the lower Senne and upper Senne by the 110 m a.s.l.-contour line (Seraphim, 1979a). Its depositional history has been an object of interest for the last century, resulting in numerous depositional models displaying a Middle Pleistocene Saalian glacifluvial (Seraphim, 1979a; Skupin et al., 1993; Lenz, 2003) or Late Pleistocene Weichselian periglacial formation (Fehrentz and Radtke, 1998, 2001; Lang and Fehrentz, 1998; Skupin, 1994). Recently, Meinsen et al. (2014) have interpreted the sedimentary succession of the upper Senne to consist of alluvial fan and aeolian sandsheet deposits that recorded rapid climatic changes throughout the Late Pleistocene.

1.2.2 The Leine valley

The studied area of the Leine valley in northern Germany is part of a larger graben system (Leinetal Graben) that formed during the Late Cretaceous to Early Cenozoic. Vollbrecht and

Tanner (2011) investigated the north-south trending structure of the Leine valley and found numerous pull-apart basins that formed during the Cretaceous and acted as depocentres for up to averagely 30 m thick ice-marginal and fluvial Pleistocene deposits.

The Leine valley is flanked by up to 450 m high Mesozoic mountain ridges (**Fig. 1**). During the last century, the Leine valley area has been extensively studied by means of landform and provenance analyses (e.g., Rausch, 1977; Rohde, 1983; Kaltwang, 1992). This was performed in order to reconstruct both the former glaciation history and the reaction of fluvial systems, which had to adapt to the repeatedly advancing and retreating ice sheets of the Elsterian and Saalian Drenthe glaciations. During both glaciations, the study area was covered by ice sheets, while the maximum extents of the Saalian Warthe and the Weichselian glaciations were located further north (Ehlers et al., 2011; **Fig. 1**). During the Saalian Drenthe, the Leine valley was characterised by the formation of glacial Lake Leine (Thome, 1998; Winsemann et al., 2007), as is indicated by the occurrence of glacial lacustrine sediments, consisting of thick fine-grained, commonly laminated lake-bottom sediments, coarse-grained ice-marginal deposits, and ice-rafted debris (e.g., Jordan, 1984; Winsemann et al., 2007; 2009, 2011b; Meinsen et al., 2011).

However, a detailed and multidisciplinary approach including numerical age determination of the ice-marginal deposits did not exist, and thus hampered a trans-regional correlation of the Leine valley-fill deposits with other well-dated sites in northern Central Europe.

1.2.3 The Weser valley

The studied area is located in the southern Weser valley (**Fig. 1**) and is characterised by a folded Variscan basement, which is overlain by Mesozoic sediments that experienced uplift during the Late Cretaceous to Neogene. As a result, the River Weser incised. The studied area in the Weser valley is characterised by up to 530 m high mountain ridges and the broad valley of the River Weser. During the Middle Pleistocene glaciations, the southern Weser valley was ice-free (Ehlers et al., 2011; **Fig. 1**), but was probably characterised by the formation of a deep proglacial lake, namely glacial Lake Weser (Klostermann, 1992; Thome, 1983, 1998; Winsemann et al., 2009; Meinsen et al., 2011). As in the Leine valley, the temporal presence of glacial Lake Weser is indicated by the occurrence of coarse-grained ice-marginal deposits and fine-grained lake-bottom sediments, overlying Middle Pleistocene fluvial deposits and/or bedrock (Winsemann et al., 2009, 2011b). Two catastrophic lake outburst events, which were attributed to the opening of overspill ways, resulted in the initial drainage of glacial Lake Weser into the Münsterland Embayment (Winsemann et al., 2011b). Final drainage was caused by a

sudden ice-lobe destabilisation (Winsemann et al., 2011a, b). However, the subsequent Late Pleistocene ice sheet did not reach the study area (**Fig. 1**).

The sedimentary succession of the Nachtigall pit near Holzminden consists of Middle Pleistocene Saalian fluvial deposits, which are intercalated with interglacial sediments (Kleinmann et al., 2011; Rohde et al., 2012). The fluvial deposits are overlain by Late Pleistocene sediments (Rohde et al., 2012). For over 100 years, the interglacial sediments of the Nachtigall pit have been subject to studies, linking the deposition to the Late Cromerian (Mangelsdorf, 1981), the Holsteinian (Grupe, 1929) or the Eemian (e.g., Siegert, 1912, 1921). However, recent uranium-thorium ($^{230}\text{U}/\text{Th}$) datings proposed a deposition during the Middle Pleistocene Saalian MIS 7c to early MIS 6 (Waas et al., 2011), associating the deposition of the overlying fluvial deposits with the Saalian Drenthe glaciation (Kleinmann et al., 2011; Waas et al., 2011; Rohde et al., 2012).

1.3 Methods

1.3.1 Field work

Field work was carried out in several sand and gravel pits in the Münsterland Embayment and the Leine and Weser valleys. Additionally, three cores (KB01, KB02, KB03) were acquired in the Leine valley. Outcrops and cores were characterised from vertical sediment logs which were measured at the scale of individual beds, noting grain size, bed thickness, bed contacts, bed geometry, and internal sedimentary structures. In outcrop sections, the larger-scale facies architecture was mapped from two-dimensional photo panels. Palaeoflow directions were obtained on the basis of clast imbrications and cross-stratification. In the Leine valley, additional provenance analyses were performed using both the heavy mineral associations of the sands and the clast composition of the gravels. For further information on the detailed procedures regarding provenance analyses, see publication 2 (Chapter 3.3.2).

1.3.2 Shear wave seismic profiles

In order to obtain a high-resolution image of the subsurface to investigate the larger-scale depositional architecture along the position of the three newly acquired cores in the Leine valley, three shear wave seismic reflection profiles were acquired. Publication 2 (Chapter 3.3.3) offers a detailed description of the seismic acquisition parameters and procedures. The seismic profiles exhibited a range of seismic facies types which were defined by external geometry and internal reflector pattern. These were described using the scheme of Mitchum et al. (1977). Seismic facies types were grouped into seismic-stratigraphic units, bounded by seismic reflec-

tors (Brown and Fischer, 1977; Posamentier and Vail, 1988). The three newly acquired cores and additional borehole data provided a substantial lithological control and supported the interpretation of the seismic data.

1.3.3 Three-dimensional subsurface modeling (GOCAD®)

In the Leine valley, the final reconstruction of the large-scale depositional architecture was based on the determined outcrop and borehole data which was integrated into a three-dimensional subsurface model (GOCAD®). Reconstructions of the bedrock relief surface and the thickness and spatial distribution of the overlying Pleistocene deposits subsequently allowed for the creation of maps. These maps revealed zones of increased sediment thickness, whose spatial arrangement was used as an indicator for possible ice-advance directions.

1.3.4 Luminescence dating

For numerical age determination, luminescence dating techniques on aeolian, waterlain and glacial deposits were performed. In the past decades, luminescence dating has been extensively used as a powerful chronological tool. Thermoluminescence (TL) dating of archaeological findings (pottery, burnt flints, and burnt stones) gave the last heating event. TL dating gradually developed towards OSL and IRSL dating, which has become a common and widely used dating technique for Quaternary sediments in order to directly determine the sediment's last exposure to sunlight, giving the last depositional age (cf. Aitken, 1998).

1.3.4.1 The basic principles of luminescence dating

Luminescence dating is a radiation dosimetric method which is based on charge transfer processes in the crystal lattice of minerals such as quartz and feldspar (Bøtter-Jensen et al., 2003). These minerals act as natural dosimeters and are able to record the amount of radiation they have been exposed to over the time. The longer a mineral is exposed to radiation, the greater the number of charge (i.e. electrons) that is trapped in deficiencies or structural defects within the crystal lattice, and the greater the light-sensitive luminescence signal (Aitken, 1985). The number of available deficiencies within the crystal lattice is, however, not infinite and will reach a saturation dose when the mineral is kept under burial conditions long enough. In a natural environment, when the mineral is exposed to sunlight and thus optically stimulated, the trapped charge is released and recombines at luminescence centres causing light (photon) emission. This light emission is also referred to as luminescence or the luminescence signal. Ideally, this signal is completely reduced (bleached) and reset to zero (**Fig. 2**). During subse-

quent burial, the mineral is sealed from sunlight and the luminescence signal accumulates again (Fig. 2).

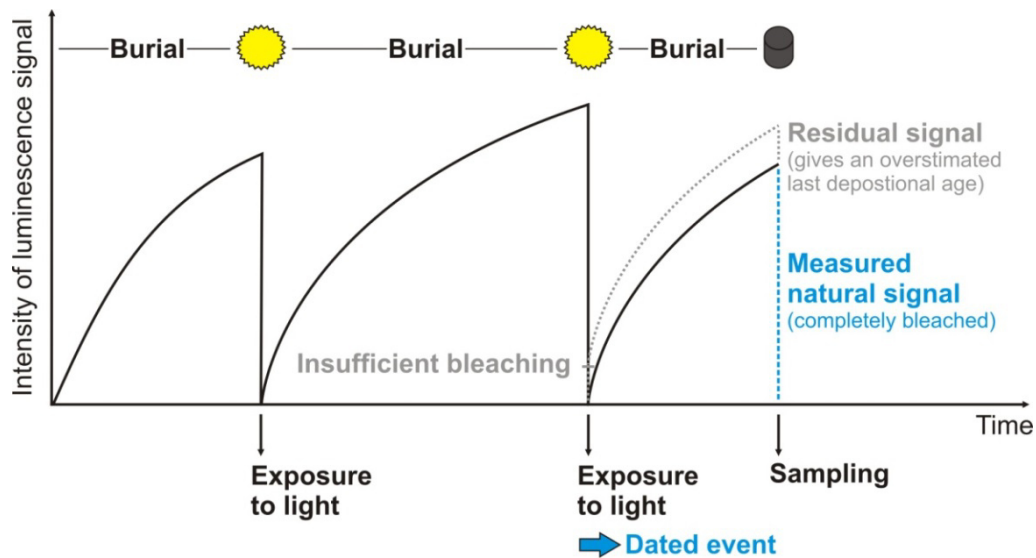


Fig. 2: The luminescence signal accumulates during burial and is ideally set to zero (bleached) when the mineral grain has been exposed to sufficient light. The measured luminescence signal of a sufficiently bleached sample is therefore equivalent to the age of the last dated event. In case of insufficient bleaching, a residual signal will ultimately lead to an age overestimation of the last depositional event.

In the laboratory, optical stimulation is mimicked by light stimulation and the emitted photons of the natural luminescence signal are measured and counted using a photomultiplier. By doing so, the natural luminescence signal is bleached and the aliquot is irradiated again. The induced luminescence signals are measured and subsequently form a growth curve. Interpolation of the natural luminescence signal allows for estimation of the past radiation dose, which is equivalent to the total stored energy since the last bleaching event, referred to as the equivalent dose (D_e in Gy). Division by the dose rate (D_R in Gy ka^{-1}), which is measured by gamma spectrometry of the surrounding sediment and describes the annual dose rate of the surrounding environment including cosmic radiation, allows for calculation of the time elapsed since the last exposure to sunlight prior to deposition. The equation is as follows:

$$\text{Age (ka)} = \text{Equivalent dose (Gy)} / \text{Dose rate (Gy ka}^{-1}\text{)}$$

Further insights on luminescence basics, including details on the physical background, can be found in Aitken (1985, 1998), Wintle (1997, 2008), Preusser et al. (2008) and references therein.

1.3.4.2 Luminescence dosimeters – their advantages and disadvantages

Although several other minerals (e.g., zircon, halite) show the same phenomenon, the most commonly used luminescence dosimeters for dating purposes are quartz and potassium-rich feldspar minerals. Yet, both minerals have advantages and disadvantages over the other.

The quartz luminescence signal is much more light-sensitive and thus bleaches faster than that of feldspar. It may, however, be contaminated by feldspar micro-inclusions, which can lead to additional complications when trying to detect the quartz luminescence signal. The major disadvantage of quartz is assigned to its low saturation dose, which limits its application as a dosimeter to comparably young sediments.

Contrary to this, the feldspar luminescence signal grows to a much higher dose and thus makes it possible to date older sediments. Nevertheless, bleaching of the feldspar luminescence signal takes much more time that might not always be given naturally, thus leading to insufficiently bleached minerals and overestimated depositional ages. The effect of insufficient bleaching and its detection is one of the greatest challenges in luminescence dating. The feldspar luminescence signal is also known to suffer from a spontaneous signal loss over time, which is referred to as anomalous fading (Wintle, 1973; Spooner, 1994). The reason for this phenomenon is linked to quantum-mechanical tunnelling (Visocekas, 1985) and, if left undetected and uncorrected, ultimately leads to underestimated depositional ages and, just like overestimated depositional ages, false interpretations of the investigated successions.

1.3.4.3 Dose rate determination

Determination of the dose rate within the sediment is fundamental when the last depositional age is to be calculated. Besides the internal radiation from within the mineral grain itself (mainly ^{40}K), the external radiation from adjacent mineral grains (^{40}K ; ^{232}Th , ^{235}U , ^{238}U) and the cosmic radiation (neutrons, electrons, photons etc.) from outer space have to be taken into account. For determination of the external dose rate, the water content needs to be known. For this thesis, the water content of all samples was measured and set to an average value close to the measured one. For the determination of the cosmic radiation, the geographical position, altitude and thickness of the overburden have been considered.

Concentrations of the natural radionuclides were not directly measured during field work but were obtained using high-resolution gamma-ray spectrometry in the laboratory. Respectively, 50 g or 700 g of the dry and homogenized sample were stored in N-Type or Marinelli beakers for at least four to six weeks before measurements were conducted to assure equilibri-

um between radon and its daughter nuclides. Final dose rates were calculated using conversion factors reported by Adamiec and Aitken (1998).

1.3.4.4 Equivalent dose determination

Luminescence measurements are commonly performed using an automated Risø TL/OSL reader (DA-20) with a calibrated $^{90}\text{Sr}/^{90}\text{Y}$ beta source (1.48 GBq = 40 mCi), delivering between 0.11 and 0.14 Gy s^{-1} . Feldspar signals are stimulated by infrared (IR) light emitting diodes (LED) at 870 nm and the feldspar luminescence signal is detected through a Schott BG39/Corning 7-59 filter combination in the blue-violet region (320-460 nm). Quartz signals are stimulated with blue LED, emitting at 470 nm, and the quartz luminescence signals are detected through a Hoya U-340 filter in the ultra violet region (280-380 nm). The most commonly used procedure to determine the equivalent dose is the single-aliquot regenerative (SAR) dose protocol (Murray and Wintle, 2000, 2003). Pure monomineralic potassium-rich feldspar or quartz minerals are mounted on discs, representing subsamples which are referred to as aliquots. For detailed information on laboratory procedures, see publication 2 (Chapter 3.3.5.1).

In order to give reliable, reproducible and robust luminescence results, it is essentially important to check whether the applied SAR protocol is suitable prior to the actual measurements. This is accomplished by carrying out performance tests such as dose recovery tests and recycling ratio tests. The dose recovery test checks whether a known dose, which had been given after bleaching the natural signal, can be measured and recovered accurately. If so, the ratio of the given/measured dose should be within 10% of unity (Wintle and Murray, 2006). The recycling ratio test checks whether sensitivity changes were successfully corrected for by giving the same dose at i.e. the beginning and at the end of the measurement. Acceptable values should again be within 10% of unity (Wintle and Murray, 2006).

Since all sedimentary succession were expected to have a somewhat old (Middle Pleistocene) depositional age, feldspar minerals were initially chosen as dosimeters. For the alluvial and aeolian deposits in the Münsterland Embayment, test measurements gave unexpectedly low equivalent doses, therefore additional quartz measurements were performed. For the ice-marginal and fluvial deposits of the Leine and Weser valleys, a pulsed IRSL SAR protocol was applied on monomineralic potassium-rich feldspar minerals and only the off-time signal was recorded to obtain a stable luminescence signal (Tsukamoto et al., 2006). In order to reduce anomalous fading, the pulsed IRSL signal measured at 50°C was used due to its greater light-

sensitivity, which makes it more suitable for dating deposits deriving from a challenging environment.

If possible, additional quartz measurements were performed. The reason for this double-dating approach is assigned to the different bleaching behaviours of both minerals. An age agreement is considered a proof for good bleaching conditions prior to deposition (Murray et al., 2012). Another useful tool to prove the accuracy and reliability of the determined luminescence ages is the comparison of the obtained ages with results of other numerical age determination methods of the exact same sediment and/or the over- and/or underlying deposits. By doing so and given the fact that all obtained ages are consistent and in stratigraphic order, all applied dating methods can be proved to have worked accurately.

1.3.4.5 Incomplete bleaching

Ideally, the luminescence signal is completely reset by sufficient light exposure during transport (**Fig. 2**). However, the chance of complete bleaching in nature depends on the depositional environment. While the best bleaching conditions are known for aeolian sediments, waterlain (such as fluvial, alluvial, lacustrine) and especially glacial sediments (such as glacialfluvial, glaciallacustrine) have a greater potential for having been incompletely bleached due to e.g. short transport distances, various modes of transport, high suspension loads, and high sedimentation rates. Incomplete bleaching is considered the main cause for overestimated depositional ages. When dating younger sediments, the impact of incompletely bleached minerals is of greater importance than dating comparably older sediments because for the latter a residual signal will most likely be within the error range (Duller, 2008).

The degree of incomplete bleaching can be detected by using different approaches such as comparison with independent age control (publication 3, Chapter 4), performing double-datings using two dosimeters (as mentioned above), creating and evaluating equivalent dose vs. time-plots (publication 2, Chapter 3) and/or measuring single-grains or small-sized aliquots which are close to single-grain conditions (publication 1, Chapter 2). However, it has been shown that glacial sediments are not necessarily insufficiently bleached (e.g., Fuchs and Owen, 2008; Houmark-Nielsen, 2008; Alexanderson and Murray, 2012) and luminescence dating of these deposits can be successful (e.g., Fehrentz and Radtke, 1998; Preusser, 1999; Pawley et al., 2008, 2010; Houmark-Nielsen, 2011; Alexanderson and Murray, 2012; Pitkäranta et al., 2014).

1.4 Outline of the thesis – Publications and their contents

This thesis is composed of three publications which have been submitted to peer-reviewed international journals.

Publication 1: Luminescence dating of an Upper Pleistocene alluvial fan and aeolian sandsheet complex: The Senne in the Münsterland Embayment, NW Germany

by J. Roskosch, S. Tsukamoto, J. Meinsen, M. Frechen, J. Winsemann published in *Quaternary Geochronology* 10 (2012), 94-101, DOI: 10.1016/j.quageo.2012.02.012.

In this chapter, the objective was to shed new light into the long lasting controversial discussion regarding the origin and depositional age of the upper Senne deposits. Twelve samples from two localities were dated by luminescence techniques using both an elevated temperature post-infrared infrared stimulated luminescence (pIRIR₂₉₀) protocol (Thiel et al., 2011) for monomineralic coarse-grained potassium-rich feldspar minerals and a double SAR protocol for monomineralic coarse-grained quartz minerals. The central age model (CAM) and the 3-parameter minimum age model (MAM-3; Galbraith et al., 1999) were applied in order to use only those grains for final age determination which represent the true burial dose. The most reliable results are those from both quartz CAM ages, indicating a deposition during the Late Pleistocene (Pleniglacial to Late Glacial). Feldspar pIRIR₂₉₀ ages, however, show a consistency with the quartz CAM ages of the aeolian deposits, but generally overestimate quartz ages of the alluvial plain and alluvial fan deposits.

Publication 2: Luminescence dating of ice-marginal deposits in northern Germany: evidence for repeated glaciations during the Middle Pleistocene (MIS 12 to MIS 6)

by J. Roskosch, J. Winsemann, U. Polom, C. Brandes, S. Tsukamoto, A. Weitkamp, W.A. Bartholomäus, D. Henningsen, M. Frechen published in *Boreas* 44 (2015), 103-126, DOI: 10.1111/bor.12083.

This paper presents new luminescence data from Middle Pleistocene ice-marginal and fluvial deposits from the Leine valley in northwestern Germany. In combination with digital elevation models, high-resolutions shear wave seismic profiles, outcrop and borehole data and generated GOCAD models, the dataset allows for the reconstruction of the stratigraphical valley-fill architecture, and can thus contribute to the ongoing discussion considering the number, extent and timing of the Middle Pleistocene glaciations in northern Central Europe. Luminescence dating techniques were performed on monomineralic coarse-grained potassium-rich feldspar and quartz minerals derived from twelve ice-marginal and two fluvial samples. Equivalent

doses were determined using a pulsed IRSL SAR protocol with IR stimulation at 50°C for 400 s with 50 µs on-time and 200 µs off-time. Final feldspar ages were discussed with respect to their reliability and robustness due to possible causes for both age under- and age overestimation. The overall results of the large dataset indicate that ice advances into the study area occurred during both the Elsterian (MIS 12 and MIS 10) and the Saalian (MIS 8? and MIS 6), extending to approximately the same position, probably controlled by proglacial lakes.

Publication 3: Luminescence dating of fluvial deposits from the Weser valley, Germany: a comparison with independent age control

by J. Roskosch, S. Tsukamoto, M. Frechen, *Geochronometria* (in review).

This publication focuses on new luminescence results from fluvial deposits from the Nachtigall pit located in the Weser valley in northwestern Germany. Monomineralic coarse-grained potassium-rich feldspar minerals and polymineralic fine-grains of five fluvial samples were dated using a pulsed IRSL SAR protocol. Numerical age results indicate two phases of deposition as during MIS 5d and from late MIS 5b to MIS 4, leading to a revised chronostratigraphic framework of the deposits of the Nachtigall pit (Winsemann et al., *subm.*). Independent age control is given by $^{230}\text{U}/\text{Th}$ ages of interglacial sediments (MIS 7c to early MIS 6; Waas et al., 2011) underlying the fluvial deposits.

References

- Aitken, M.J., 1985. Thermoluminescence Dating. Academic Press, London.
- Aitken, M.J., 1998. An Introduction to Optical Dating. Oxford University Press, Oxford.
- Alexanderson, H., Murray, A.S., 2012. Luminescence signals from modern sediments in a glaciated bay, NW Svalbard. *Quaternary Geochronology* 10, 250-256.
- Bøtter-Jensen, L., McKeever, S.W.S., Wintle, A.G., 2003. *Optically Stimulated Luminescence Dosimetry*. Elsevier, Amsterdam, 355pp.
- Brown, L.F., Fisher, W.L., 1977. Seismic-stratigraphic interpretation of depositional systems: examples from Brazilian rift and pullapart basins. In: Payton, C.E. (ed.), *Seismic Stratigraphy – Applications to Hydrocarbon Exploration*. AAPG Memoir 26, 117-133.
- Busschers, F.S., van Balen, R.T., Cohen, K.M., Kasse, C., Weerts, H.J.T., Wallinga, J., Bunnik, F.P.M., 2008. Response of the Rhine-Meuse fluvial system to Saalian ice-sheet dynamics. *Boreas* 37, 377–398.

- Caspers, G., Jordan, H., Merkt, J., Meyer K.-D., Müller, H., Streif, H., 1995. III. Niedersachsen. In: Benda, L. (ed.), *Das Quartär von Deutschland*, Gebrüder Borntraeger, Berlin, 23-58.
- Drozdowski, G., 1995. Geologischer Bau. Krefeld. In: *Geologisches Landesamt Nordrhein-Westfalen* (ed.), *Geologie im Münsterland*, 14-18.
- Duller, G.A.T., 2008. Single-grain optical dating of Quaternary sediments: why aliquot size matters in luminescence dating. *Boreas* 37, 589-612.
- Ehlers, J., Grube, A., Stephan, H.J., Wansa, S., 2011. Chapter 13 – Pleistocene Glaciations of North Germany - new results. In: Ehlers, J., Gibbard, P.L., Hughes, P.D. (eds.), *Quaternary Glaciations - Extent and Chronology – A closer look*. *Developments in Quaternary Science* 15, Elsevier, Amsterdam, 149-162.
- Eissmann, L., 2002. Quaternary geology of eastern Germany (Saxony, Saxon-Anhalt, South Brandenburg, Thuringia), type area of the Elsterian and Saalian Stages in Europe. *Quaternary Science Reviews* 21, 1275-1346.
- Fehrentz, M., Radtke, U., 1998. Lumineszenzdatierung an pleistozänen Schmelzwassersanden der Senne (östliches Münsterland). *Kölner Geographische Arbeiten* 70, 103-115.
- Fehrentz, M., Radtke, U., 2001. Luminescence dating of Pleistocene outwash sediments of the Senne area (Eastern Münsterland, Germany). *Quaternary Science Reviews* 20, 725-729.
- Fuchs, M., Owen, L.A., 2008. Luminescence dating of glacial and associated sediments: review, recommendations and future directions. *Boreas* 37, 636–659.
- Galbraith, R.F., Roberts, R.G., Laslett, G.M., Yoshida, H., Olley, J.M., 1999. Optical dating of single and multiple grains of quartz from Jinmium rock shelter, Northern Australia: part I, experimental design and statistical models. *Archaeometry* 41, 339-364.
- Gast, R., Gundlach, T., 2006. Permian strike slip and extensional tectonics in Lower Saxony, Germany. *Zeitschrift der Deutschen Gesellschaft für Geowissenschaften* 157, 41-56.
- Geyh, M.A., Müller, H., 2005. Numerical $^{230}\text{Th}/\text{U}$ dating and a palynological review of the Holsteinian/Hoxnian Interglacial. *Quaternary Science Reviews* 24, 1861-1872.
- Grobe, M., Machel, H.G., 2002. Saline groundwater in the Münsterland Cretaceous Basin, Germany: clue to its origin and evolution. *Marine and Petroleum Geology* 19, 307-322.
- Grupe, O., 1929. Erläuterungen zur Geologische Karte von Preußen und benachbarten deutschen Ländern 1:25 000, Blatt 4122 Holzminden. *Preußische Geologische Landesanstalt*, Berlin, 71pp.

- Herget, J., 2002. Sedimentary traces as indicator of temporary ice-marginal channels in the Westphalian Bight, Germany. In: Martini, P.I., Baker, V.R., Garzón, G. (eds.), Flood and Megaflood Processes and Deposits: recent and Ancient Examples. Special Publications of the International Association of Sedimentologists 32, 283-290.
- Houmark-Nielsen, M. 2008. Testing OSL failures against a regional Weichselian glaciation chronology from southern Scandinavia. *Boreas* 37, 660-677.
- Houmark-Nielsen, M., 2011. Chapter 5 - Pleistocene Glaciations in Denmark: A Closer Look at Chronology, Ice Dynamics and Landforms. In: Ehlers, J., Gibbard, P.L., Hughes, P.D. (eds.), Quaternary Glaciations - Extent and Chronology – A closer look. *Developments in Quaternary Science* 15, Elsevier, Amsterdam, 47-58.
- Huuse, M., Lykke-Andersen, H., 2000. Overdeepened Quaternary valleys in the eastern Danish North Sea: morphology and origin. *Quaternary Science Reviews* 19, 1233-1253.
- Jordan, H., 1984. Geologische Karte von Niedersachsen 1:25 000 - Erläuterungen zu Blatt Nr. 4325 Nörten-Hardenberg. Hannover, 146pp.
- Kaltwang, J., 1992. Die pleistozäne Vereisungsgrenze im südlichen Niedersachsen und im östlichen Westfalen. *Mitteilungen des Geologischen Instituts der Universität Hannover* 33, 1-161.
- Kleinmann, A., Müller, H., Lepper, J., Waas, D., 2011. Nachtigall: A continental sediment and pollen sequence of the Saalian Complex in NW-Germany and its relationship to the MIS-framework. *Quaternary International* 241, 97-110.
- Kley, J., Voigt, T., 2008. Late Cretaceous intraplate thrusting in central Europe: effect of Africa-Iberia-Europe convergence, not Alpine collision. *Geology* 36, 839-842.
- Klostermann, J., 1992. Das Quartär der Niederrheinischen Bucht. Geologisches Landesamt Nordrhein-Westfalen, Krefeld, 200pp.
- Klostermann, J., 1995. Nordrhein-Westfalen. In: Benda, L. (ed.), *Das Quartär von Deutschland*, 59-94.
- Krbetschek, M.R., Degering, D., Alexowsky, W., 2008. Infrarot-Radiofluoreszenz-Alter (IR-RF) unter-saalezeitlicher Sedimente Mittel- und Ostdeutschlands. *Zeitschrift der Deutschen Gesellschaft für Geowissenschaften* 159, 133-140.
- Laban, C., van der Meer, J.J.M., 2011. Chapter 20 – Pleistocene Glaciation in the Netherlands. In: Ehlers, J., Gibbard, P.L., Hughes, P.D. (eds.), *Quaternary Glaciations - Extent and Chronology – A closer look. Developments in Quaternary Science* 15, Elsevier, Amsterdam, 247-260.

- Lambeck, K., Purcell, A., Funder, S., Kjær, K.H., Larsen, E., Möller, P., 2006. Constraints on the Late Saalian to early Middle Weichselian ice sheet of Eurasia from field data and rebound modeling. *Boreas* 35, 539-575.
- Lang, M., Fehrentz, M., 1998. GR-OSL- und IR-OSL-Datierungen an spätpleistozänen und holozänen Dünensanden der Senne (östliches Münsterland). *Kölner Geographische Arbeiten* 70, 47-58.
- Lang, J., Winsemann, J., Steinmetz, D., Polom, U., Pollok, P., Böhner, U., Serangeli, J., Brandes, C., Hampel, A., Winghart, S., 2012. The Pleistocene of Schöningen, Germany: a complex tunnel valley fill revealed from 3D subsurface modelling and shear wave seismics. *Quaternary Science Reviews* 39, 86–105.
- Lee, J.R., Rose, J., Hamblin, R.J.O., Moorlock, B.S.P., Riding, J.B., Phillips, E., Barendregt, R.W., Candy, I., 2011. Chapter 6 – The Glacial History of the British Isles during the Early and Middle Pleistocene: Implications for the long-term development of the British Ice Sheet. In: Ehlers, J., Gibbard, P.L., Hughes, P.D. (eds.), *Quaternary Glaciations - Extent and Chronology – A closer look*. *Developments in Quaternary Science* 15, Elsevier, Amsterdam, 59-74.
- Lenz, A., 2003. Geologische Karte von Nordrhein-Westfalen 1:25000 - Erläuterungen zu Blatt 4016 Gütersloh. Krefeld.
- Litt, T., Behre, K.-E., Meyer, K.-D., Stephan, H.-J., Wansa, S., 2007. Stratigraphische Begriffe für das Quartär des norddeutschen Vereisungsgebietes. *E&G Quaternary Science Journal* 56, 7-65.
- Littke, R., Bayer, U., Gajewski, D., 2005. Dynamics of sedimentary basins: the example of the Central European Basin system. *International Journal of Earth Sciences* 94, 779-781.
- Lotze, F., 1951. Neue Ergebnisse der Quartärgeologie Westfalens V. Zur Stratigraphie des Senne-Diluviums. *Neues Jahrbuch für Geologie und Paläontologie, Monatshefte* 4, 97-102.
- Lutz, R., Kalka, S., Gaedicke, C., Reinhardt, L., Winsemann, J., 2009. Pleistocene tunnel valleys in the German North Sea: spatial distribution and morphology. *Zeitschrift der Deutschen Gesellschaft für Geowissenschaften* 160, 225-235.
- Mangelsdorf, P., 1981. Quartärgeologische und paläobotanische Untersuchungen in der Tongrube „Nachtigall“ N Höxter/Weser. Unpublished diploma thesis, University of Hannover, 63pp.

- Marks, L., 2011. Chapter 23 – Quaternary Glaciation in Poland. In: Ehlers, J., Gibbard, P.L., Hughes, P.D. (eds.), *Quaternary Glaciations - Extent and Chronology – A closer look. Developments in Quaternary Science 15*, Elsevier, Amsterdam, 299-303.
- Meinsen, J., Winsemann, J., Weitkamp, A., Landmeyer, N., Lenz, A., Dölling, N., 2011. Middle Pleistocene (Saalian) lake outburst floods in the Münsterland Embayment (NW Germany): impacts and magnitudes. *Quaternary Science Reviews* 30, 2597-2625.
- Meinsen, J., Winsemann, J., Roskosch, J., Brandes, C., Frechen, M., Dultz, S., Böttcher, J., 2014. Climate control on the evolution of Late Pleistocene alluvial-fan and aeolian sand-sheet systems in NW Germany. *Boreas* 43, 42-66.
- Mitchum, R.M., Vail, P.R., Sangree, J.B., 1977. Seismic stratigraphy and global changes of sea-level, Part 6: stratigraphic interpretation of seismic reflection patterns in depositional sequences. In: Payton, C.E. (ed.), *Seismic Stratigraphy – Applications to Hydrocarbon Exploration*. AAPG Memoir 26, 117-133.
- Murray, A.S., Wintle, A.G., 2000. Luminescence dating of quartz using an improved single aliquot regenerative-dose protocol. *Radiation Measurements* 32, 57-73.
- Murray, A.S., Wintle, A.G., 2003. The single aliquot regenerative dose protocol: potential for improvements in reliability. *Radiation Measurements* 37, 377-381.
- Murray, A.S., Thomsen, K.J., Masuda, N., Buylaert, J.-P., Jain, M., 2012. Identifying well-bleached quartz using the different bleaching rates of quartz and feldspar luminescence signals. *Radiation Measurements* 47, 688-695.
- Posamentier, H.W., Vail, P.R., 1988. Eustatic controls on clastic deposition II – sequence and system tract models. In: Wilgus, C.K., Hastings, B.S., Kendall, C.G.S.C., Posamentier, H. W., Ross, C.A., Van Wagoner, J.C. (eds.), *Sea Level Changes – An Integrated Approach*. SEPM Special Publication 42, 125-154.
- Pawley, S.M., Bailey, R.M., Rose, J., Moorlock, B.S.P., Hamblin, R.J.O., Booth, S.J., Lee, J.R., 2008. Age limits on Middle Pleistocene glacial sediments from OSL dating, north Norfolk, UK. *Quaternary Science Reviews* 27, 1363-1377.
- Pawley, S.M., Toms, P., Armitage, S.J., Rose, J., 2010. Quartz luminescence dating of Anglian Stage (MIS 12) fluvial sediments: comparison of SAR age estimates to the terrace chronology of the Middle Thames valley, UK. *Quaternary Geochronology* 5, 569-582.
- Pitkäranta, R., Lunkka, J.-P., Eskola, K., 2014. Lithostratigraphy and Optically Stimulated Luminescence age determinations of pre-Late Weichselian deposits in the Suupohja area, western Finland. *Boreas* 43, 193-207.

- Preusser, F., 1999. Lumineszenzdatierung fluviatiler Sedimente: Fallbeispiele aus der Schweiz und Norddeutschland. *Kölner Forum für Geologie und Paläontologie* 3, 1-62.
- Preusser, F., Degering, D., Fuchs, M., Hilgers, A., Kadereit, A., Klasen, N., Krbetschek, M., Richter, D., Spencer, J.Q.G., 2008. Luminescence dating: basics, methods and applications. *E&G Quaternary Science Journal* 57, 95-149.
- Rausch, M., 1977. Fluß-, Schmelzwasser- und Solifluktuationsablagerungen im Terrassengebiet der Leine und der Innerste. *Mitteilungen des Geologischen Instituts der Technischen Universität Hannover* 14, 1-84.
- Rohde, P., 1983. Erläuterungen zu Blatt Nr. 3742 Pattensen. *Geologische Karte von Niedersachsen – 1:25 000*. Niedersächsisches Landesamt für Bodenforschung, Hannover, 192pp.
- Rohde, P., Lepper, J., Thiem, W., 2012. Younger Middle Terrace - Saalian pre-Drenthe deposits overlying MIS 7 Nactigall interglacial strata near Höxter/Weser, NW-Germany. *E&G Quaternary Science Journal* 61, 133-145.
- Siegert, L., 1912. Über die Entwicklung des Wesertales. *Zeitschrift der Deutschen Geologischen Gesellschaft* 64, 233-264.
- Siegert, L., 1921. Beiträge zur Kenntnis des Pliocäns und der diluvialen Terrassen im Flußgebiet der Weser. *Abhandlungen der Preußischen Geologischen Landesanstalt, Neue Folge* 90, Berlin, 130pp.
- Sierralta, M., Frechen, M., Urban, B. 2011. $^{230}\text{Th}/\text{U}$ dating results from opencast mine Schöningen. In: Behre, K.-E. (ed.), *Die chronologische Einordnung der paläolithischen Fundstellen von Schöningen*. Forschungen zur Urgeschichte im Tagebau von Schöningen. Schriftenreihe Forschungen im Tagebau Schöningen 1. Verlag des Römisch-Germanischen Zentralmuseums, Mainz, 143-154.
- Skupin, K., 1994. Aufbau, Zusammensetzung und Alter der Flugsand- und Dünenbildungen im Bereich der Senne (Östliches Münsterland). *Geologie und Paläontologie in Westfalen* 28, 41-72.
- Skupin, K., 2002. *Geologische Karte von Nordrhein-Westfalen 1:100 000 – Erläuterungen zu Blatt C4314 Gütersloh, Krefeld*, 120pp.
- Skupin, K., Speetzen, E., Zandstra, J.G., 1993. *Die Eiszeit in Nordwestdeutschland. Zur Vereisung der Westfälischen Bucht und angrenzender Gebiete*. Geologisches Landesamt NRW, Krefeld, 143pp.
- Spooner, N.A., 1994. The anomalous fading of infrared-stimulated luminescence from feldspars. *Radiation Measurements* 23, 625-632.

- Stackebrandt, W., 2009. Subglacial channels of Northern Germany – a brief review *Zeitschrift der Deutschen Gesellschaft für Geowissenschaften* 60, 203-210.
- Stewart, M.A., Lonergan, L., 2011. Seven glacial cycles in the middle-late Pleistocene of northwest Europe: Geomorphic evidence from buried tunnel valleys. *Geology* 39, 283-286.
- Thiel, C., Buylaert, J.P., Murray, A., Terhorst, B., Hofer, I., Tsukamoto, S., Frechen, M., 2011. Luminescence dating of the Stratzing loess profile (Austria) – Testing the potential of an elevated temperature post-IR IRSL protocol. *Quaternary International* 234, 23-31.
- Thome, K.N., 1983. Gletschererosion und eakkumulation im Münsterland und angrenzenden Gebieten. *Neues Jahrbuch für Geologie und Paläontologie, Abhandlungen* 166, 116-138.
- Thome, K.N., 1998. Einführung in das Quartär: Das Zeitalter der Gletscher. Springer, Berlin, 309pp.
- Toucanne, S., Zaragosi, S., Bourillet, J.F., Gibbard, P.L., Eynaud, F., Giraudeau, J., Turon, T.L., Cremer, M., Cortijo, E., Martinez, P., Rossignol, L., 2009b. A 1.2 Ma record of glaciation and fluvial discharge for the west European Atlantic margin. *Quaternary Science Reviews* 28, 2974-2981.
- Tsukamoto, S., Denby, P.M., Murray, A.S., Bøtter-Jensen, L., 2006. Time-resolved luminescence from feldspars: New insight into fading. *Radiation Measurements* 41, 790-795.
- Visocekas, R., 1985. Tunnelling radiative recombination in labradorite: its association with anomalous fading of thermoluminescence. *Nuclear Tracks and Radiation Measurements* 10, 521-529.
- Waas, D., Kleinmann, A., Lepper, J., 2011. Uranium-thorium dating of fen peat horizons from pit Nachtigall in northern Germany. *Quaternary International* 241, 111-124.
- Winsemann, J., Asprion, U., Meyer, T., Schramm, C., 2007. Facies characteristics of Middle Pleistocene (Saalian) ice-margin subaqueous fan and delta deposits, glacial Lake Leine, NW Germany. *Sedimentary Geology* 193, 105-129.
- Winsemann, J., Hornung, J.J., Meinsen, J., Asprion, U., Polom, U., Brandes, C., Bußmann, M., Weber, C., 2009. Anatomy of a subaqueous ice-contact fan and delta complex, Middle Pleistocene, North-west Germany. *Sedimentology* 56, 1041-1076.
- Winsemann, J., Brandes, C., Polom, U., 2011a. Response of a proglacial delta to rapid high-amplitude lake level change: an integration of outcrop data and high resolution shear wave seismic. *Basin Research* 23, 22-52.

- Winsemann, J., Brandes, C., Polom, U., Weber, C., 2011b. Depositional architecture and palaeogeographic significance of Middle Pleistocene glaciolacustrine ice marginal deposits in northwestern Germany: a synoptic overview. *E&G Quaternary Science Journal* 60, 212-235.
- Winsemann, J., Lang, J., Böhner, U., Polom, U., Brandes, C., Roskosch, J., Glotzbach, C., Frechen, M., submitted to *Quaternary Science Reviews*. Terrace styles and timing of terrace formation in the Weser and Leine Valley, northern Germany: response of a fluvial system to climate change and glaciation.
- Wintle, A.G., 1973. Anomalous fading of thermoluminescence in minerals. *Nature* 245, 143-144.
- Wintle, A.G., 1997. Luminescence dating: laboratory procedures and protocols. *Radiation Measurements* 27, 769-817.
- Wintle, A.G, Murray, A.S., 2006. A review of quartz optically stimulated luminescence characteristics and their relevance in single-aliquot regeneration dating protocols. *Radiation Measurements* 41, 369-391.
- Yoshida, H., Roberts, R.G., Olley, J.M., Laslett, G.M., Galbraith, R.F., 2000. Extending the age range of optical dating using single 'supergrains' of quartz. *Radiation Measurements* 32, 439-446.

Chapter 2

Publication 1

This chapter has been published as *Roskosch et al., 2012* in *Quaternary Geochronology*, 10, 94-101, DOI: 10.1016/j.quageo.2012.02.012 and can be found at:

<http://www.sciencedirect.com/science/article/pii/S1871101412000374>

Luminescence dating of an Upper Pleistocene alluvial fan and aeolian sandsheet complex: The Senne in the Münsterland Embayment, NW Germany

Julia Roskosch¹⁾, Sumiko Tsukamoto²⁾, Janine Meinsen¹⁾,
Manfred Frechen²⁾, Jutta Winsemann¹⁾

- 1) Institut für Geologie, Leibniz Universität Hannover, Callinstraße 30, D-30167 Hannover, Germany
- 2) Leibniz Institute for Applied Geophysics (LIAG), Geochronology and Isotope Hydrology, Stilleweg 2, D-30655 Hannover, Germany

Abstract

An up to 15 m thick alluvial fan and aeolian sandsheet complex is exposed in the upper Senne area, on the southern slope of the Teutoburger Wald Mountains (NW Germany). The origin and age of these deposits have been controversially discussed for many years, ranging from Saalian glaci-fluvial to Weichselian periglacial deposits. In order to provide a high-resolution chronological framework for the deposits, we conducted luminescence dating of 12 samples from two localities (Oerlinghausen and Augustdorf pits). Both coarse-grain potassium-rich feldspar and quartz minerals were used for luminescence dating. Feldspar was measured using an elevated temperature post-IR infrared stimulated luminescence (IRSL). Quartz was measured using optically stimulated luminescence (OSL) with a conventional single aliquot regenerative dose (SAR) protocol. Feldspar results tend to overestimate quartz ages for the lower part of the sections (alluvial plain and alluvial fan facies) but are consistent with quartz ages

for the upper part of the sections (aeolian facies). Quartz ages from both central and minimum age models suggest deposition during the Late Pleistocene Pleniglacial to Late Glacial.

2.1 Introduction

The sediments of the upper Senne are located on the southern slope of the Teutoburger Wald Mountains, south of the North German Lowlands. The origin and depositional age of these sediments have long been controversial and interpretations considered either a Saalian glacialfluvial (e.g., Seraphim, 1979a; Skupin, 1985, 2002; Klostermann, 1995; Lenz, 2003) or a Weichselian periglacial deposition (Fehrentz and Radtke, 1998, 2001; Lang and Fehrentz, 1998; Skupin, 1994).

This study forms part of a larger project, re-examining the Pleistocene depositional history of the Münsterland Embayment, including a detailed analysis of depositional systems and soft sediment deformation structures (Brandes et al., 2012). In this paper, we present new luminescence ages from two outcrop sections of the upper Senne. The objective of this paper is to provide a high-resolution chronostratigraphic framework for the periglacial deposits of the upper Senne.

2.2 Study area and previous research

The Münsterland Embayment is located south of the North German Lowlands, bounded by the Teutoburger Wald Mountains towards the North (Drozdowski, 1995). The Mesozoic basement rocks of the Teutoburger Wald Mountains and the Münsterland Embayment are overlain by Pleistocene and Holocene deposits (e.g., Lotze, 1951; Seraphim, 1979b; Klostermann, 1992, 1995; Skupin et al., 1993; Skupin, 2002).

Northern Germany was affected by three major glaciations during the Elsterian, Saalian and Weichselian glacial periods (**Fig. 1A**). The Elsterian ice-margin probably terminated north of the Teutoburger Wald Mountains. During the maximum extent of the Saalian (Drenthe) glaciation, the Münsterland Embayment was probably completely covered by ice and ice lobes, advanced from a northwesterly or northerly direction into the Münsterland Embayment (**Fig. 1A**; Skupin et al., 1993; Ehlers et al., 2011). The Late Pleistocene (Weichselian) glaciation did not affect the Münsterland Embayment (**Fig. 1A**).

The study area is located on the southern slope of the Teutoburger Wald Mountains. This area is referred to as Senne (Harbort and Keilhack, 1918) and is characterised by an up to 30 m thick sediment body, covering an area of about 250 km² (Hesemann, 1975; Seraphim, 1979a; **Fig. 1B**). The Senne has a stepped profile with two major plains at ~110 m and ~145 m a.s.l.

The deposits of the Senne consist of Holsteinian and Early Saalian pre-glacial fluvial and lacustrine deposits, overlain by late Saalian meltwater deposits and patchy occurrences of till. The westernmost part of the Senne has been affected by late Saalian lake outburst floods of glacial Lake Weser, leading to a strong erosion and the formation of streamlined hills (Meinsen et al., 2011), formerly interpreted as drumlins (Seraphim, 1973; Skupin et al., 1993). This Middle Pleistocene succession is overlain by alluvial fan and aeolian sandsheet deposits, which are exposed in two major outcrops (Oerlinghausen and Augustdorf pits) over an altitude range of 185-215 m a.s.l. Up to six palaeosols have been mapped within the Aeolian deposits of the upper Senne thought to range in age from the Allerød to the Atlanticum (Skupin, 1994). Lang and Fehrentz (1998) studied aeolian dune deposits NW of Schlangen (**Fig. 1B**) using optically stimulated luminescence (OSL) of quartz and infrared stimulated luminescence (IRSL) of feldspar. Determined quartz and feldspars ages point to a Late Pleistocene (15.8 ± 1.5 ka) to Holocene (7.5 ± 1.2 ka) formation of the sediments.

Fehrentz and Radtke (1998, 2001) investigated quartz and feldspar minerals of sediments from the sand pit Schlegel in Augustdorf (**Fig. 1B**) using multiple aliquot additive dose and regenerative dose techniques to find the boundary between Pleistocene and Holocene deposits. Their quartz results indicate ages between 50 and 25 ka, whereas their feldspar ages (26-7 ka) underestimate the quartz ages, presumably due to anomalous fading.

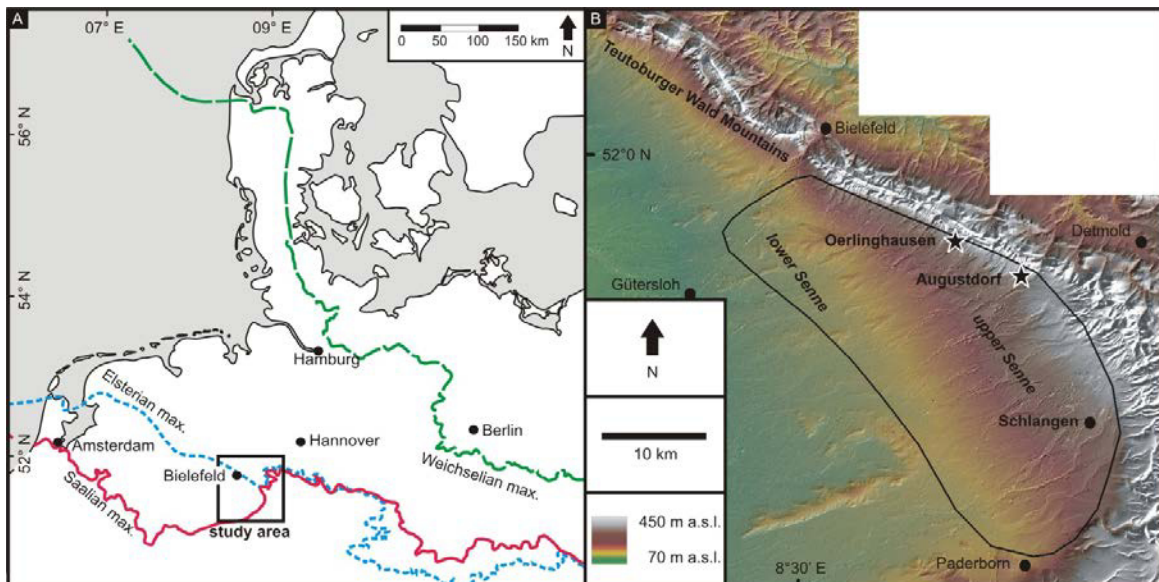


Fig. 1: (A) Map of northern Europe, showing the maximum extent of Pleistocene ice sheets (modified after Ehlers et al., 2004; Winsemann et al., 2011) and the study area; (B) Hill-shaded relief model of the Senne area (eastern part of the Münsterland Embayment) based on data from the Bezirksregierung Köln (Germany). Stars indicate the studied sites.

2.3 Study sites and samples

2.3.1. Field work

Field work including a detailed logging of sections and sampling for luminescence and dosimetry measurements was carried out in April and November 2010. The outcrops were characterised from vertically measured sections and two-dimensional photo panels of the outcrop walls. Sediment logs were measured at the scale of individual beds, noting grain size, bed thickness, bed contacts, bed geometry and internal sedimentary structures. Palaeoflow directions were obtained from cross-bedding and clast imbrications. The larger-scale facies architecture was mapped from photo panels. A detailed analysis of the sedimentary facies will be provided elsewhere. The soft sediment deformation structures have recently been analysed by Brandes et al. (2012). Altogether 12 samples were taken for OSL dating, eight from the Oerlinghausen (**Fig. S1**) and four from the Augustdorf pit (**Fig. S2**).

2.3.2 The outcrop section

In the Oerlinghausen sand pit (N 51°56'28.57", E 8°40'22.95"; **Fig. 1B**) up to 15 m thick deposits are exposed over an altitude range of 190-205 m a.s.l. The sedimentary succession is characterised by an overall subhorizontal geometry. The basal succession consists of an up to 2 m thick alternation of fine-grained sand, silt and mud, interpreted as alluvial plain deposits. These fine-grained floodplain deposits are unconformably overlain by 4-13 m thick channelized and subhorizontally stratified gravel and sand, representing alluvial fan deposits. This succession is bounded by an erosion surface and overlain by 1-4 m thick, subhorizontally stratified, fine- and medium-grained sand with intercalated layers rich in mudstone clasts, reflecting alternating periods of aeolian and alluvial deposition. Within these deposits a wide range of soft sediment deformation structures are developed, which are probably seismically induced (Brandes et al., 2012). The location of OSL samples is shown in **Fig. S1**.

The Augustdorf outcrop section (N 51°55'9.39", E 8°44'41.54") is located approximately 7 km SE of the Oerlinghausen pit. The sediments are exposed over an altitude range of 185-215 m a.s.l. The lower section consists of trough cross-stratified and planar-parallel stratified fine- to coarse-grained sand and gravel, interpreted as alluvial fan deposits. This succession is overlain by 6-8 m thick aeolian sandsheet deposits. The location of the samples for OSL dating is shown in **Fig. S2**.

2.4 Luminescence dating

2.4.1 Preparation and laboratory procedures

In the laboratory, sample preparation and treatment were performed under subdued red light to avoid bleaching of luminescence signal (Preusser et al., 2008). The material of both ends of the sample tubes was removed due to possible light exposure during sampling. Coarse-grained (100-150 μm ; except for Sen10 and Aug1 where the 150-200 μm fraction was used) potassium-rich feldspar and quartz grains were prepared using a procedure of drying, sieving and chemical treatment with hydrochloric acid, disodium oxalate and hydrogen peroxide. Heavy liquid separations followed. Quartz fractions were treated with hydrofluoric acid to avoid contribution of the alpha-irradiated outer part of the quartz mineral and to remove remaining feldspar minerals. Feldspar and quartz aliquots of 2.5 mm (feldspar) and 1 mm (quartz; 20 to 45 grains) size were used for luminescence measurements. Luminescence measurements were performed using an automated Risø TL/OSL reader (DA-20) with a calibrated $^{90}\text{Sr}/^{90}\text{Y}$ beta source. The feldspar signal was stimulated with infrared light diodes emitting at 870 nm and detecting the luminescence signal in the blue-violet region (320 nm-460 nm) with a Schott BG39/Corning 7-59/ND 1.0 filter combination. The quartz signal was stimulated with blue light diodes emitting at 470 nm and was detected through a Hoya U-340 filter, which transmits between 280 nm and 380 nm in the ultra violet region.

2.4.2 Dose rate determination

After drying at $\leq 50^\circ\text{C}$ and homogenization, 700 g of each dosimetry sample was packed in Marinelli beakers, sealed and stored for six weeks to assure equilibrium between radon and its daughter nuclides. High-resolution gamma-ray spectrometry was used to determine the concentrations of uranium, thorium and potassium and the dose rates were calculated using the conversion factors of Adamiec and Aitken (1998) considering a measured average water content of $10 \pm 5\%$. For feldspar dose rate determination, an internal potassium content of $12.5 \pm 0.5\%$ (Huntley and Baril, 1997) and an a-value of 0.150 ± 0.015 (Balescu and Lamothe, 1994) were assumed. The cosmic radiation was corrected for altitude and sediment thickness (Prescott and Hutton, 1994). Dosimetry results and dose rates can be found in **Table 1**.

2.4.3 Equivalent dose rate determination

Due to Saalian age assumptions of previous literature (e.g., Seraphim, 1979a; Skupin, 1985), we started equivalent dose (D_e) determination using potassium-rich feldspar minerals. A total of 16 aliquots per sample were measured. An elevated temperature post-IR IRSL (pIRIR)

Table 1: Dosimetry results and dose rates for the samples of Oerlinghausen (Sen1-10) and Augustdorf (Aug1-4). For feldspar dose rate calculation, an internal potassium content of $12.5 \pm 0.5\%$ and an α -val

Sample	Depth (m)	Dosimetry			Dose rates					Total dose rates	
		Uranium (ppm)	Thorium (ppm)	Potassium (%)	D_α (Gy ka^{-1})	D_β (Gy ka^{-1})	D_γ (Gy ka^{-1})	D^{internal} (Gy ka^{-1})	D^{cosmic} (Gy ka^{-1})	Feldspar (Gy ka^{-1})	Quartz (Gy ka^{-1})
Sen5	0.20	0.59±0.01	1.97±0.02	0.55±0.01	0.06±0.06	0.46±0.06	0.24±0.05	0.51±0.09	0.20±0.02	1.48±0.13	0.91±0.08
Sen9	0.65	0.46±0.01	1.53±0.02	0.64±0.00	0.05±0.06	0.50±0.05	0.23±0.05	0.51±0.09	0.19±0.02	1.48±0.13	0.92±0.08
Sen8	1.25	0.66±0.01	2.11±0.02	0.73±0.01	0.06±0.06	0.59±0.05	0.29±0.05	0.51±0.09	0.17±0.02	1.63±0.13	1.05±0.08
Sen4	3.00	0.63±0.01	2.06±0.02	0.62±0.01	0.06±0.06	0.51±0.06	0.26±0.05	0.51±0.09	0.13±0.01	1.48±0.13	0.90±0.08
Sen3	4.20	0.43±0.01	1.40±0.02	0.54±0.00	0.04±0.06	0.43±0.05	0.21±0.05	0.51±0.09	0.11±0.01	1.29±0.13	0.74±0.07
Sen2	5.18	0.38±0.01	1.23±0.02	0.49±0.00	0.04±0.06	0.39±0.05	0.18±0.05	0.51±0.09	0.09±0.01	1.21±0.13	0.66±0.07
Sen1	7.58	0.55±0.01	1.76±0.01	0.54±0.00	0.05±0.06	0.45±0.05	0.23±0.05	0.51±0.09	0.07±0.01	1.30±0.13	0.74±0.07
Sen10	8.15	0.83±0.01	2.51±0.02	0.61±0.01	0.06±0.06	0.52±0.05	0.30±0.05	0.69±0.09	0.06±0.01	1.63±0.13	0.88±0.07
Aug4	0.55	0.46±0.01	1.53±0.01	0.55±0.01	0.03±0.06	0.44±0.05	0.22±0.05	0.51±0.09	0.19±0.02	1.39±0.13	0.85±0.08
Aug3	1.55	0.33±0.01	1.09±0.01	0.54±0.00	0.03±0.06	0.42±0.05	0.19±0.05	0.51±0.09	0.16±0.02	1.31±0.13	0.76±0.07
Aug2	6.85	0.32±0.01	1.17±0.02	0.52±0.00	0.03±0.06	0.40±0.05	0.18±0.05	0.51±0.09	0.07±0.01	1.19±0.13	0.65±0.07
Aug1	8.65	0.45±0.01	1.40±0.02	0.44±0.01	0.03±0.06	0.36±0.05	0.19±0.05	0.69±0.09	0.06±0.01	1.32±0.13	0.60±0.07

protocol after Thiel et al. (2011; **Table 2A**), using a preheat at 320°C and a post-IR stimulation at 290°C after stimulating with IR at 50°C for 100 s was used, which has been proved to show negligible anomalous fading (Thiel et al., 2011; Buylaert et al., 2012). Both D_e values of IRSL signal at 50°C (IR_{50}) and pIRIR signal at 290°C ($pIRIR_{290}$) were calculated. The $pIRIR_{290}$ signal has a typical residual dose of ~5 Gy at the time of deposition (Buylaert et al., 2012). This residual dose of 5 Gy was subtracted from the D_e values for age calculation. Residual doses could be slightly sample-dependent, however, there is no modern analogue material in our study site and it was impossible for us to determine residual doses specifically for our samples. Additionally, dose recovery and fading tests were performed on two samples of both sections (Oerlinghausen pit: samples Sen3 and Sen5; Augustdorf pit: samples Aug2 and Aug3), using six aliquots of each of these samples, which were bleached by a solar stimulator. Recovery ratios (minus a residual dose of 5 Gy) are within the 1 σ -level (0.98-1.07; **Fig. S3**). Fading rates (g-values) were calculated after Huntley and Lamothe (2001).

For quartz measurements, a conventional SAR protocol (Murray and Wintle, 2000, 2003) was used (**Table 2B**) and slightly modified to a so called double SAR protocol, which includes an IR stimulation to reduce the feldspar signal prior to stimulation of the aliquots with blue LEDs (post-IR OSL signal). Dose recovery tests at different preheat temperatures were performed to find the best preheat condition and to get accurate dose estimations. A selected preheat temperature (180°C) was conducted for samples Sen1 to Sen5 using six aliquots each. Recovery ratios (0.91-0.94) are consistent with unity at 1 σ -level, other than Sen5 (0.85) which is consistent with the 2 σ -level (**Fig. S3**). 96 aliquots per sample were used for D_e measurements.

Table 2: (A) Post-IR IRSL SAR protocol for coarse-grain potassium feldspar measurements, (B) pIRIR protocol for coarse-grain quartz measurements.

Step	Treatment	
	(A) Feldspar	(B) Quartz
1	Give dose	Give dose
2	Preheat, 60 s @ 320°C	Preheat, 10 s @ 180°C
3	IR stimulation, 100 s @ 50°C	IR stimulation, 100 s @ 50°C
4	IR stimulation, 210 s @ 290°C	OSL stimulation, 40 s @ 125°C
5	Give test dose	Give test dose
6	Cutheat, 60 s @ 320°C	Cutheat, 0 s @ 160°C
7	IR stimulation, 100 s @ 50°C	IR stimulation, 100 s @ 50°C
8	IR stimulation, 210 s @ 290°C	OSL stimulation, 40 s @ 125°C
9	IR stimulation, 100 s @ 325°C	Return to step 1
10	Return to step 1	

Acceptance criteria for SAR measurements are: recycling ratio limit, within 10% from the unity; maximal test dose error 10%; signal intensity larger than 3 sigma above background. Dose response curves were fitted with a saturating exponential function to calculate D_e values. A measurement error of 2.0% was included for the D_e calculation. For feldspar samples, the integrated signal of the first 5 s from the decay curve was used after subtracting the last 50 s as a background. For quartz samples, the initial 0.5 s of the signal was used after subtracting an early background of 0.7 s-4.0 s (Cunningham and Wallinga, 2010).

2.4.4 Age models and age calculations

For feldspar age calculations, the mean D_e values (after subtracting the residual of 5 Gy for the pIRIR₂₉₀) were used. For the IR₅₀ ages, a fading correction after Huntley and Lamothe (2001) was performed. Feldspar grains in our samples might have been heterogeneously bleached, however, unlike quartz most of the feldspar grains give luminescence, and thus even D_e values from small aliquots are not suitable for any statistical analysis. On the other hand, our quartz OSL measurements are close to single-grain conditions, and we therefore used two statistical methods that have been developed to isolate grains which represent a true burial dose: central age model (CAM) and the 3-parameter minimum age model (MAM-3; Galbraith et al., 1999). The CAM generates a representative estimate of the average burial dose which can be compared to a weighted average with the difference that it does not select one true value (Arnold et al., 2007). The standard deviation of this distribution is called overdispersion (σ_{OD}) and describes the scatter within the sample which cannot be explained by instrumental errors. The MAM-3 was developed for heterogeneously bleached sediments (Galbraith and Laslett, 1993; Galbraith et al., 1999). An σ_{OD} value of 35% obtained from well bleached aeolian samples (Sen5, Aug3, Aug4) was used to calculate MAM-3 ages for all samples (see chapter 4.6 why we think these samples are well bleached). In order to consider which age model is more suitable for our samples, the single-aliquot age model decision process by Arnold et al. (2007) was used. Specific D_e distribution characteristics (e.g., overdispersion, skewness) were taken to identify the appropriate statistical approach.

2.4.5 Feldspar: luminescence signal characteristics, dose distribution and ages

For post-IR IRSL measurements of feldspar the test dose measurements corrected properly for sensitivity changes, since the average recycling ratio of all aliquots was 1.01 ± 0.10 . For the IR₅₀ signal, a mean g-value of $2.5 \pm 0.3\%$ per decade ($2.2 \pm 0.5\%$ per decade for the Oerlinghausen pit and $2.8 \pm 0.4\%$ per decade for the Augustdorf pit) was obtained. For the pIRIR₂₉₀ signal,

the mean g-value was $1.0 \pm 0.2\%$ per decade ($0.8 \pm 0.3\%$ per decade for the Oerlinghausen pit and $1.2 \pm 0.3\%$ per decade for the Augustdorf pit). Only the IR_{50} ages were corrected for anomalous fading. Mean recuperation was 5.5% (Oerlinghausen pit) and 7.1% (Augustdorf pit). The IR_{50} and $pIRIR_{290}$ ages are given in **Table 3**. All ages are given with the 1σ uncertainty. Feldspar ages are in stratigraphic order and indicate a Late Pleistocene deposition: IR_{50} ages range from 31.0 ± 3.1 ka to 17.3 ± 1.8 ka (Oerlinghausen pit) and from 21.7 ± 2.5 ka to 17.0 ± 2.1 ka (Augustdorf pit). $pIRIR_{290}$ ages are slightly older ranging from 34.0 ± 2.7 ka to 20.6 ± 1.6 ka (Oerlinghausen pit) and from 27.1 ± 4.3 ka to 19.7 ± 1.9 ka (Augustdorf pit) but are in agreement in 1-sigma standard deviation.

2.4.6 Quartz: luminescence signal characteristics, dose distribution and ages

All quartz samples show a dim signal (<800 counts per 0.10 s; **Fig. S4**), which decays very quickly during the first seconds of stimulation, indicating that the OSL signal is dominated by the fast component. A representative dose response and decay curve as well as a D_e histogram are shown in **Fig. 2**. The average recycling ratio of all aliquots for all samples is close to unity (1.04 ± 0.10 for samples of the Oerlinghausen pit; 1.05 ± 0.10 for samples of the Augustdorf pit), implying that the test dose measurement corrected for sensitivity changes appropriately.

The OSL ages are given in **Table 3**. All ages are given with the 1σ uncertainty. The quartz dose distributions for all samples, plotted in histograms and radial plots, are shown in **Figs S5** and **S6**. Quartz ages determined using the CAM model are in stratigraphic order, ranging in age from 29.3 ± 3.2 ka to 13.1 ± 1.5 ka (except for the uppermost sample Sen5 from the Oerlinghausen pit) and 25.4 ± 3.6 ka to 19.5 ± 2.0 ka (Augustdorf pit), indicating a Pleniglacial to Late Glacial age. MAM-3 ages are consistent with CAM ages within 1σ -level except for three samples: Sen10, Sen3 and Sen8 (**Table 3B**, **Fig. 3**); the two ages of Sen3 and Sen10 are also consistent within 2σ -level. The ages cover ranges from 21.0 ± 3.5 ka to 7.6 ± 1.5 ka (Oerlinghausen pit) and from 21.3 ± 4.1 ka to 18.5 ± 2.8 ka (Augustdorf pit), indicating a Late Pleniglacial and Late Glacial to Holocene age of the Oerlinghausen deposits and a Late Pleniglacial age of the Augustdorf section.

The D_e histograms shown in **Fig. S5** display a Gaussian-like distribution for most of the samples (e.g., Sen9, Sen5). Some samples (e.g., Sen1, Sen2, Sen4, Aug1) are skewed towards lower doses. All histograms have a broad distribution. The three samples from the uppermost part of the sections (Sen5, Aug3, Aug4) are well bleached, probably because of their aeolian origin. Moreover, these samples show a Gaussian-like and normal dose distribution (**Fig. S6**) and their quartz and feldspar ages (IR_{50} and $pIRIR_{290}$ – a residual dose of 5 Gy) agree

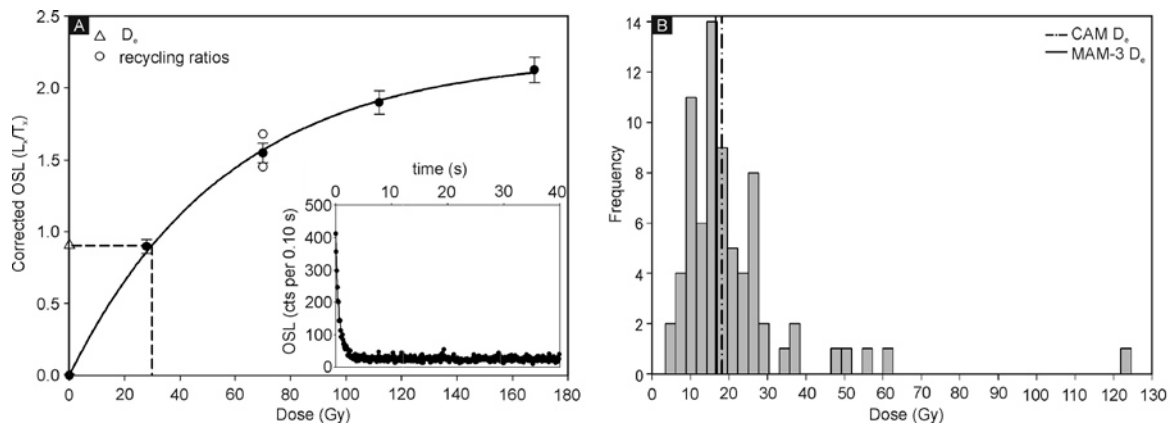


Fig. 2: (A) Dose response and decay curve for quartz sample Sen1; those for the rest of the samples can be found in **Fig. S4**. The dose response curve shows an exponential growth, the decay curve shows a rapid decrease of the OSL signal within the first three seconds, indicating a dominance of fast components. One of the recycling points is an IR depletion ratio. (B) D_e histogram for quartz sample Sen1; those for the rest of the samples can be found in **Fig. S5**.

perfectly (**Fig. 3**). Since quartz bleaches more rapidly than feldspar (Godfrey-Smith et al., 1988), such an agreement can only occur with well bleached samples. Additionally, these samples have the lowest σ_{OD} values among the samples (**Table 3B**), but the values themselves are still high (~33 to 38%). The reason of the high σ_{OD} values is unknown but may be due to natural beta dose heterogeneity and/or post-depositional mixing. The mean σ_{OD} of 35% obtained from these three samples was used for the calculation of MAM-3 ages. Radial plots shown in **Fig. S6** also indicate sufficient bleaching, as measured aliquots are mostly within the 2 σ -level of the average D_e values. For all samples, MAM-3 D_e values have a greater relative error and a lower precision. CAM D_e values are more precise with a smaller relative error.

For 9 of 12 samples, D_e distribution characteristics favour MAM-3 for age calculation due to an σ_{OD} value of $\geq 40\%$ (**Table 3B**; Arnold et al., 2007). However, the decision process may not be appropriate for our samples, because the σ_{OD} values are ~35% even for well bleached samples.

2.5 Discussion

Samples are derived both from the alluvial fan and overlying aeolian deposits. The best bleaching results were found in samples Sen5, Aug3 and Aug4, representing samples from the uppermost aeolian-dominated parts of both sections. Samples from the alluvial deposits are generally less well bleached. Both quartz and feldspar luminescence dating results point to a Late Pleistocene age of the studied sediments, contradicting a Saalian formation of the uppermost Senne deposits (e.g., Seraphim, 1979a; Skupin, 1985). Also, determined quartz and feldspar

Table 3: (A) Feldspar and (B) quartz luminescence ages from the Oerlinghausen (Sen1-10) and Augustdorf pits (Aug1-4). Feldspar results are divided into pIRIR₂₉₀ and IR₅₀ ages. Quartz results are divided according to statistical methods (CAM, MAM-3) and D_e distribution characteristics. Bold numbers indicate the age which is rather reliable due to Arnold et al. (2007); n = total number of aliquots measured per sample; n₁ = number of measured aliquots accepted for D_e analysis; σ_{OD} = overdispersion; c = skewness; 2σ_c = 2σ uncertainty of skewness; k = kurtosis; 2σ_k = 2σ uncertainty of kurtosis; RSD = relative standard deviation; * see Arnold et al., 2007; ** see Tabachnick and Fidell, 1996.

Sample	(A) Feldspar				(B) Quartz											
	pIRIR ₂₉₀ D _e (Gy)	pIRIR ₂₉₀ age (ka)	IR ₅₀ D _e (Gy)	IR ₅₀ age (ka)	CAM D _e (Gy)	CAM age (ka)	MAM-3 D _e (Gy)	MAM-3 age (ka)	n	n ₁	σ _{OD} (%)	c	2σ _c ***	k	2σ _k ***	RSD (%)
Sen5	31.1±0.4	21.1±1.9	21.1±0.5	17.3±1.8	14.3±0.7	15.6±1.5	14.3±1.4	15.5±2.0	96	59	33.36	0.38	0.64	8.47	1.28	6.00
Sen9	31.1±0.8	21.0±1.9	22.4±1.0	18.4±2.0	14.8±0.9	15.9±1.6	10.8±1.7	11.6±2.1	96	57	44.66	0.86	0.65	0.67	1.30	7.80
Sen8	33.5±0.4	20.6±1.6	23.9±0.4	19.6±1.8	13.9±1.2	13.1±1.5	8.0±1.5	7.6±1.5	96	51	57.69	0.89	0.69	0.94	1.53	7.80
Sen4	32.8±0.9	22.2±2.0	22.4±0.8	21.1±2.2	17.0±1.1	18.7±1.9	13.5±1.9	14.9±2.4	96	64	48.10	2.32	0.61	0.42	1.22	11.83
Sen3	31.5±0.9	24.4±2.5	21.3±1.0	20.1±2.4	15.7±1.2	21.0±2.6	9.5±1.7	12.8±2.6	96	56	54.96	1.48	0.65	2.42	1.31	11.19
Sen2	36.5±0.8	30.2±3.3	25.3±0.8	23.7±2.8	15.0±1.0	22.4±2.8	13.3±1.8	19.9±3.4	96	77	54.06	3.90	0.56	20.51	1.12	14.36
Sen1	42.0±1.1	32.2±3.3	29.8±1.3	27.9±3.3	18.1±1.2	24.4±2.9	15.6±2.1	21.0±3.5	96	73	52.33	3.90	0.57	21.29	1.15	16.52
Sen10	55.5±1.1	34.0±2.7	37.7±1.2	31.0±3.1	25.8±1.9	29.3±3.2	15.6±2.4	17.7±3.1	96	59	55.60	1.02	0.64	1.29	1.28	16.77
Aug4	27.7±0.7	19.7±1.9	18.9±0.8	17.6±1.9	16.7±0.9	19.5±2.0	15.9±2.0	18.5±2.8	96	61	38.22	1.30	0.63	2.90	1.40	8.65
Aug3	27.0±1.0	20.6±2.2	18.3±1.0	17.0±2.1	15.1±0.7	19.6±2.1	15.1±1.5	19.5±2.6	96	58	33.55	0.71	0.64	1.91	1.44	6.15
Aug2	31.3±1.2	26.2±3.0	22.7±1.4	20.8±2.7	15.5±1.1	23.7±3.1	12.6±1.8	19.3±3.5	96	49	43.80	0.91	0.70	0.05	1.56	9.20
Aug1	35.9±0.9	27.1±2.7	23.7±0.9	21.7±2.5	15.3±1.2	25.4±3.6	12.8±1.9	21.3±4.1	96	51	55.53	2.67	0.69	8.24	0.77	7.80

ages partly considerably differ. It is known that quartz bleaches more rapidly than feldspar. Moreover, Buylaert et al. (2012) have recently compared the bleachability of quartz OSL, feldspar IR₅₀ and pIRIR₂₉₀ signals and showed that the pIRIR₂₉₀ signal is much less sensitive to light than the IR₅₀ signal. A good agreement between quartz CAM ages and feldspar IR₅₀ ages for all the samples except Sen8 (**Fig. 3**) suggests that these samples are reasonably well bleached at deposition; at least quartz OSL and feldspar IR₅₀ signals were bleached for the majority of the grains. However, the difference between the OSL/IR₅₀ ages and the pIRIR₂₉₀ ages tends to be larger in the lower part of the sections. The increasing discrepancy between the quartz and feldspar pIRIR₂₉₀ ages towards the lower part probably suggests that the bleaching environment for the lower part of the sections was not as good as the upper part, as may be expected for an alluvial fan setting, periodically affected by high-energy floods.

2.5.1 CAM vs. MAM-3: What is the appropriate age model?

We have shown that CAM and MAM-3 ages are in agreement in 1 σ -level for 9 of 12 samples except for Sen10, Sen3 and Sen8. The MAM-3 ages for these samples are mainly based upon aliquots having relatively low precisions (**Fig. S6**). The distributions of all the three samples are not skewed but very broad, suggesting that the application of the minimum age model may not be really suitable.

Moreover, the CAM and MAM-3 ages broadly cover the same age ranges, indicating a Pleniglacial to Late Glacial deposition. Despite the favouring of most MAM-3 results due to the decision process by Arnold et al. (2007), CAM ages are used for interpretation because results of D_e histograms (**Fig. S5**) and radial plots (**Fig. S6**) indicate a constant reliability of CAM D_e values. There are no significant age inversions and ages can be put into a palaeo-environmental context. As stated above, MAM-3 ages were likely to be derived using only a few and very imprecise aliquots (**Fig. S6**). However, it might be possible that the CAM ages from the alluvial fan and floodplain facies are slightly overestimated, because most of these samples show different ages between quartz and feldspar, suggesting that the bleaching environment was not ideal.

2.5.2 Comparison of results with previous studies

Luminescence dating of quartz and feldspar by Fehrentz and Radtke (1998, 2001) for the uppermost Augustdorf pit strongly differs from our results. Their quartz ages range from ~50 to 25 ka and feldspar ages from ~26 to 7 ka, ours from 25 to 19 ka (quartz) and 27 to 20 ka (feldspar). This large difference in age might be explained by the applied method of

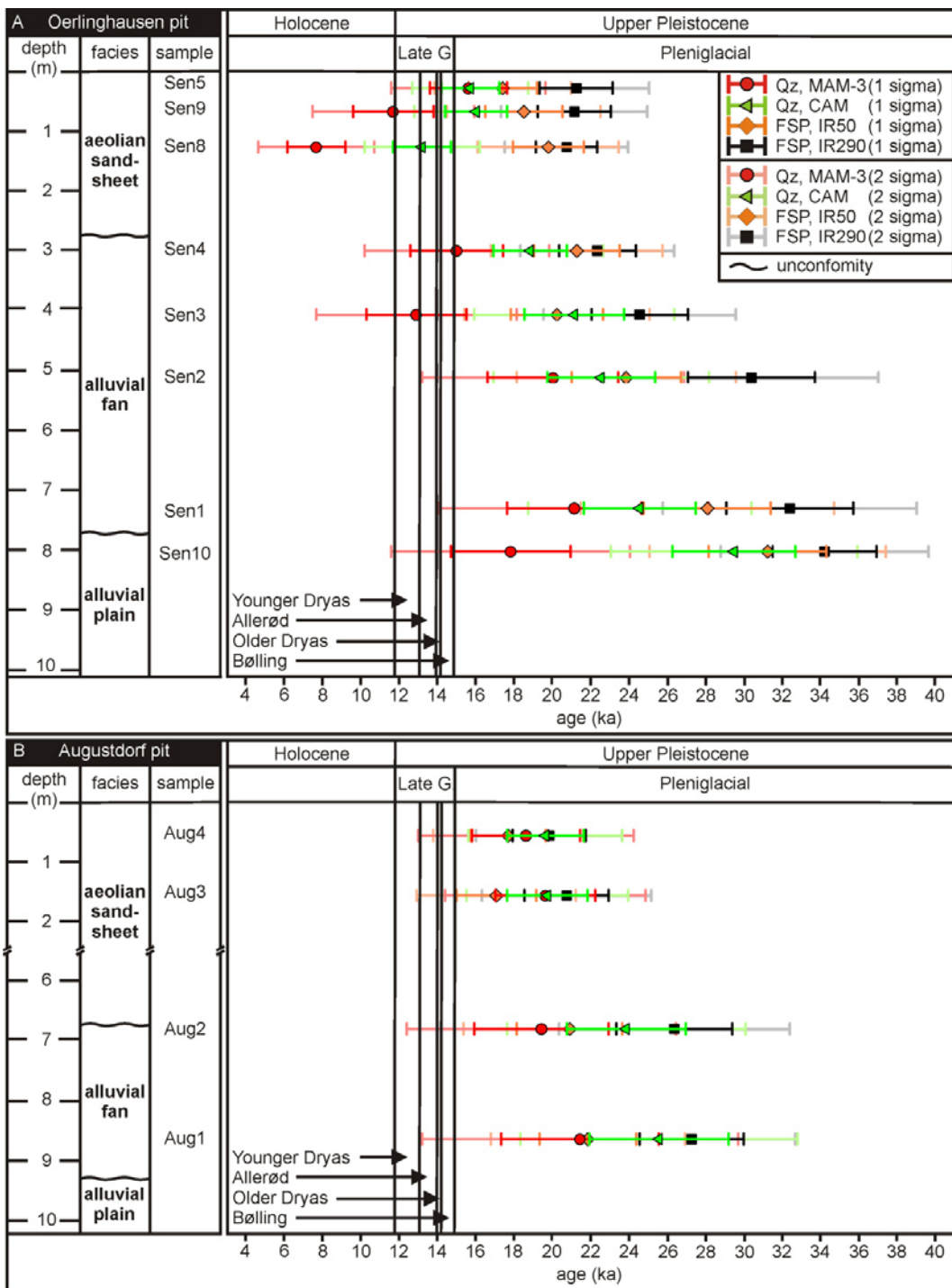


Fig. 3: Facies associations, age and stratigraphy of all samples of the (A) Oerlinghausen and (B) Augustdorf pit. For all samples, the age is given with 1 and 2 σ uncertainty.

luminescence measurements (multiple aliquot additive dose and regenerative dose techniques). However, luminescence ages of quartz and feldspar by Lang and Fehrentz (1998) for aeolian dune deposits northwest of Schlangen are not consistent with our results as well. Their quartz

ages range from ~16 to ~7 ka and feldspar ages from ~10 to ~5 ka. This difference in age might have various reasons. 1) The aeolian deposits from the Schlangen area (**Fig. 1B**) might be younger in age than those exposed in the Oerlinghausen and Augustdorf pits. 2) The different applied luminescence methods (additive dose-methods) used for stimulation (quartz signal stimulation with green light diodes emitting at 500-550 nm) may have led to the determination of different ages.

2.5.3 Sedimentology

The drying-upward succession of the upper Senne resembles Upper Pleistocene fluvial-aeolian deposits from the Netherlands (e.g., Kasse et al., 2007) and Poland (e.g., Zieliński et al., 2011). Calculated CAM ages for the alluvial deposits of the Senne indicate a deposition during ~30 to 20 ka. This succession is overlain by aeolian sandsheet deposits, which range in age from approximately 20 to 13 ka. An important marker horizon in northwest European Upper Pleistocene fluvial-aeolian deposits is the so-called Beuningen Gravel bed that resulted from deflation under polar desert conditions, indicating strong cooling and increasing aridity between 17 ka and 15 ka (Kasse et al., 2007; Bateman, 2008; Vandenberghe et al., 2009).

The observed prominent unconformity on top of the alluvial fan deposits might be correlated with the Beuningen gravel event. Subsequently, aeolian sandsheets were deposited post-dating this unconformity. The intercalated palaeosols in the uppermost aeolian deposits indicate a rapid climatic warming during the Late Glacial (Skupin, 1994; Kasse et al., 2007). Pedostratigraphical marker horizons (palaeosols) in Late Glacial deposits are common (e.g., the Usselo and Finow soil) and known from many areas in NW and Central Europe. Radiocarbon dates of the Usselo and Finow soil indicate an Allerød pedogenesis, separating deposits of the Older and Younger Dryas (Skupin, 1994; Kasse, 2002; Kasse et al., 2007; Kaiser et al., 2009) and reflecting a phase of surface stability (Kasse et al., 2007). Unlike the Dutch fluvial-aeolian deposits, evidences for permafrost, such as ice-wedge casts (Kasse, 1997, 2002) and cryoturbation features, have not been found in the upper Senne deposits.

2.6 Conclusions

This study presents new luminescence ages from 12 samples from two outcrop sections of the upper Senne. Coarse-grain feldspar and quartz measurements were performed and age results of two statistical models (CAM, MAM-3) are discussed. The following conclusions can be drawn:

- The deposits of the uppermost Senne consist of an alluvial fan and aeolian sandsheet succession that was deposited during the Pleniglacial to Late Glacial;
- Feldspar pIRIR₂₉₀ results tend to be older than quartz and feldspar IR₅₀ ages for the alluvial deposits, probably indicating heterogeneous bleaching of the pIRIR₂₉₀ signal of the alluvial deposits;
- Results from quartz CAM ages (~30-13 ka) seem to be most reliable because D_e values show the best precision and the lowest relative error;
- The alluvial fan deposits (~30-20 ka) are unconformably overlain by aeolian sandsheet deposits, which range in age from approximately 20 to 13 ka. The unconformity at the base of the aeolian sandsheet deposits might be correlated with the Beuningen gravel event that is thought to represent a deflation lag, formed under polar desert conditions, indicating strong cooling and increasing aridity between 17 ka and 15 ka;
- Intercalated palaeosols in the uppermost aeolian deposits point to a rapid climatic warming during the Late Glacial.

Acknowledgements

We are grateful to one anonymous reviewer for the constructive review, which helped to improve the manuscript, and editor Rainer Grün for helpful comments and discussion. We would like to thank the owner of the Oerlinghausen pit (Oerlinghausen Sandgrube GmbH, A. Stöltzing) and the Augustdorf pit (Ernst Schlegel GmbH&Co. KG) for the permission to enter and work on their properties. Alexander Kunz, Tony Reimann, Thomas Stevens and Christine Thiel are gratefully acknowledged for discussion. Eventually, we thank Sonja Riemenschneider for her technical assistance in the laboratory.

References

- Adamic, G., Aitken, M.J., 1998. Dose-rate conversion factors: update. *Ancient TL* 16, 37-50.
- Arnold, L.J., Bailey, R.M., Tucker, G.E., 2007. Statistical treatment of fluvial dose distributions from southern Colorado arroyo deposits. *Quaternary Geochronology* 2, 162-167.
- Balescu, S., Lamothe, M., 1994. Comparison of TL and IRSL age estimates of feldspar coarse grains from waterlain sediments. *Quaternary Science Reviews* 13 (5-7), 437-444.
- Bateman, M.D., 2008. Luminescence dating of periglacial sediments and structures. *Boreas* 37, 574-588.

- Brandes, C., Winsemann, J., Roskosch, J. Meinsen, J., Tanner, D.C., Frechen., M., Steffen, H., Wu, P., in press. Activity along the Osning Thrust in Central Europe during the Lateglacial: ice-sheet and lithosphere interaction. *Quaternary Science Reviews* 38, 49-62.
- Buylaert, J.-P., Jain, M., Murray, A.S., Thomsen, K., Thiel, C., Sohbati, R., 2012. A robust feldspar luminescence dating method for Middle and Late Pleistocene sediments. *Boreas* 41, 435-451.
- Cunningham, A.C., Wallinga, J., 2010. Selection of integration time intervals for quartz OSL decay curves. *Quaternary Geochronology* 5, 657-666.
- Drozdowski, G., 1995. Geologischer Bau. In: *Geologisches Landesamt Nordrhein-Westfalen* (ed.), *Geologie im Münsterland*, Krefeld, 14-18.
- Ehlers, J., Eissmann, L., Lippstreu, L., Stephan, H.-J., Wansa, S., 2004. Pleistocene glaciations of North Germany. In: Ehlers, J., Gibbard, P.L. (eds.), *Quaternary Glaciations Extent and Chronology. Developments in Quaternary Science 2*, Elsevier, Amsterdam, 135-146.
- Ehlers, J., Grube, A., Stephan, H.J., Wansa, S., 2011. Chapter 13 – Pleistocene Glaciations of North Germany - new results. In: Ehlers, J., Gibbard, P.L., Hughes, P.D. (eds.), *Quaternary Glaciations - Extent and Chronology – A closer look. Developments in Quaternary Science 15*, Elsevier, Amsterdam, 149-162.
- Fehrentz, M., Radtke, U., 1998. Lumineszenzdatierung an pleistozänen Schmelzwassersanden der Senne (östliches Münsterland). *Kölner Geographische Arbeiten* 70, 103-115.
- Fehrentz, M., Radtke, U., 2001. Luminescence dating of Pleistocene outwash sediments of the Senne area (Eastern Münsterland, Germany). *Quaternary Science Reviews* 20, 725-729.
- Galbraith, R.F., Laslett, G., 1993. Statistical models for mixed fission track ages. *Radiation Measurements* 21, 459-470.
- Galbraith, R.F., Roberts, R.G., Laslett, G.M., Yoshida, H., Olley, J.M., 1999. Optical dating of single and multiple grains of quartz from Jinmium rock shelter, Northern Australia: part I, experimental design and statistical models. *Archaeometry* 41, 339-364.
- Godfrey-Smith, D.I., Huntley, D.J., Chen, W.-H., 1988. Optical dating studies of quartz and feldspar sediment extracts. *Quaternary Science Reviews* 7, 373-380.
- Harbort, E., Keilhack, K., 1918. Erläuterungen zu Blatt 4118 Senne. *Geol. Kt. Preußen u. benachb. dt. Länder*, 1:25 000. Berlin.
- Hesemann, J., 1975. *Geologie Nordrhein-Westfalens. Bochumer Geographische Arbeiten, Sonderreihe Band 2*, Paderborn.

- Huntley, J.D., Baril, M.R., 1997. The K content of the K-feldspars being measured in optical dating or in thermoluminescence dating. *Ancient TL* 15, 11-13.
- Huntley, J.D., Lamothe, M. 2001. Ubiquity of anomalous fading in K-feldspars and the measurement and correction for it in optical dating. *Canadian Journal of Earth Sciences* 38, 1093-1106.
- Kaiser, K., Hilgers, A., Schlaak, N., Jankowski, M., Kühn, P., Bussemer, S., Przegiętka, K., 2009. Palaeopedological marker horizons in northern central Europe: characteristics of lateglacial Usselo and Finow soils. *Boreas* 38, 591-609.
- Kasse, C., 1997. Cold-climate aeolian sand-sheet formation in North-Western Europe (c. 14 ± 12.4 ka); a response to permafrost degradation and increased aridity. *Permafrost and Periglacial Processes* 8, 295-311.
- Kasse, C., 2002. Sandy aeolian deposits and environments and their relation to climate during the last glacial maximum and lateglacial in northwest and central Europe. *Progress in Physical Geography* 26, 507-532.
- Kasse, C., Vandenberghe, D., de Corte, F., van den Haute, P., 2007. Late Weichselian fluvio-aeolian sands and coversands of the type locality Grubbenvorst (southern Netherlands): sedimentary environments, climate record and age. *Journal of Quaternary Science* 22, 695-708.
- Klostermann, J., 1992. *Das Quartär der Niederrheinischen Bucht*. Geologisches Landesamt Nordrhein-Westfalen, Krefeld, 200pp.
- Klostermann, J., 1995. Nordrhein-Westfalen. In: Benda, L. (ed.), *Das Quartär von Deutschland*, 59-94.
- Lang, M., Fehrentz, M., 1998. GR-OSL- und IR-OSL-Datierungen an spätpleistozänen und holozänen Dünen sanden der Senne (östliches Münsterland). *Kölner Geographische Arbeiten* 70, 47-58.
- Lenz, A., 2003. *Geologische Karte von Nordrhein-Westfalen 1:25000 - Erläuterungen zu Blatt 4016 Gütersloh*. Krefeld.
- Lotze, F., 1951. Neue Ergebnisse der Quartärgeologie Westfalens V, Zur Stratigraphie des Senne-Diluviums. *Neues Jahrbuch für Geologie und Paläontologie, Monatshefte* 4, 97-102.
- Meinsen, J., Winsemann, J., Weitkamp, A., Landmeyer, N., Lenz, A., Dölling, M., 2011. Middle Pleistocene (Saalian) lake outburst floods in the Münsterland Embayment (NW Germany): impacts and magnitudes. *Quaternary Science Reviews* 30, 2597-2625.

- Murray, A.S., Wintle, A.G., 2000. Luminescence dating of quartz using an improved single-aliquot regenerative-dose protocol. *Radiation Measurements* 32, 57-73.
- Murray, A.S., Wintle, A.G., 2003. The single aliquot regenerative dose protocol potential form improvements in reliability. *Radiation Measurements* 37, 377-381.
- Prescott, J.R., Hutton, J.T., 1994. Cosmic ray contribution to dose rates for luminescence and ESR dating: large depths and long-term time variations. *Radiation Measurements* 23, 497-500.
- Preusser, F., Degering, D., Fuchs, M., Hilgers, A., Kadereit, A., Klasen, N., Krbetschek, M., Richter, D., Spencer, J.Q.L., 2008. Luminescence dating: basics, methods and application. *E&G Quaternary Science Journal* 57, 95-149.
- Seraphim, E.Th., 1973. Drumlins des Drenthe-Stadiums am Nordostrand der Westfälischen Bucht. *Osnabücker Naturwissenschaftliche Mitteilunge* 2, 41-87.
- Seraphim, E.Th., 1979a. Der sog. Senne-Sander, eine Kame-Terrasse - Drenthestadiale Grundmoräne und post-moränale Schmelzwasser-Sedimente der Oberen Senne. *Berichte der Naturwissenschaftliche Vereinigung Bielefeld* 24, 319-344.
- Seraphim, E.Th., 1979b. Zur Inlandvereisung der Westfälischen Bucht im Saale- (Rib) Glazial. *Münstersche Forschungen zur Geologie und Paläontologie* 47, 1-51.
- Skupin, K., 1985. Eiszeitliche Halte am Osning. In: *Geologisches Landesamt Nordrhein-Westfalen* (ed.), *Geologische Karte von Nordrhein-Westfalen 1:100.000. Erläuterungen zu Blatt C 4318, Paderborn, Krefeld.*
- Skupin, K., 1994. Aufbau, Zusammensetzung und Alter der Flugsand- und Dünenbildungen im Bereich der Senne (Östliches Münsterland). *Geologie und Paläontologie Westfalens* 28, 41-72.
- Skupin, K., 2002. *Geologische Karte von Nordrhein-Westfalen 1:100000. Erläuterungen zu Blatt C4314 Gütersloh. Krefeld.*
- Skupin, K., Speetzen, E., Zandstra, J.G., 1993. Die Eiszeit in Nordwestdeutschland. Zur Vereisung der Westfälischen Bucht und angrenzender Gebiete. *Geologisches Landesamt Nordrhein-Westfalen, Krefeld, 143pp.*
- Tabachnick, B.G., Fidell, L.S., 1996. *Using Multivariate Statistics, 3rd edition, Harper collins, New York.*

- Thiel, C., Buylaert, J.-P., Murray, A.S., Terhorst, B., Hofer, I., Tsukamoto, S., Frechen, M., 2011. Luminescence dating of the Stratzing loess profile (Austria) - testing the potential of an elevated temperature post-IR IRSL protocol. *Quaternary International* 234, 23-31.
- Vandenbergh, D., Vanneste, K., Verbeeck, K., Paulissen, E., Buylaert, J.-P., de Corte, F., van den Haute, P., 2009. LateWeichselian and Holocene earthquake events along the Geleen found in NE Belgium: OSL age constraints. *Quaternary International* 199, 56-74.
- Winsemann, J., Brandes, C., Polom, U., Weber, C., 2011. Depositional architecture and palaeogeographic significance of Middle Pleistocene glaciolacustrine ice marginal deposits in northwestern Germany: a synoptic overview. *E&G Quaternary Science Journal* 60, 212-235.
- Zieliński, P., Sokołowski, R.J., Fedorowicz, S., Jankowski, M., 2011. Stratigraphic position of fluvial and aeolian deposits in the Żabinko site (W Poland) based on TL dating. *Geochronometria* 38, 64-71.

Online supplementary data to publication 1

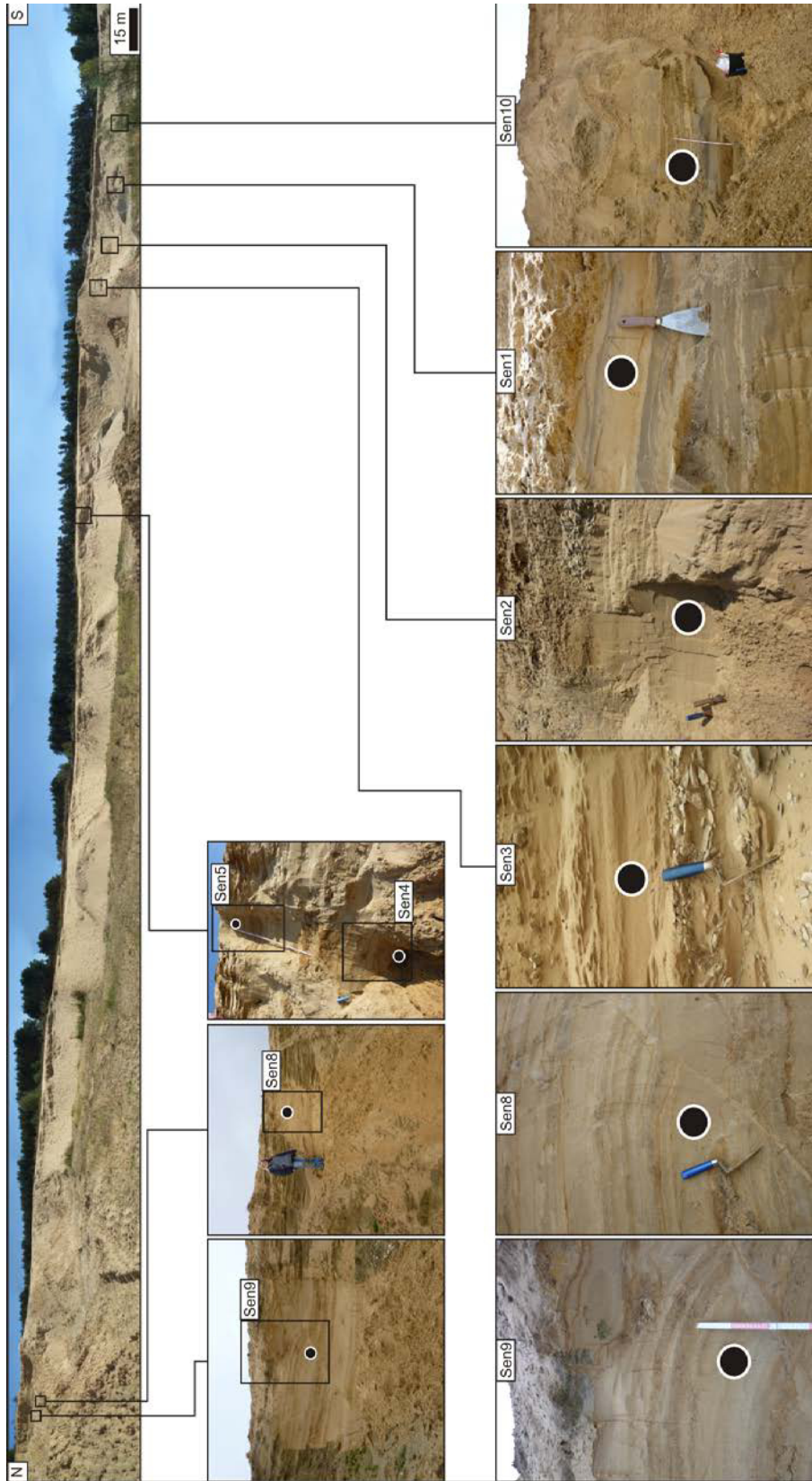


Fig. S1: Photo panel of the Oerlinghausen sand pit with locations of OSL samples. Length of the panel is about 250 m. Note: Dimensions may be distorted due to panorama view.

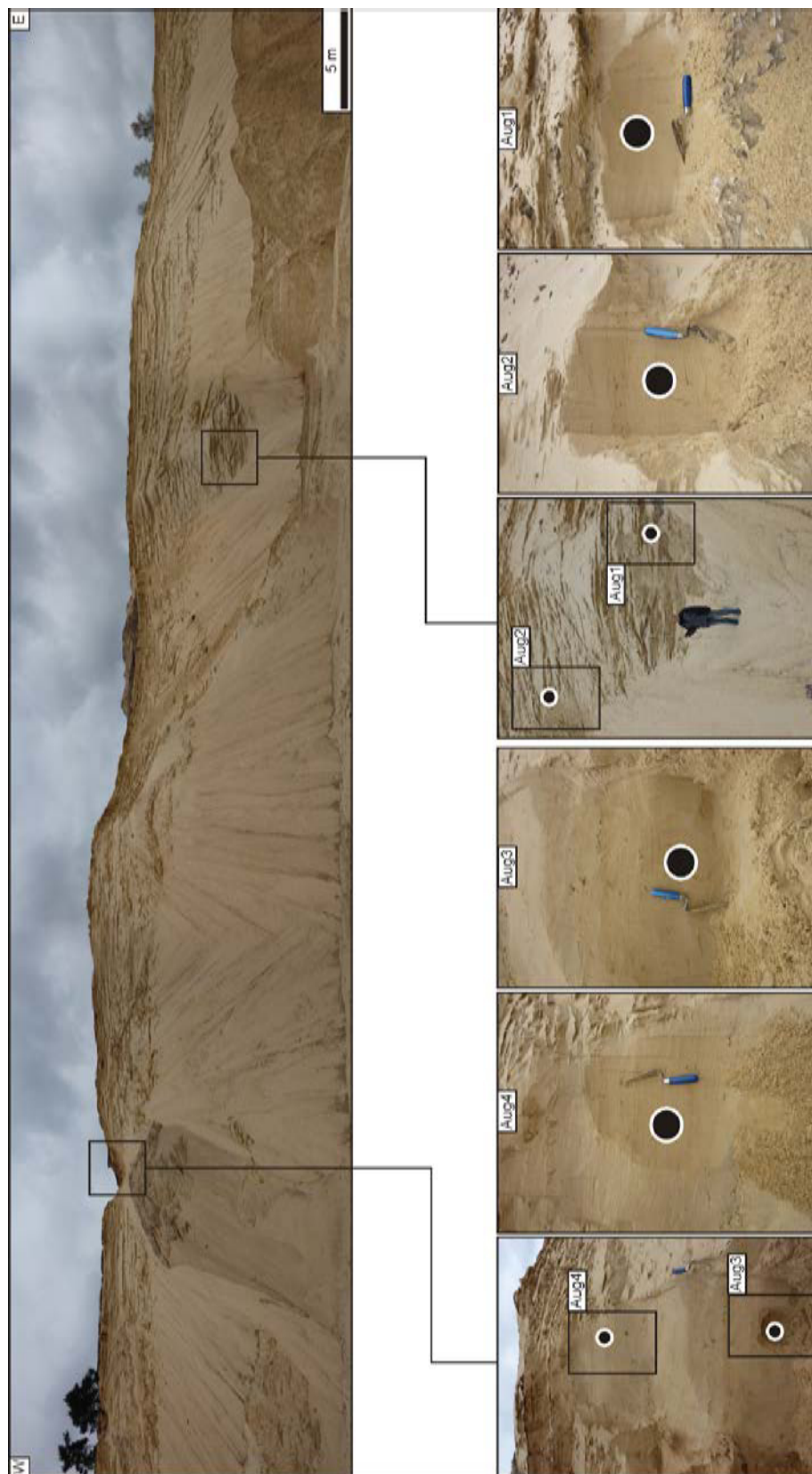


Fig. S2: Photo panel of the Augustdorf sand pit with locations of OSL samples. Length of the panel is about 50 m. Note: Dimensions may be distorted due to panorama view.

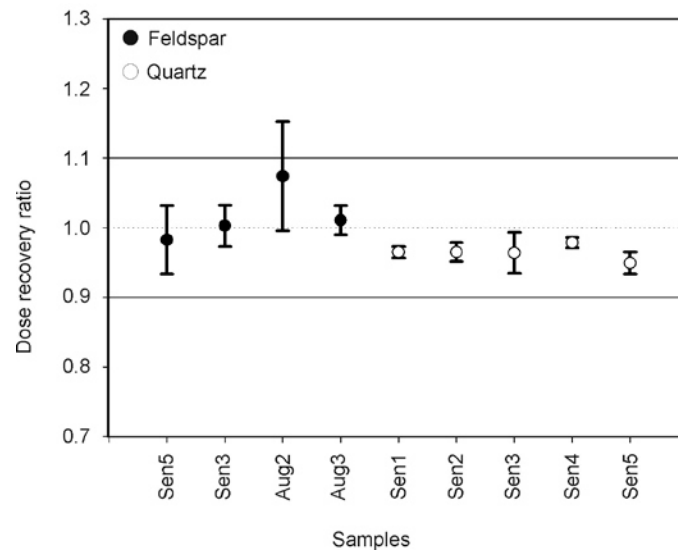


Fig. S3: Dose recovery ratios of selected feldspar and quartz samples.

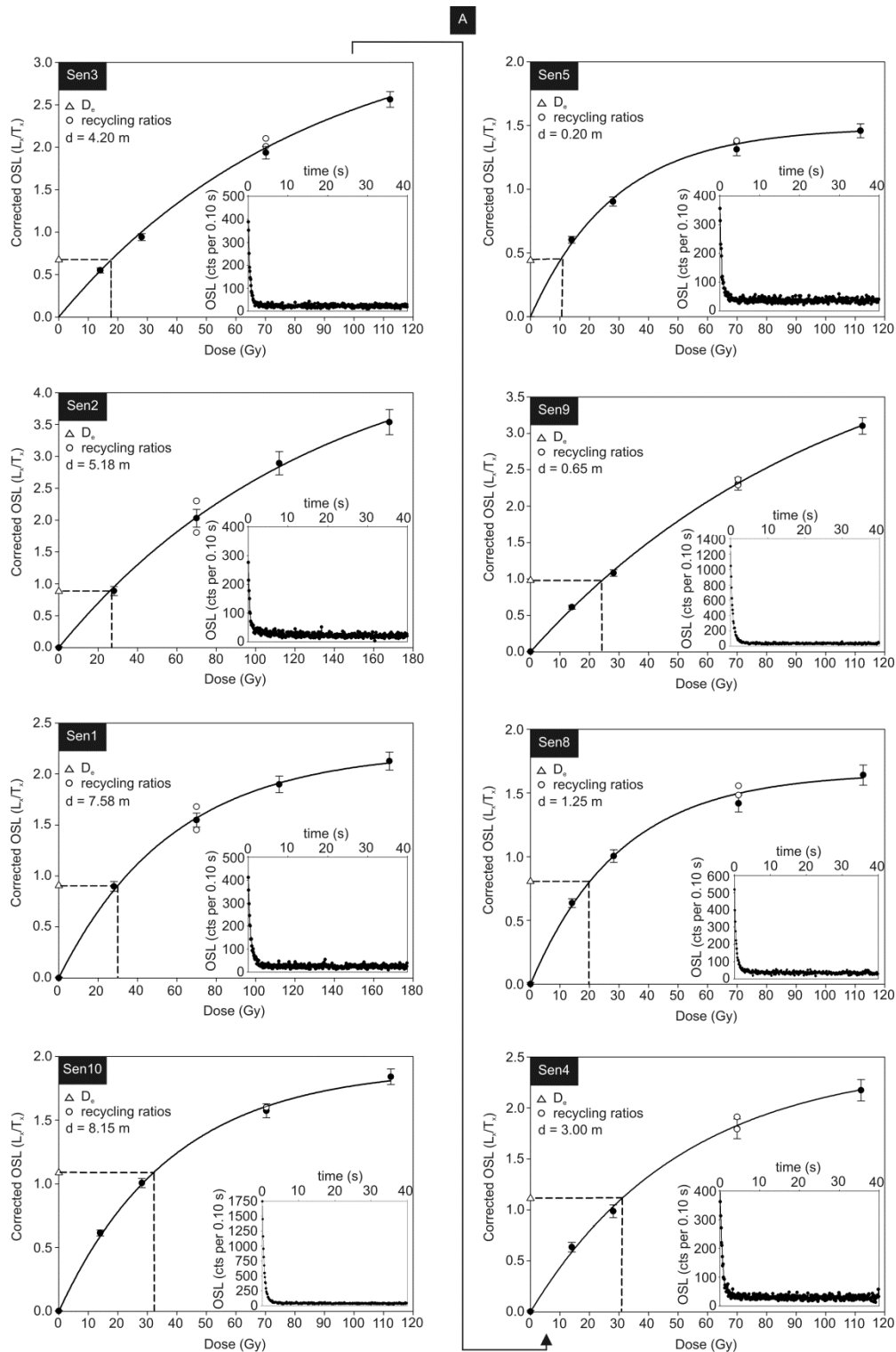


Fig. S4: (A) Dose response and decay curve for the Oerlinghausen samples in order of depth (d) (continued on the next page).

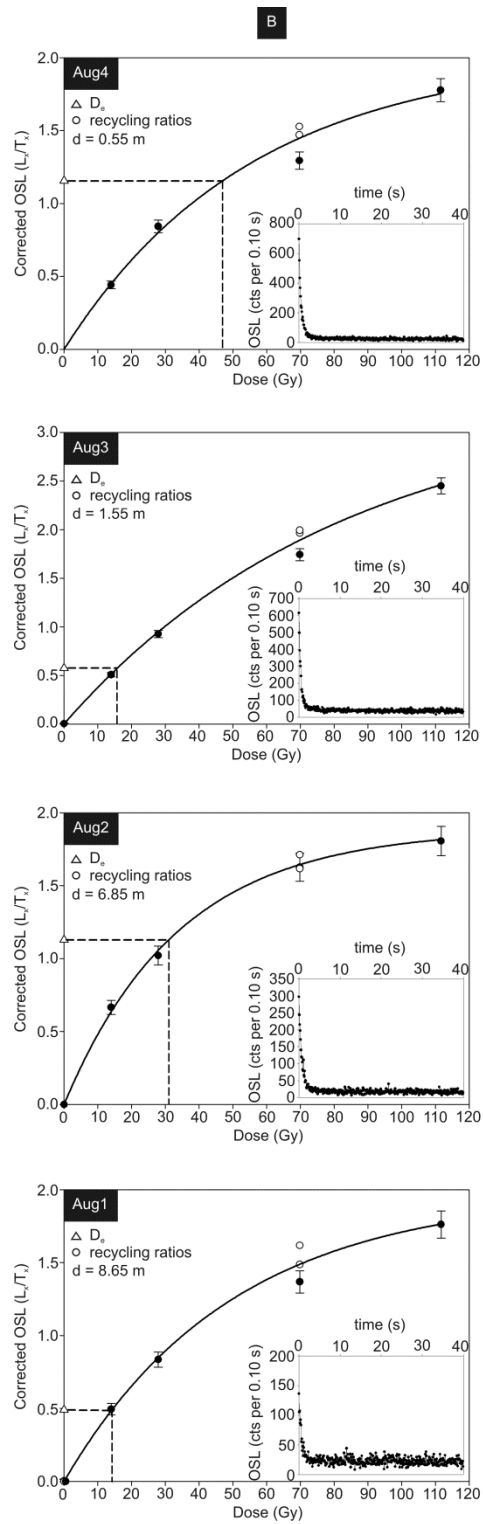


Fig. S4: (B) Dose response and decay curve for the Augustdorf samples in order of depth (d).

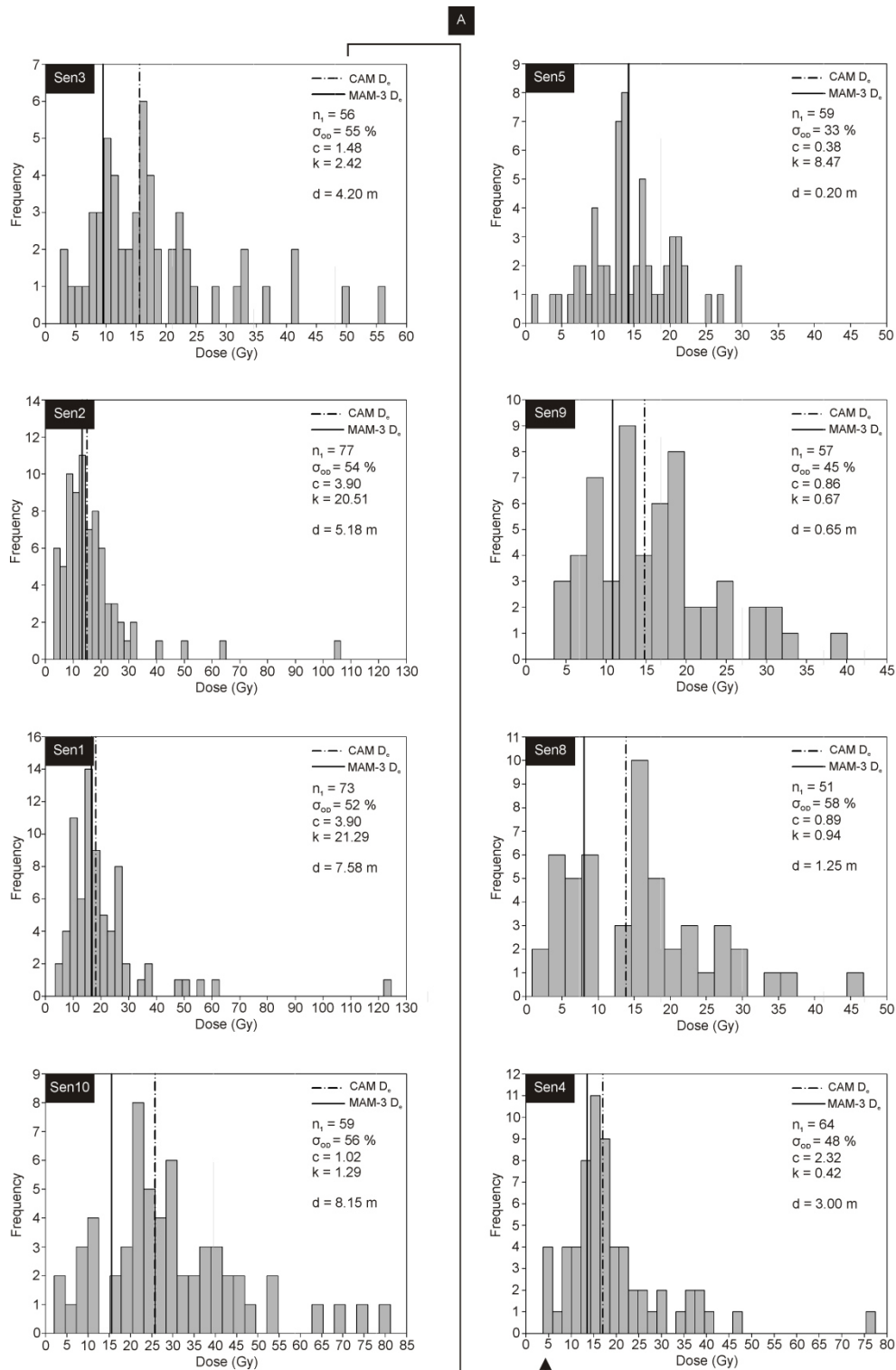


Fig. S5: (A) D_e histograms of the Oerlinghausen samples in order of depth (d) including CAM D_e and MAM-3 D_e values. n_1 = number of accepted aliquots, σ_{OD} = overdispersion, c = skewness, k = kurtosis (continued on the next page).

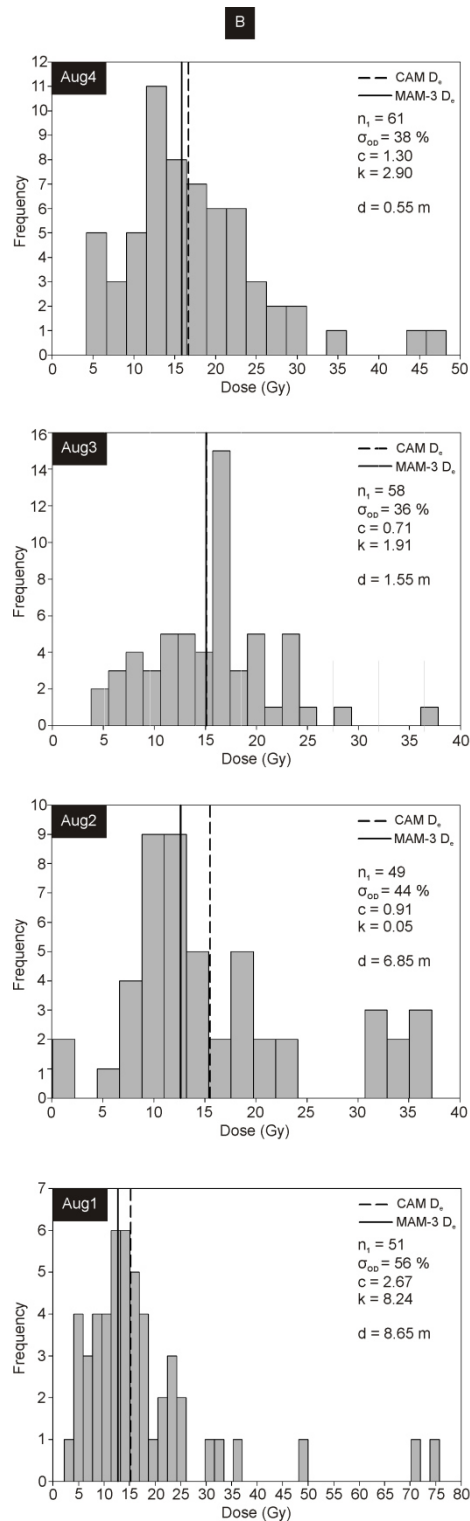


Fig. S5: (B) D_e histograms of the Augustdorf samples in order of depth (d) including CAM D_e and MAM-3 D_e values. n_1 = number of accepted aliquots, σ_{OD} = overdispersion, c = skewness, k = kurtosis.

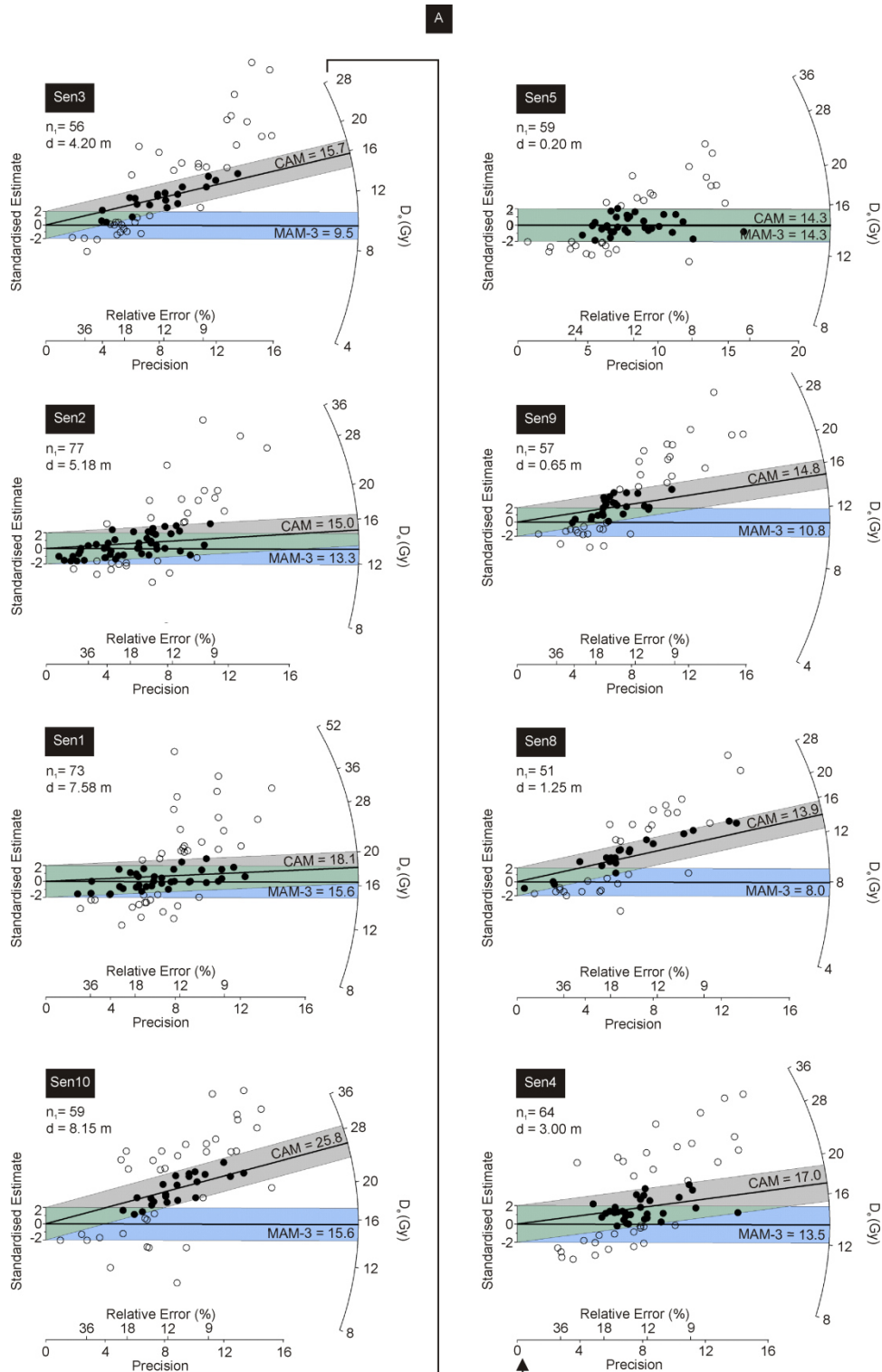


Fig. S6: (A) Radial plots of the Oerlinghausen samples in order of depth (d). CAM D_e values and their 2σ uncertainty are grey, MAM-3 D_e values and their 2σ uncertainty are blue. n_1 = number of accepted aliquots (continued on the next page).

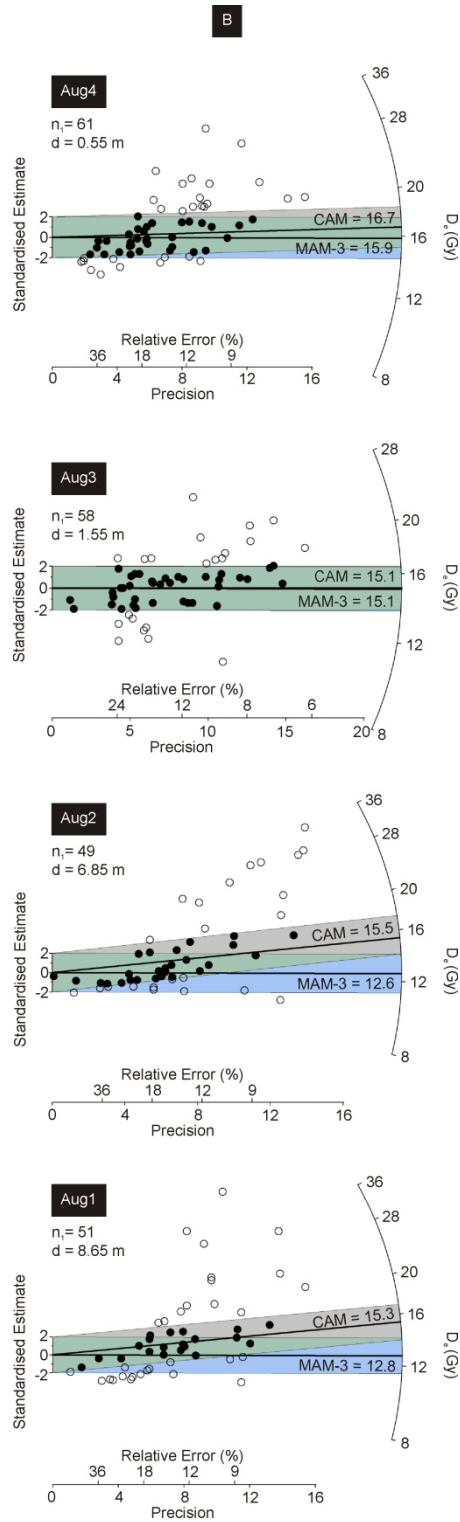


Fig. S6: (B) Radial plots of the Augustdorf samples in order of depth (d). CAM D_e values and their 2σ uncertainty are grey, MAM-3 D_e values and their 2σ uncertainty are blue. n_1 = number of accepted aliquots.

Chapter 3

Publication 2

This chapter has been published as *Roskosch et al., 2015* in *Boreas*, 44, 103-126,

DOI: 10.1111/bor.1208 and can be found at:

<http://onlinelibrary.wiley.com/doi/10.1111/bor.12083/abstract>

Luminescence dating of ice-marginal deposits in northern Germany: evidence for glaciations during the Middle Pleistocene (MIS 12 to MIS 6)

Julia Roskosch¹, Jutta Winsemann¹, Ulrich Polom², Christian Brandes¹,
Sumiko Tsukamoto², Axel Weitkamp¹, Werner A. Bartholomäus¹,
Dierk Henningsen¹, Manfred Frechen²

- 1) Institut für Geologie, Leibniz Universität Hannover, Callinstraße 30, D-30167 Hannover, Germany
- 2) Leibniz Institute for Applied Geophysics (LIAG), Geochronology and Isotope Hydrology, Stilleweg 2, D-30655 Hannover, Germany

Abstract

The exact number, extent and chronology of the Middle Pleistocene Elsterian and Saalian glaciations in northern Central Europe are still controversial. This study presents new luminescence data from Middle Pleistocene ice-marginal deposits in northern Germany, giving evidence for repeated glaciations during the Middle Pleistocene (MIS 12 to MIS 6). The study area is located in the Leine valley south of the North German Lowlands. The data set includes digital elevation models, high-resolution shear wave seismic profiles, outcrop and borehole data integrated into a 3D subsurface model to reconstruct the bedrock relief surface. For numerical age determination, we performed luminescence dating on 12 ice-marginal and two fluvial samples. Luminescence ages of ice-marginal deposits point to at least two ice advances during MIS 12 and MIS 10 with ages ranging from 461 ± 34 to 421 ± 25 ka and from 376 ± 27

to 337 ± 21 ka. The bedrock relief model and different generations of striations indicate that the older ice advance came from the north and the younger one from the northeast. During rapid ice-margin retreat, subglacial overdeepenings were filled with glacialacustrine deposits, partly rich in re-worked Tertiary lignite and amber. During MIS 8 and MIS 6, the study area may have been affected by two ice advances. Luminescence ages of glacialacustrine delta deposits point to a deposition during MIS 8 or early MIS 6, and late MIS 6 (250 ± 20 to 161 ± 10 ka). The maximum extent of both the Elsterian (MIS 12 and MIS 10) and Saalian glaciations (MIS 8? and MIS 6) approximately reached the same position in the Leine valley and was probably controlled by the formation of deep proglacial lakes in front of the ice sheets, preventing a further southward advance.

3.1 Introduction

Considerable uncertainty still exists regarding the exact timing and number of Middle Pleistocene glacial advances into northern Central Europe. The most complete glaciation record is preserved in the North Sea Basin where continuous subsidence created accommodation space for Pleistocene glacial and interglacial sediments (Stewart and Lonergan, 2011). Since 2000, numerous seismic studies have been carried out in the North Sea area, providing evidence for seven glaciations during the Middle and Late Pleistocene (Huuse and Lykke-Andersen, 2000; Sejrup et al., 2005; Lutz et al., 2009; Stewart and Lonergan, 2011). However, the age control is poor and age estimations are mainly based on a correlation with borehole data from the Bay of Biscay (Toucanne et al., 2009b).

The oldest glaciation probably occurred during Marine Isotope Stage (MIS) 12, which is in accordance with data from the Bay of Biscay, from where a first significant clastic pulse is recorded (Toucanne et al., 2009b). The coalescence of the Fennoscandian and British ice sheets in the North Sea Basin favoured a re-direction of the Central European drainage system, a higher meltwater discharge and an increased clastic input into the English Channel and Bay of Biscay (Toucanne et al., 2009a, b). Further glaciations, mainly indicated by the formation of tunnel valleys, are attributed to ice advances during MIS 10, MIS 8, MIS 6, MIS 4 and MIS 2 (Stewart and Lonergan, 2011).

Three major glaciations have been reconstructed from the terrestrial record of northern Central Europe (Ehlers et al., 2011; Houmark-Nielsen, 2011; Marks, 2011), referred to as Elsterian, Saalian and Weichselian glaciations (**Fig. 1A**). Data from Great Britain (Gibbard and Clark, 2011; Lee et al., 2011), Denmark (Houmark-Nielsen, 2011), the Netherlands (Laban and

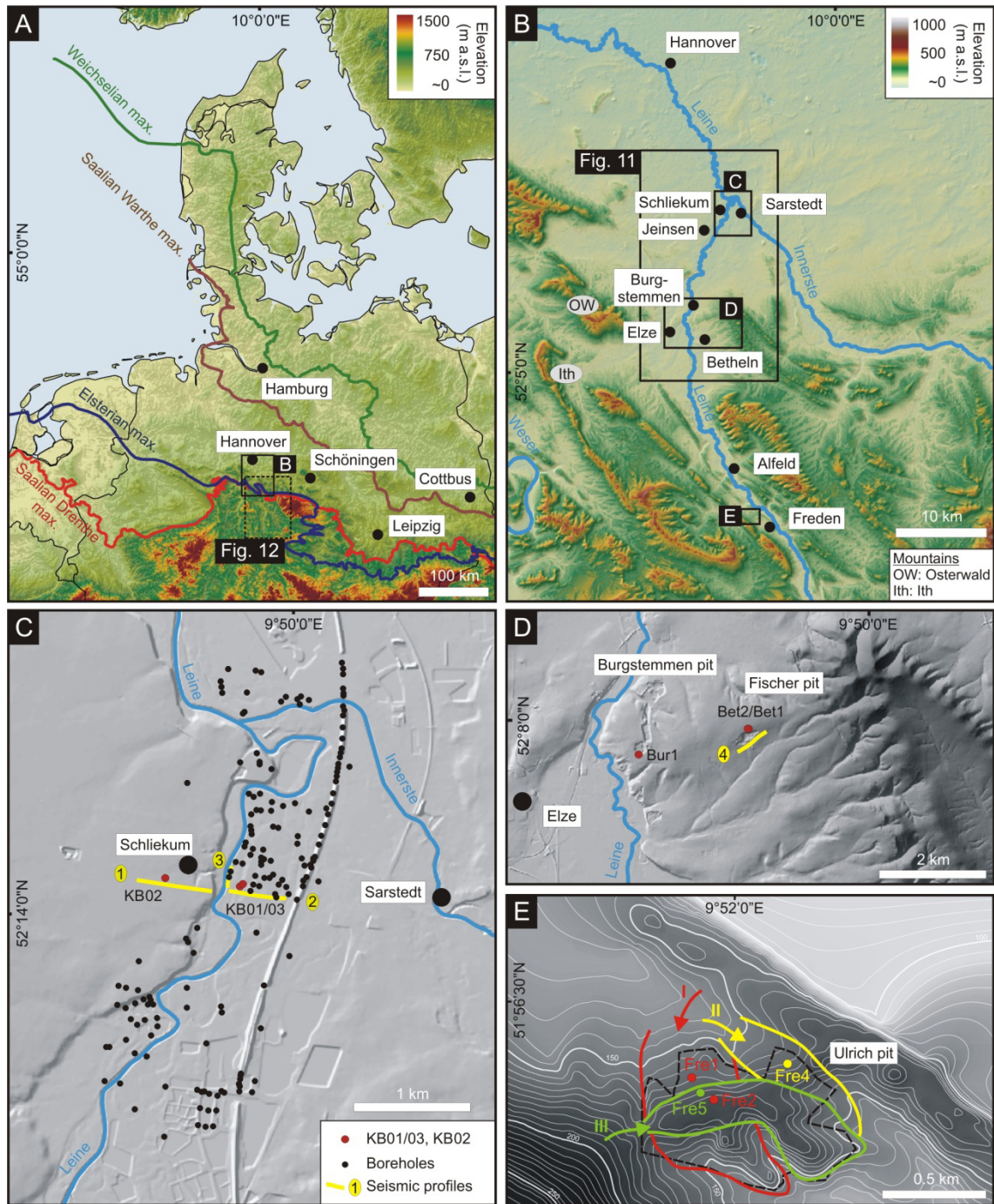


Fig. 1: (A) Hill-shaded relief model (SRTM data) of northern Central Europe, showing the maximum extent of Pleistocene ice sheets (modified after Ehlers et al., 2011). (B) Close-up view of the study area. Black boxes refer to close-ups of the studied areas (C, D, E) and the bedrock relief model (Fig. 11). (C) Hill-shaded relief model of the Schliekum/Sarstedt area with location of boreholes and seismic profiles. For sedimentary logs see Figs 8 and 9. The hill-shaded relief model is based on data from the Landesvermessung und Geobasisinformation Niedersachsen LGLN. (D) Hill-shaded relief model of the Betheln delta with location of the seismic profile and luminescence samples. The hill-shaded relief model is based on data from the Landesvermessung und Geobasisinformation Niedersachsen LGLN. (E) Hill-shaded relief model of the Freden ice-marginal complex, showing different sediment bodies with palaeocurrent directions and location of luminescence samples. The hill-shaded relief model is reconstructed from old topographic maps (1901/1937).

van der Meer, 2011) and Poland (Marks, 2011) indicate that the Elsterian glaciation occurred during MIS 12 (**Fig. 2**), whereas data from northern Germany point to this glaciation during MIS 10 (Geyh and Müller, 2005; Litt et al., 2007). The correlation with Marine Isotope Stages was mostly performed on the basis of overlying interglacial sediments and only very few absolute ages of glacial deposits exist (Pawley et al., 2008).

The number of MIS 12 and MIS 10 ice advances is somewhat unclear and varies from one in Poland and Great Britain (Gibbard and Clark, 2011; Marks, 2011), two in the North Sea area (Cohen and Gibbard, 2010; Gibbard and Clark, 2011; Houmark-Nielsen, 2011; Marks, 2011; Stewart and Lonergan, 2011) to up to three in Denmark (Houmark-Nielsen, 2011) and northern Germany (Caspers et al., 1995; Eissmann, 2002; Litt et al., 2007; Ehlers et al., 2011; Stephan, 2014). The ice advances occurred from the north and/or northeast (Caspers et al., 1995; Eissmann, 2002; Litt et al., 2007; Gibbard and Clark, 2011; Houmark-Nielsen, 2011; Laban and van der Meer, 2011; Stewart and Lonergan, 2011; Stephan, 2014), indicated by the clast composition of tills and the orientation of the subglacial tunnel valleys.

Well-preserved Holsteinian interglacial deposits in northern Central Europe are mainly found in tunnel valleys or overdeepened glacial basins that acted as depocentres and kept the fine-grained interglacial deposits from erosion (Eissmann, 2002; Lang et al., 2012). New U/Th dating proves a MIS 9 age for Holsteinian deposits in northern Germany (Geyh and Müller, 2005; Frechen et al., 2007; Sierralta et al., 2011; Urban et al., 2011).

In a few sites in the Netherlands, Denmark and Poland, glacial deposits occur that might indicate a glaciation during MIS 8. During this time, the North Sea Basin was most likely occupied by an extensive ice sheet (Beets et al., 2005; Hall and Migoń, 2010; Houmark-Nielsen, 2011; Laban and van der Meer, 2011; Marks, 2011; Kars et al., 2012). In contrast, infrared radiofluorescence ages of fluvial deposits in eastern Germany range from 306 ± 23 ka to 149 ± 8 ka, pointing to a long period without glaciations during MIS 9 to early MIS 6 (Krbetschek et al., 2008).

Sediments of the MIS 6 Drenthe and Warthe glaciation are widespread in northern Central Europe and well dated (Wallinga et al., 2004; Busschers et al., 2005, 2008; Houmark-Nielsen, 2011; Kars et al., 2012). These two ice advances probably occurred during a short time span of approximately 20 000 years at the end of MIS 6 (155 to 135 ka) (Litt et al., 2007; Busschers et al., 2008; Krbetschek et al., 2008), although luminescence ages cluster at around ~ 250 ka, ~ 190 ka and ~ 155 ka (Fehrentz and Radtke, 1998; Preusser, 1999; Wallinga et al., 2004; Lüthgens et al., 2011; Kars et al., 2012).

In total, three Saalian ice advances have been mapped in northern Germany. The glaciers advanced from the north and northeast and the southernmost advance is linked to the older Saalian Drenthe glaciation (Caspers et al., 1995; Eissmann, 2002; Litt et al., 2007; Ehlers et al., 2011). In this study, we provide new luminescence ages of Middle Pleistocene ice-marginal deposits of the Leine-valley fill south of the North German Lowlands. The data set, including digital elevation models, outcrop data, borehole data, and high-resolution shear wave seismic profiles, allows for a reconstruction of the stratigraphic valley-fill architecture, which will contribute to a better understanding of the glaciation history of northern Central Europe.

Marine isotopic stages and British Isles (Cohen and Gibbard, 2010)		Northwest Europe (Cohen and Gibbard, 2010)		Northern Germany (Litt et al., 2007)		(this study)	
MIS 1	Holocene	Holocene		Holocene			
MIS 2-4	Late Pleistocene	Devensian	Weichselian	Weichselian			
MIS 5		Ipswichian	Eemian	Eemian			
MIS 6	Middle Pleistocene	Wolostonian	Saalian	Warthe Drenthe	Saalian-Complex	Warthe Drenthe	ice advance
MIS 7						Dömnitz	
MIS 8						Fuhne	ice advance?
MIS 9				Wacken/Dömnitz	Holsteinian		
MIS 10				Fuhne	Elsterian		ice advance
MIS 11				Hoxnian	Holsteinian		Cromerian-Complex
MIS 12	Anglian	Elsterian			2 ice advances?		

Fig. 2: Chronostratigraphy of the Pleistocene in northern Central Europe.

3.2 Regional setting and previous research

The study area is located in the Leine valley between Hannover and Freden, south of the North German Lowlands (**Fig. 1A, B**). The valley is flanked by several up to 450 m high mountain ridges, built-up by Mesozoic sedimentary rocks. The north-south trending structure of the Leine valley was recently investigated by Vollbrecht and Tanner (2011). It partly belongs to a larger graben system (Leinetal Graben), which initially formed in the Late Cretaceous to Early Cenozoic as a response to north-south compression, causing east-west extension. Significant tectonic movements continued until the Pliocene and strike-slip movements, caused by the northwest-southeast directed alpine compression, led to the formation of several small pull-apart basins, which provided local accommodation space for Pleistocene deposits.

Since the beginning of the 20th century, numerous studies have been carried out in the Leine valley area to reconstruct the former ice-margins and map economically important ice-marginal and fluvial deposits. More detailed studies were based on landform and provenance analysis of Pleistocene fluvial and ice-marginal deposits (Rausch, 1977; Rohde 1983, 1994; Kaltwang, 1992). Based on these previous studies, the Leine valley was probably overridden by both the Middle Pleistocene Elsterian and Saalian ice sheets (**Fig. 1A**). The Saalian Warthe and Weichselian ice sheets did not reach the study area and were located approximately 100 and 150 km further towards the northeast, respectively (**Fig. 1A**; Caspers et al., 1995; Ehlers et al., 2011).

The southernmost occurrence of ice-marginal deposits in the Leine valley is recorded from Freden (**Fig. 1B**), which has been related to the ice front position of the Saalian Drenthe ice sheet. During both Middle Pleistocene glaciations, glacial lakes were dammed in the Leine valley and its tributaries due to the northward blockage of drainage pathways. Mapped glacial-lacustrine sediments consist of up to 50 m thick fine-grained lake bottom sediments and up to 60 m thick coarse-grained ice-marginal deposits, which have been used as water-surface indicators (Winsemann et al., 2007, 2011b).

3.3 Methodology

3.3.1 Sedimentology

Three sand and gravel pits and 1730 borehole logs were used to analyse the Leine-valley fill deposits. Additionally, three new cores (KB01, KB02, KB03) were acquired near Schliekum (**Fig. 1C**). Fourteen samples were taken from these cores and from outcrops for luminescence dating (**Fig. 1C, D, E**; **Table S1**). Outcrops and cores were measured at the scale of individual beds, documenting grain size, bed thickness, bed contacts, bed geometries, and internal sedimentary structures. In outcrop sections, palaeoflow directions were determined from clast imbrications and planar cross-stratification.

3.3.2 Provenance analysis

For heavy mineral analysis, transparent heavy minerals with a density greater than 2.70 g cm⁻³ were taken. A total of 250-300 grains were counted per mount under an optical microscope (Henningsen, 1983). In two cases (KB02_373-385, KB02_1060-1074), only 180 grains could be counted because of the scarcity of transparent heavy minerals. Minerals were divided into two groups regarding their provenance: (i) Scandinavian/Baltic provenance, represented mainly by garnet and mostly green-coloured hornblende, as well as minerals of the epidote group

and kyanite; and (ii) a southern provenance of the catchment area of the River Leine and Weser, characterised especially by augite, orthopyroxene, and basaltic hornblende, in the second place also by tourmaline, zircon and apatite (Henningesen, 1983).

For clast composition analysis of the cores, at least 300 pebble-sized gravel clasts (6.3 to >20 mm) were counted per sample. Clasts were divided into three groups regarding their provenance: (i) Scandinavian/Baltic provenance, represented mainly by crystalline rocks (gneiss, granite), quartzite and flint; (ii) clasts derived from the adjacent Mesozoic bedrock and river catchments, mainly characterised by Triassic and Cretaceous sandstone, limestone (Muschelkalk and Plänerkalk), and marlstones (Flammenmergel); and (iii) clasts derived from the Palaeozoic bedrock of the river catchments, represented mainly by lydite and greywacke (Rausch, 1977; Rohde, 1983; Lepper, 1984).

3.3.3 Shear wave seismic profiles

Three shear wave seismic reflection profiles were acquired and analysed in order to determine the larger-scale architecture of the Leine-valley fill near Schliekum/Sarstedt. Seismic lines 1 and 2 trend approximately west-east and are 643 and 500 m long, respectively. Seismic line 3 runs north-south perpendicular to seismic line 1 and is 185 m long. Lithological control is provided by the newly acquired cores (KB01, KB02, KB03) and older borehole logs (**Fig. 1C**). For the seismic survey, we combined a shear wave land streamer consisting of 120 transverse horizontal (SH) geophones (10 Hz resonant frequency) in 1-m intervals with a small, electrodynamic-driven SH shaker source system mounted on a wheel barrow unit (Polom, 2006), operating in transverse horizontal (SH) mode (**Table S2**). Maximum target depth was 70 m. The seismic SH body wave type was used because it achieves up to 10 times higher resolution than P-wave seismic, resulting in a vertical resolution of ~0.5 m and a lateral resolution starting at 0.5 m near the surface, decreasing to ~12 m at 50 m depth (Polom et al., 2013). The shear wave vibroseis method (Crawford et al., 1960; Ghose et al., 1996) was utilised with a 20-160 Hz linear increasing sinusoidal sweep of 10 s duration as seismic source signal.

Seismic data processing focussed on shear wave velocity analysis after pre-processing of the raw data. Elevation static corrections have been applied relative to the highest peaks of the profiles. Post stack Finite Difference (FD) migration using a maximum dip aperture of 70 degrees was applied in the time domain to reduce diffraction effects of point and edge scattering above basement reflections and for true dip imaging. Time-to-depth conversion by a carefully smoothed velocity field derived from stacking velocities has been undertaken. Further information on seismic acquisition parameters are summarised in **Table S2**.

The seismic profiles were described using the scheme of Mitchum et al. (1977). The seismic attributes amplitude and continuity were used for the analysis of the reflector patterns. In the standard seismic interpretation workflow, the seismic facies types are grouped into packages, referred to as seismic-stratigraphic units, bounded by seismic reflectors (Brown and Fischer, 1977; Posamentier and Vail, 1988).

3.3.4 3D subsurface modeling (GOCAD®)

To reconstruct the Mesozoic bedrock relief and the thickness and spatial distribution of the Pleistocene deposits, the 3D subsurface modeling software GOCAD® was used. The bedrock relief model is based on 1730 borehole logs. It is 25 km long and 15 km wide, covering an area of 375 km². For borehole log interpretation, the software GeODin was used, allowing the rapid display of logs and cross-sections. The high-resolution digital elevation model (DEM 5) was integrated as reference surface. The geological input data were then integrated into GOCAD to reconstruct the bedrock relief surface and the thickness and spatial distribution of the overlying Pleistocene deposits. Subsequently, the modelled surfaces were used to create maps.

3.3.5 Luminescence dating

For numerical age determination, we performed luminescence dating using coarse-grained feldspar and quartz minerals from 12 ice-marginal and two fluvial samples. Outcrop samples were taken using opaque metal tubes with a length of 11 cm and a diameter of 10 cm. Tubes were hammered into the freshly cleaned sediment face and sealed with aluminium foil. Cores were collected in opaque PVC liners with a diameter of 10 cm. The opaque liner was subsequently split lengthwise using an electric saw and a stainless steel plate was hammered into the core to divide it into halves. One half was immediately packed in opaque black plastic bags to avoid exposure to light. Sampling for luminescence dating was carried out under subdued red light in the luminescence laboratory. The outer ends of cores as well as the upper parts of the core halves were discarded to avoid sampling material possibly exposed to light.

3.3.5.1 Laboratory procedures and analytical equipment

From outcrops and undisturbed cores, 350-750 grams of sand were taken. Pure monomineralic coarse-grained (100-200 µm) quartz and potassium-rich feldspar minerals were prepared using a procedure of drying at $\leq 50^{\circ}\text{C}$, sieving and a subsequent chemical treatment with hydrochloric acid, disodium oxalate and hydrogen peroxide. In order to separate potassium-rich feldspar and quartz minerals, density separations were carried out. Quartz minerals were addition-

ally etched with hydrofluoric acid to avoid contribution of the alpha-irradiated outer part of the mineral and to remove feldspar contamination. Aliquots with 2.5 mm diameter were mounted on 9.8 mm stainless steel discs using silicone spray as an adhesive.

Both feldspar and quartz luminescence signals were measured with three automated Risø TL/OSL readers (DA-20) with calibrated $^{90}\text{Sr}/^{90}\text{Y}$ beta sources ($1.48 \text{ GBq} = 40 \text{ mCi}$), delivering between 0.11 and 0.14 Gy s^{-1} . Feldspar signal was stimulated by pulsing by infrared (IR) light emitting diodes (LED) at 870 nm. The feldspar luminescence signal was detected during the off-periods of each pulse cycle in the blue-violet region (320–460 nm) with a Schott BG39/Corning 7-59 filter combination. Stimulation of the quartz signal was performed with blue LED, emitting at 470 nm. The quartz luminescence signal was detected through a Hoya U-340 filter, transmitting in the ultra violet region (280–380 nm). Measurements were carried out in 2012 at the Leibniz Institute for Applied Geophysics (Hannover, Germany).

3.3.5.2 Dose rate determination

After drying at $\leq 50^\circ\text{C}$, either 50 or 700 g of the homogenised samples were filled in plastic containers. To assure equilibrium between radon and its daughter nuclides, beakers were sealed and stored for at least six weeks before measurement. Concentrations of uranium, thorium and potassium were obtained using high-resolution gamma spectrometry. Dose rates were then calculated using conversion factors of Adamiec and Aitken (1998). The water content for all samples was measured and set to an average value close to the measured one. Dosimetry results and dose rates are documented in **Table 1**.

3.3.5.3 Equivalent dose D_e determination

Feldspar D_e values were determined using a pulsed infrared stimulated luminescence (IRSL) single aliquot regenerative (SAR) dose protocol. IR stimulation was carried out at 50°C for 400 s with 50 μs on-time and 200 μs off-time, and only off-time signal was recorded to obtain a stable luminescence signal (Tsukamoto et al., 2006; **Table S3A**). Pulsed IRSL signal measured at 50°C (IR_{50}) was used to reduce anomalous fading from feldspar (see Fading tests and Luminescence characteristics) because this signal is much more light-sensitive than more commonly used elevated temperature post-IR IRSL (pIRIR) signal (Thiel et al., 2011; Buylaert et al., 2012). It is therefore more suitable for dating glacial sediments. Nonetheless, we also tested an elevated temperature pIRIR protocol after Thiel et al. (2011) using a preheat at 320°C for 60 s, IR stimulation at 50°C for 100 s, and a post-IR stimulation at 290°C for 200 s (pIRIR₂₉₀). pIRIR₂₉₀ results were then compared to pulsed IR_{50} results. D_e values of the pIRIR₂₉₀

signal were about 100-150 Gy higher than those of the pulsed IR₅₀ signal (**Fig. 3A, B**). However, some agreement does exist regarding the lower doses of both signals as the mean D_e value of the pulsed IR₅₀ signal (734 Gy) corresponds with the 'leading edge' of the pIRIR₂₉₀ (721-750 Gy; **Fig. 3B**). This is probably because some grains measured by pIRIR₂₉₀ were not well bleached prior to deposition and yielded higher D_e values, but well bleached grains gave the same D_e values by both method. We used the pulsed IR₅₀ signal for D_e and age determination because this signal is faster to bleach than the pIRIR₂₉₀ signal. For quartz measurements, a double SAR protocol was used (Murray and Wintle, 2000, 2003; **Table S3B**).

At least 10 aliquots per sample were measured, and only aliquots passing the following criteria were used: recycling ratio limit within 10% of unity; maximal test dose error 10%; signal intensity larger than 3 sigma above background. Dose response curves were fitted with a saturating exponential function to calculate D_e values. Measurement error of 2.0% was assumed. For feldspar samples, after subtracting a late background of the last 50 s, the middle part of the decay curve (21-60 s) was used, which showed negligible anomalous fading when compared to the initial parts (0-10 s and 11-20 s, respectively) of the decay curve (**Fig. 3C**) (see Luminescence characteristics). For quartz samples, the initial 0.5 s of the signal were used after subtracting an early background of 0.7-4.0 s (Cunningham and Wallinga, 2010).

3.3.5.4 Dose recovery and recycling ratio tests

Dose recovery tests were conducted to check the suitability of the SAR protocol towards our samples under laboratory conditions. Initially, minerals were bleached for 4 h by a solar simulator. A dose close to the expected natural one was given and the same SAR protocol was applied to check if the given dose could be accurately recovered. The SAR protocol is considered to be suitable when dose recovery ratios are within 1-sigma standard error of unity (0.9-1.1; Wintle and Murray, 2006).

However, dose recovery ratios were too low, with values of 0.76 ± 0.01 (Fre2) and 0.78 ± 0.01 (KB02_656-670), which may have been a result of possible sensitivity changes prior to or during preheat, which could not be corrected by the SAR protocol. In order to check whether the low dose recovery ratio originated from the solar simulator bleaching, we decided to apply both the pIRIR₂₉₀ (three aliquots) and the pulsed IR₅₀ (six aliquots) protocols to sample KB01_664-675. Aliquots were bleached within the reader for 2000 s using IR diodes, followed by a pause of 5000 s, bleached again for 2000 s and given a dose close to the expected natural one. Dose recovery ratios of the pIRIR₂₉₀ signal were too high (1.65 ± 0.03 ; **Fig. 3D**), indicating that the pIRIR₂₉₀ protocol does not work for our samples. The pulsed IR₅₀ dose re-

covery results were excellent (see Luminescence characteristics). Ultimately, three aliquots of each sample were bleached within the reader. Feldspar samples were treated with the above mentioned procedure, whereas quartz minerals were bleached for 1000 s by blue diodes, followed by a pause of 5000 s and bleached again for 1000 s.

We also checked if the sensitivity change correction was accurately measured by conducting recycling ratio tests and calculating recycling ratios. The same dose was applied at both the beginning and the end of the SAR cycle. If sensitivity changes were properly corrected for, the ratio of these two doses should ideally be within 10% of unity (0.9-1.1; Wintle and Murray, 2006). Results of dose recovery and recycling ratio tests are documented in Table 2A.

3.3.5.5 *Fading tests*

Feldspar minerals are known to suffer from a phenomenon called anomalous fading (e.g., Spooner, 1994), which leads to underestimated IRSL ages. Several age correction models have been proposed which are mostly applicable to the 'linear' part (young samples, up to 50 ka; e.g., Huntley and Lamothe, 2001) and in some cases also to the 'non-linear' part of the dose response curve (older samples; Lamothe et al., 2003; Kars et al., 2008). However, correction models for older samples have not yet been tested thoroughly enough. Although Huntley and Lamothe (2001) advise against application of their model on older samples, Buylaert et al. (2011) successfully applied it to Eemian (MIS 5e) sediments. Their results were in good agreement with both independent age control and quartz optically stimulated luminescence (OSL) ages. Therefore, Buylaert et al. (2011) concluded that the age restriction of up to 50 ka given by Huntley and Lamothe (2001) may be too strict and that their fading correction may also be applicable to older samples. However, all of these age correction models include assumptions, which are untestable in the laboratory and it is therefore recommended to use those parts of the IRSL signal, which are less or not affected by fading (e.g., Thiel et al., 2011). We used the pulsed IR₅₀ signal, which has been proven to show less fading (Tsukamoto et al., 2006), and additionally tested for the presence of possible fading. We applied fading tests and calculated fading rates (g-values) after Huntley and Lamothe (2001) using three aliquots of six chosen samples (Bet1, Fre1, Fre4, Fre5, KB01_664-675, KB02_373-385), which were found to be representative for the rest of the samples of the same outcrop and core. For low g-values of up to 1.0-1.5% per decade (Buylaert et al., 2012), the signal fading during burial time can be considered negligible, thus uncorrected IR₅₀ feldspar ages can be used for further interpretation. Similar g-values were also measured using the post-IR IRSL signal from infinite old samples whose natural signal is in saturation (Thiel et al., 2011; Buylaert et al., 2012). The natural

signal would never reach a saturation level, if there is anomalous fading. Thus, Thiel et al. (2011) and Buylaert et al. (2012) concluded that small fading rates (less than $\sim 1.5\%$ per decade) could be laboratory artefacts. Fading rates, fading-corrected and fading-uncorrected IR_{50} feldspar ages are given in **Table 2A**.

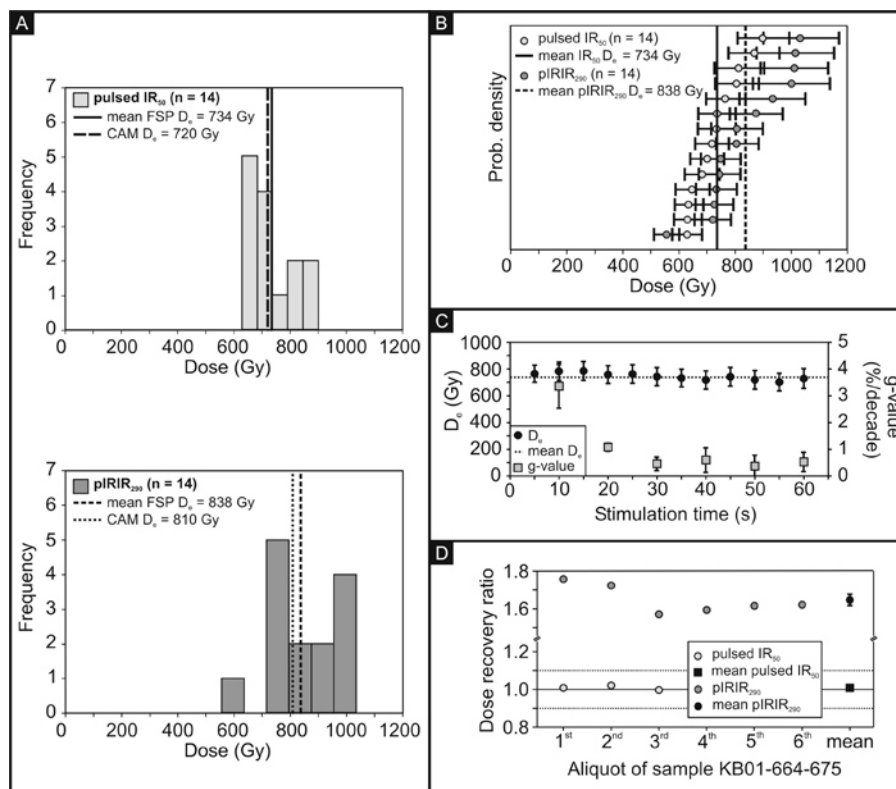


Fig. 3: (A) Histograms of the pulsed IR_{50} (upper) and $pIRIR_{290}$ (lower) protocols of sample KB01_664-675 based on 14 aliquots each, including their mean feldspar D_e and CAM D_e values. (B) Weighted histograms of D_e values derived using the pulsed IR_{50} (light grey circles, solid line) and $pIRIR_{290}$ (dark grey circles, dashed line) signals of sample KB01_664-675. The pulsed IR_{50} D_e values are consistently lower than the $pIRIR_{290}$ D_e values. (C) g-value(t) and D_e (t) plot of sample KB01_664-675 using the pulsed IR_{50} SAR protocol. The g-value(t) plot shows high g-values (grey squares) during initial stimulation time and lower g-values for the mid-part of the decay curve. The D_e (t) plot is characterised by stable D_e values (black circles), forming a flat, plateau-like trend line. The dotted line marks the mean pulsed IR_{50} D_e value (734 Gy) of the analysed aliquot. Error bars represent 1-sigma standard error. (D) Dose recovery ratios of sample KB01_664-675 using the pulsed IR_{50} (light grey circles) and the $pIRIR_{290}$ (dark grey circles) protocols, respectively. Pulsed IR_{50} dose recovery ratios are within 1-sigma standard error of unity (solid and dashed lines) (Wintle and Murray, 2006). Error bar represents 1-sigma standard error.

Table 1: Dosimetry results, dose rates and total dose rates of feldspar minerals. Uranium, thorium and potassium uncertainties are based on counting statistics of the gamma measurements. An internal potassium content of $12.5 \pm 0.5\%$ (Huntley and Baril, 1997) and an alpha efficiency value (a -value) of 0.15 ± 0.05 (cf. Balescu and Lamothe, 1994) were assumed. Cosmic radiation was corrected for altitude and sediment thickness (Prescott and Hutton, 1994).

Sample	Water content (%)	Dosimetry			Dose rates					Total dose rate (mGy a^{-1})
		Uranium (ppm)	Thorium (ppm)	Potassium (%)	D_α (mGy a^{-1})	D_β (mGy a^{-1})	D_γ (mGy a^{-1})	D_{internal} (mGy a^{-1})	D_{cosmic} (mGy a^{-1})	
Bet1	10±5	0.91±0.01	3.26±0.02	1.08±0.01	0.09±0.06	0.87±0.06	0.43±0.05	0.51±0.09	0.13±0.01	2.03±0.13
Bet2	5±2	0.77±0.01	2.75±0.03	1.03±0.01	0.06±0.04	0.84±0.03	0.41±0.02	0.69±0.09	0.16±0.02	2.17±0.11
Bur1	5±2	0.61±0.01	2.37±0.03	0.83±0.01	0.05±0.03	0.69±0.03	0.34±0.02	0.69±0.09	0.16±0.02	1.92±0.11
Fre1	10±5	0.72±0.01	2.32±0.01	1.02±0.01	0.06±0.06	0.79±0.06	0.37±0.05	0.61±0.17	0.08±0.01	1.89±0.20
Fre2	10±5	0.20±0.00	0.86±0.01	1.54±0.01	0.02±0.06	1.06±0.05	0.38±0.05	0.51±0.06	0.09±0.01	2.07±0.13
Fre4	7±4	1.05±0.01	3.83±0.03	1.58±0.01	0.08±0.06	1.24±0.05	0.59±0.04	0.69±0.09	0.16±0.02	2.77±0.13
Fre5	7±4	1.84±0.01	7.22±0.01	1.77±0.01	0.15±0.06	1.51±0.05	0.83±0.04	0.69±0.09	0.06±0.01	3.24±0.13
KB01_664-675	15±5	0.97±0.03	2.33±0.04	1.19±0.02	0.08±0.06	0.89±0.05	0.41±0.05	0.51±0.09	0.07±0.01	1.95±0.12
KB01_1060-1074	15±5	1.40±0.03	3.84±0.06	1.29±0.02	0.12±0.06	1.02±0.05	0.51±0.05	0.51±0.09	0.04±0.00	2.20±0.13
KB01_1441-1453	15±5	1.87±0.03	5.64±0.07	1.38±0.02	0.17±0.07	1.15±0.06	0.63±0.05	0.51±0.09	0.03±0.00	2.49±0.13
KB02_373-385	10±5	0.86±0.03	2.40±0.05	1.15±0.02	0.06±0.06	0.88±0.06	0.41±0.05	0.69±0.09	0.12±0.01	2.15±0.13
KB02_656-670	10±5	1.43±0.03	4.58±0.05	1.21±0.01	0.10±0.06	1.01±0.06	0.55±0.05	0.69±0.09	0.08±0.01	2.43±0.13
KB02_1344-1355	10±5	0.99±0.03	2.74±0.05	1.15±0.02	0.07±0.06	0.90±0.06	0.43±0.05	0.69±0.09	0.04±0.00	2.12±0.13
KB02_1579-1590	10±5	0.63±0.02	1.95±0.05	0.98±0.00	0.04±0.06	0.74±0.06	0.34±0.05	0.69±0.09	0.03±0.00	1.84±0.13

Table 2: Results of (A) feldspar and (B) quartz luminescence measurements, including number of measured aliquots (n_m) and number of accepted aliquots (n_a) used for age calculation, mean recycling ratios (standard error: ± 0.04), overdispersion (σ_{OD}), dose recovery ratios, total dose rates, CAM D_e values and ages, fading rates, saturation doses (D_0), mean IR_{50} , D_e values, fading-corrected and fading-uncorrected IR_{50} feldspar ages. All ages are given with their 1-sigma standard error.

(A) Feldspar												
Sample	n_m/n_a	Mean rec. ratio	σ_{OD} (%)	Dose recovery ratio	Total dose rate ($mGy a^{-1}$)	CAM D_e (Gy)	CAM age (ka)	g-value (% per decade)	$2 D_0$ (Gy)	Mean $IR_{50} D_e$ (Gy)		
										corrected	un-corrected	
Bet1	10/8	1.00	4.6	1.01 \pm 0.01	2.0 \pm 0.1	861 \pm 32	423 \pm 31	0.5 \pm 0.2	1042	875 \pm 33	451 \pm 41	430 \pm 32
Bet2	10/9	0.99	1.2	1.03 \pm 0.02	2.2 \pm 0.1	899 \pm 27	415 \pm 24	0.5 \pm 0.2	1138	912 \pm 32	439 \pm 34	421 \pm 25
Bur1	10/9	0.99	4.9	1.03 \pm 0.01	1.9 \pm 0.1	851 \pm 28	444 \pm 29	0.5 \pm 0.2	1177	867 \pm 34	473 \pm 41	452 \pm 31
Fre1	10/10	1.01	7.1	0.99 \pm 0.01	1.9 \pm 0.2	452 \pm 15	239 \pm 26	1.4 \pm 0.2	744	456 \pm 16	275 \pm 32	241 \pm 27
Fre2	10/10	1.01	11.9	1.03 \pm 0.03	2.1 \pm 0.1	509 \pm 23	246 \pm 19	1.4 \pm 0.2	704	516 \pm 25	285 \pm 26	250 \pm 20
Fre4	15/14	1.02	17.4	0.93 \pm 0.01	2.8 \pm 0.1	505 \pm 26	182 \pm 12	1.2 \pm 0.3	924	518 \pm 31	198 \pm 27	196 \pm 19
Fre5	15/14	1.02	12.9	0.97 \pm 0.01	3.2 \pm 0.1	517 \pm 21	159 \pm 9	1.2 \pm 0.8	882	533 \pm 22	182 \pm 14	161 \pm 10
KB01_664-675	16/14	1.01	6.0	1.01 \pm 0.01	2.0 \pm 0.1	720 \pm 21	369 \pm 26	0.5 \pm 0.4	910	734 \pm 24	394 \pm 40	376 \pm 27
KB01_1060-1074	16/14	1.00	6.9	1.01 \pm 0.02	2.2 \pm 0.1	791 \pm 23	359 \pm 23	0.5 \pm 0.4	1070	803 \pm 24	381 \pm 37	365 \pm 24
KB01_1441-1453	16/13	1.00	4.8	1.00 \pm 0.01	2.5 \pm 0.1	822 \pm 23	331 \pm 20	0.5 \pm 0.4	1069	838 \pm 29	352 \pm 33	337 \pm 21
KB02_373-385	10/10	1.05	16.4	0.95 \pm 0.01	2.2 \pm 0.1	243 \pm 14	113 \pm 9	1.1 \pm 0.4	747	247 \pm 15	127 \pm 14	115 \pm 10
KB02_656-670	10/10	1.05	25.8	0.97 \pm 0.01	2.4 \pm 0.1	283 \pm 24	116 \pm 12	1.1 \pm 0.4	749	295 \pm 29	134 \pm 19	121 \pm 14
KB02_1344-1355	10/9	1.00	5.8	1.00 \pm 0.01	2.1 \pm 0.1	961 \pm 35	452 \pm 33	1.1 \pm 0.4	1189	978 \pm 39	512 \pm 53	461 \pm 34
KB02_1579-1590	10/10	0.99	0.0	1.00 \pm 0.01	1.8 \pm 0.1	795 \pm 20	432 \pm 33	1.1 \pm 0.4	1301	801 \pm 18	484 \pm 50	435 \pm 33

(B) Quartz							
Samples	n_m/n_a	Mean rec. ratio	σ_{OD} (%)	Dose recovery ratio	Total dose rate ($mGy a^{-1}$)	CAM D_e (Gy)	CAM age (ka)
KB02_656-670	10/7	1.01	13.0	0.96 \pm 0.08	1.6 \pm 0.1	192 \pm 11	117 \pm 9

3.3.5.6 Age calculation

Uncorrected IR₅₀ feldspar ages were calculated using the mean D_e value of all accepted aliquots. Additionally, weighted means were calculated using the central age model (CAM; Galbraith et al., 1999), which assumes a natural distribution of the D_e values and takes additional dispersion resulting from measurement uncertainties into account. The standard deviation of this distribution is called overdispersion (σ_{OD}) and represents statistically unaccounted variations, which are due to extrinsic (incomplete bleaching, post-depositional mixing, small-scale dosimetry variations) and intrinsic factors (instrument reproducibility, thermal transfer, counting statistics). The impact of the latter on the D_e values is reflected by dose recovery tests (cf. Hilgers, 2007).

Additional quartz OSL measurements were performed for samples KB02_373-385 and KB02_656-670, which gave young IR₅₀ feldspar ages (**Table 2B**). As both quartz and feldspar signals have different bleaching behaviours, agreement of quartz and feldspar ages is indicative of good bleaching conditions; thus pointing to well-bleached feldspar samples. Therefore, an age discrepancy implies that the feldspar minerals had been insufficiently bleached (Murray et al., 2012). Depositional quartz ages were obtained using the CAM (**Table 2B**).

3.4 Results

3.4.1 Luminescence characteristics

Feldspar dose recovery ratios range from 0.93 ± 0.01 (Fre4) to 1.03 ± 0.03 (Fre2) and quartz dose recovery ratios are 0.88 ± 0.04 (KB02_373-385) and 0.96 ± 0.08 (KB02_656-670; **Table 2**). These values are within the 1-sigma standard error of unity (0.9-1.1; Wintle and Murray, 2006), confirming the applicability of the used SAR protocol.

Feldspar recycling test ratios range from 0.99 ± 0.04 (Bet2, Bur1, KB02_1579-1590) to 1.05 ± 0.04 (KB02_373-385, KB02_656-670), quartz recycling ratios are 0.99 ± 0.04 (KB02_373-385) and 1.01 ± 0.04 (KB02_656-670; **Table 2**). All values are within 10% of unity (0.9-1.1; Wintle and Murray, 2006), implying that the applied SAR protocol corrects properly for sensitivity changes.

Based on the accepted D_e values, we created D_e histograms and dose response and decay curves. Six representative D_e histograms and dose response and decay curves (KB01_1060-1074, KB02_656-670, KB02_1579-1590, Fre1, Fre4, Bet2) are shown in **Fig. 4**. Most of the D_e histograms show Gaussian-like and narrow distributions, suggesting good bleaching conditions. Two samples (KB02_656-670, Fre4) have slightly positively skewed distributions

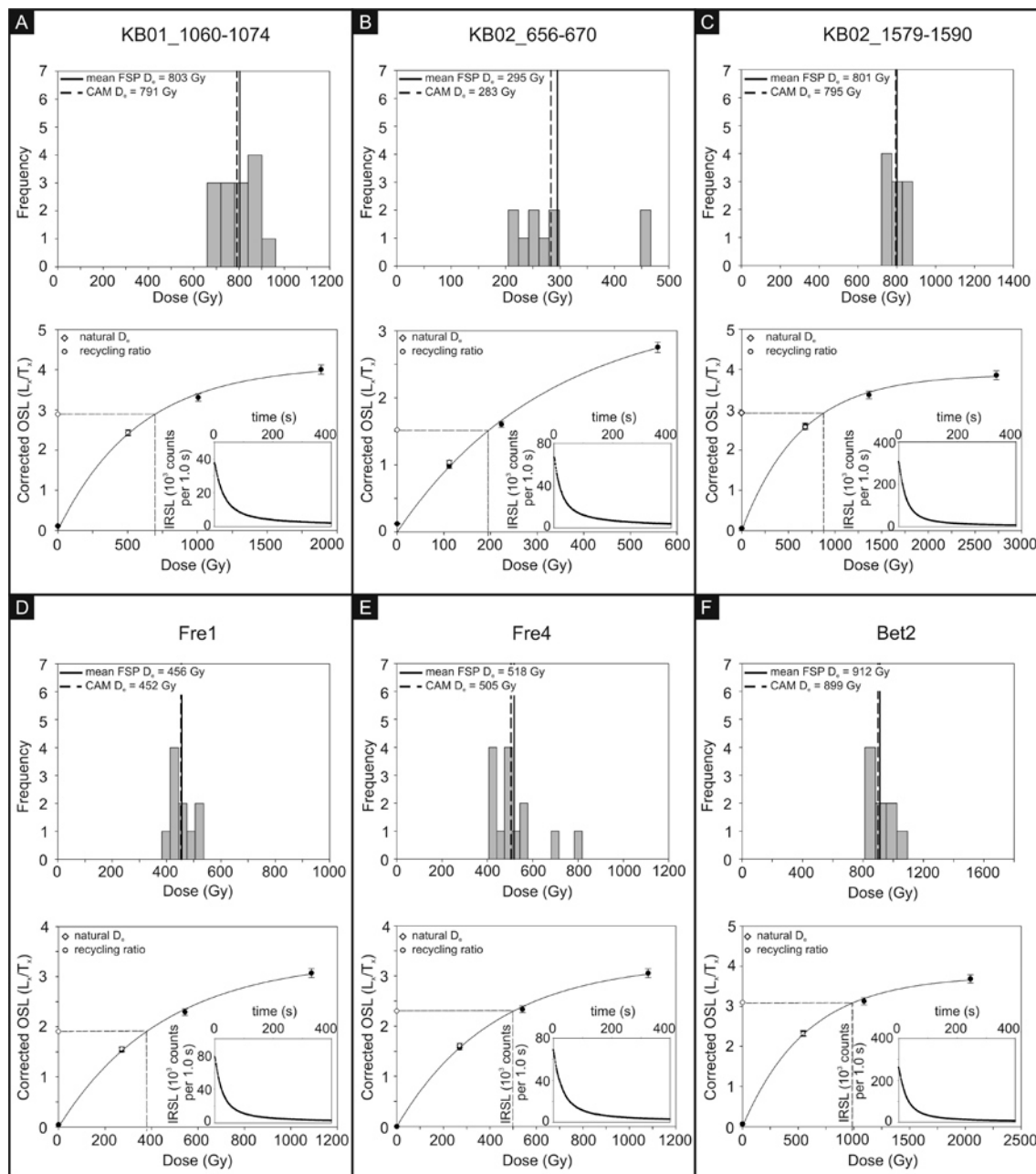


Fig. 4: D_e histograms (top) and dose response and decay curves (bottom) of luminescence samples (A) sample KB01_1060-1074, (B) sample KB02_656-670, (C) sample KB02_1579-1590, (D) sample Fre1, (E) sample Fre4 and (F) sample Bet2. D_e histograms are characterised by mainly Gaussian-like and narrow D_e distributions. Mean feldspar D_e (solid line) and CAM D_e values (dashed black line) are shown. Dose response curves display exponential growth. Natural doses (white diamonds), recycling ratios (white circles) and decay curves (insets) are shown.

with outliers at higher doses (**Fig. 4B, E**), suggesting that some grains may have not been sufficiently bleached (Olley et al., 1999), which may lead to a possible overestimation of the determined depositional age.

Fading tests results were analysed to decide which part of the decay curve is associated with the most stable part of the signal (lowest g-values). The initial part of the decay curve (0-

10 s, 11-20 s) is characterised by considerably higher g-values (up to $4.42 \pm 0.46\%$ /decade; Fre4), whereas the middle part (21-60 s) shows low g-values ($\sim 1.0 \pm 0.3\%$ /decade; Fre4; **Fig. 3C**). We therefore chose the middle part of the decay curve for D_e and g-value determination. Calculated g-values range from $0.5 \pm 0.4\%$ /decade (Fre4, KB01_664-675, KB01_1060-1074, KB01_1441-1453) to $1.4 \pm 0.2\%$ /decade (Fre1, Fre2; **Table 2A**), which is considered to be negligible (see Fading test; Buylaert et al., 2012). We therefore used uncorrected IR_{50} feldspar ages for interpretation.

Quartz CAM ages range from 117 ± 9 ka (KB02_656-670) to 116 ± 10 ka (KB02_373-385; **Table 2B**). They are in perfect agreement with the determined uncorrected IR_{50} feldspar ages of 121 ± 14 ka (KB02_656-670) and 115 ± 10 ka (KB02_373-385; **Table 2A**), implying that the feldspar minerals have been well bleached (Murray et al., 2012).

3.4.2 Depositional architecture and luminescence ages of Middle Pleistocene ice-marginal sediments

The depositional architecture of the Leine-valley fill has been reconstructed from geological maps (1:25 000, 1:50 000), borehole logs, outcrop data and high-resolution shear wave seismic profiles.

The clast composition of ice-marginal deposits mainly consists of material derived from the adjacent Mesozoic bedrock (67-89%) or re-sedimented older fluvial material (2-19%), including clasts from Palaeozoic bedrock of the river catchment area. Clasts with a Scandinavian/Baltic provenance commonly amount to 14-16% (**Table S4**). The heavy mineral association is characterised by a high percentage of garnet (21-46%), hornblende (14-31%) and epidote (21-29%; **Table S5**), indicating a Scandinavian/Baltic provenance. Both clast and heavy mineral associations are characteristic for meltwater deposits (Rausch, 1977; Henningsen, 1983).

3.4.2.1 The Freden delta

The Freden delta and subaqueous fan complex marks the southernmost occurrence of ice-marginal deposits in the Leine valley (**Fig. 1B**). The deposits are up to 60 m thick, directly overlie Mesozoic bedrock and form part of a larger ice-marginal complex, which was formerly exposed in several pits approximately 4 km northwest of Freden over an altitude range of 140-200 m a.s.l. (Winsemann et al., 2007). Parts of the Freden delta and subaqueous fan complex are still exposed in the large Ulrich pit (**Figs 1E, 5**), consisting of steeply to moderately dipping, planar and trough cross-stratified pebbly sand and climbing-ripple cross-laminated

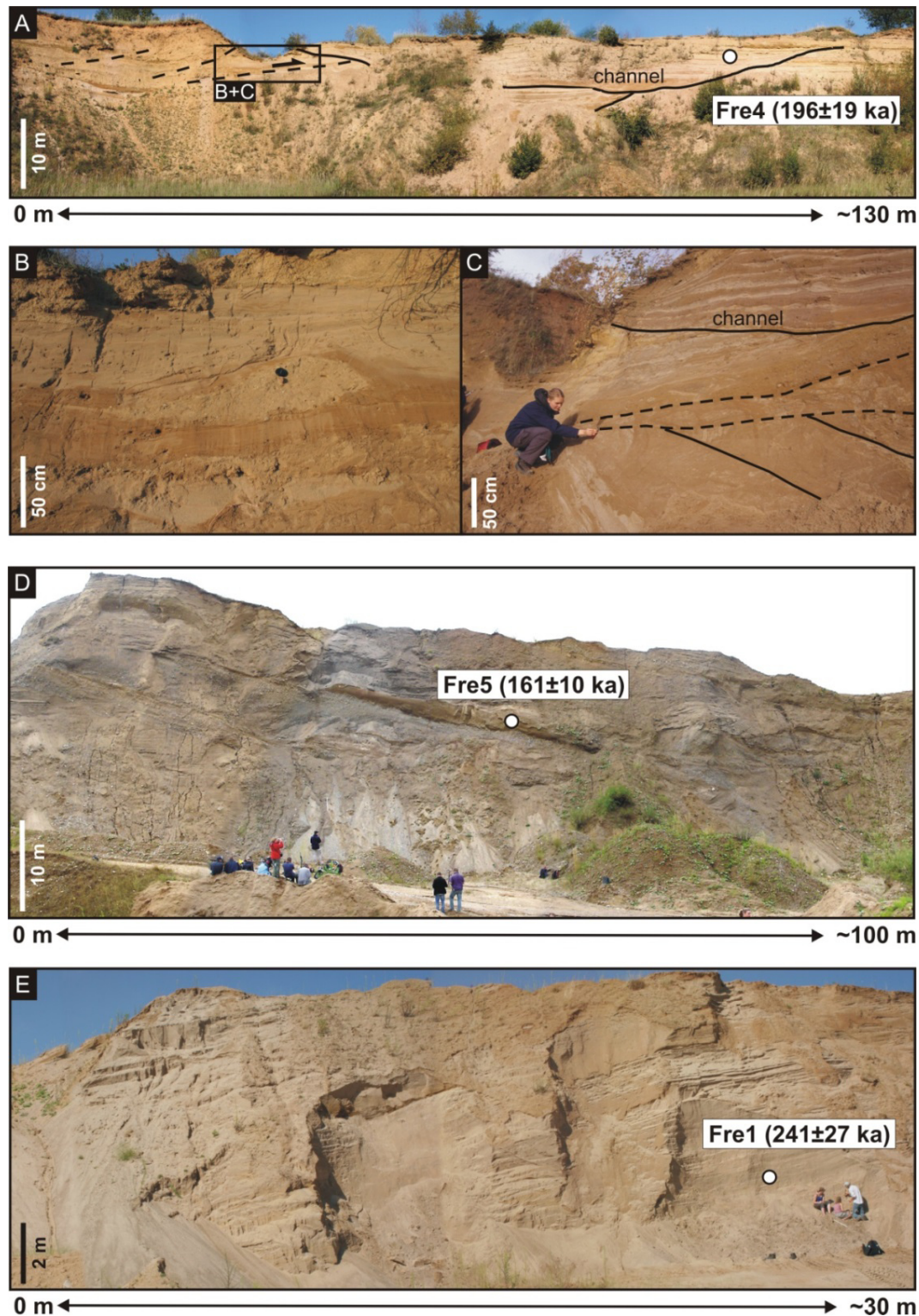


Fig. 5: Sedimentary facies of the Freden ice-marginal deposits with sample location and luminescence age estimates. For location see **Fig. 1E**. **(A)** Glacitectonic thrust sheets, erosively overlain by sandy channel-fill deposits. **(B)** Close-up view of A, showing a till layer in the hanging wall of a thrust fault. **(C)** Close-up view of A, showing the deformed zone below a glacitectonic thrust sheet. **(D)** Large slope-cutting channel complex, deeply incised into delta-foreset deposits. **(E)** Steeply dipping delta-foreset deposits, characterized by planar and trough cross-stratified pebbly sand. Sample Fre2 was taken from delta-toeset deposits approximately 200 m further to the south (left).

sand. Winsemann et al. (2007) assumed that the oldest ice-marginal deposits consist of a subaqueous fan complex, which was overlain by delta deposits during ice-margin retreat. However, new data from outcrops, boreholes and geomorphology indicate that the Freden ice-marginal deposits have a more complex depositional architecture. The oldest deposits are probably exposed in the western part of the Ulrich pit, comprising steeply dipping sand-rich delta-foreset and delta-toeset deposits (delta body I; **Figs 1E, 5E**). These sediments were shed from a north-eastern source. In the northeastern pit, this delta body is overlapped by fine-grained channelised delta or subaqueous fan deposits (delta body II), which differ in sedimentary facies and palaeo-current directions (**Figs 1E, 5A**). These sediments comprise flow till layers, are partly affected by glaciectonic deformation and are overlain by till (**Fig. 5B, C**). In the western pit, the sand-rich lowermost delta body (I) is erosively overlain by coarse-grained channelised deposits that belong to a younger delta body (III) that was shed from a western source (**Fig. 1E**).

Four samples were taken from delta-foreset (Fre1) and delta-toeset (Fre2) deposits (delta body I) and two slope-cutting channel complexes (Fre4, Fre5) of delta body II and delta body III (**Figs 1E, 5**). Uncorrected IR₅₀ feldspar ages range from 250±20 (Fre2) to 241±27 ka (Fre1) and from 196±19 (Fre4) to 161±10 ka (Fre5; **Table 2A**).

3.4.2.2 *The Betheln delta*

The Betheln delta is located about 23 km northeast of Freden (**Fig. 1B**). It is ~1.5 km wide and ~3.5 km long (**Fig. 1D**), and overlies Mesozoic bedrock. Deposits are exposed in two large sand and gravel pits (Fischer pit and Burgstemmen pit; **Fig. 1D**).

In the upper portion of the Betheln delta, coarse-grained deposits are exposed over an altitude range of ~135-150 m a.s.l., characterised by the typical tripartite structure of Gilbert-type deltas, comprising delta-topset, delta-foreset and delta-bottomset deposits (**Fig. 6A**). Delta-bottomset beds consist of trough cross-stratified and climbing-ripple cross-laminated pebbly sand and medium- and fine-grained sand. Delta-foreset beds consist of matrix- or clast-supported, massive or normally graded gravel and planar-parallel and trough cross-stratified pebbly sand. Delta-foreset beds dip steeply towards the southwest and west.

The lower portion of the delta complex is exposed over an altitude range of 100-116 m a.s.l. in the Burgstemmen pit (**Fig. 1D**). The succession consists of climbing-ripple cross-laminated fine-grained sand, silt and clay, overlain by large-scale cross-stratified gravel and coarse- to fine-grained sand (**Fig. 6C**).

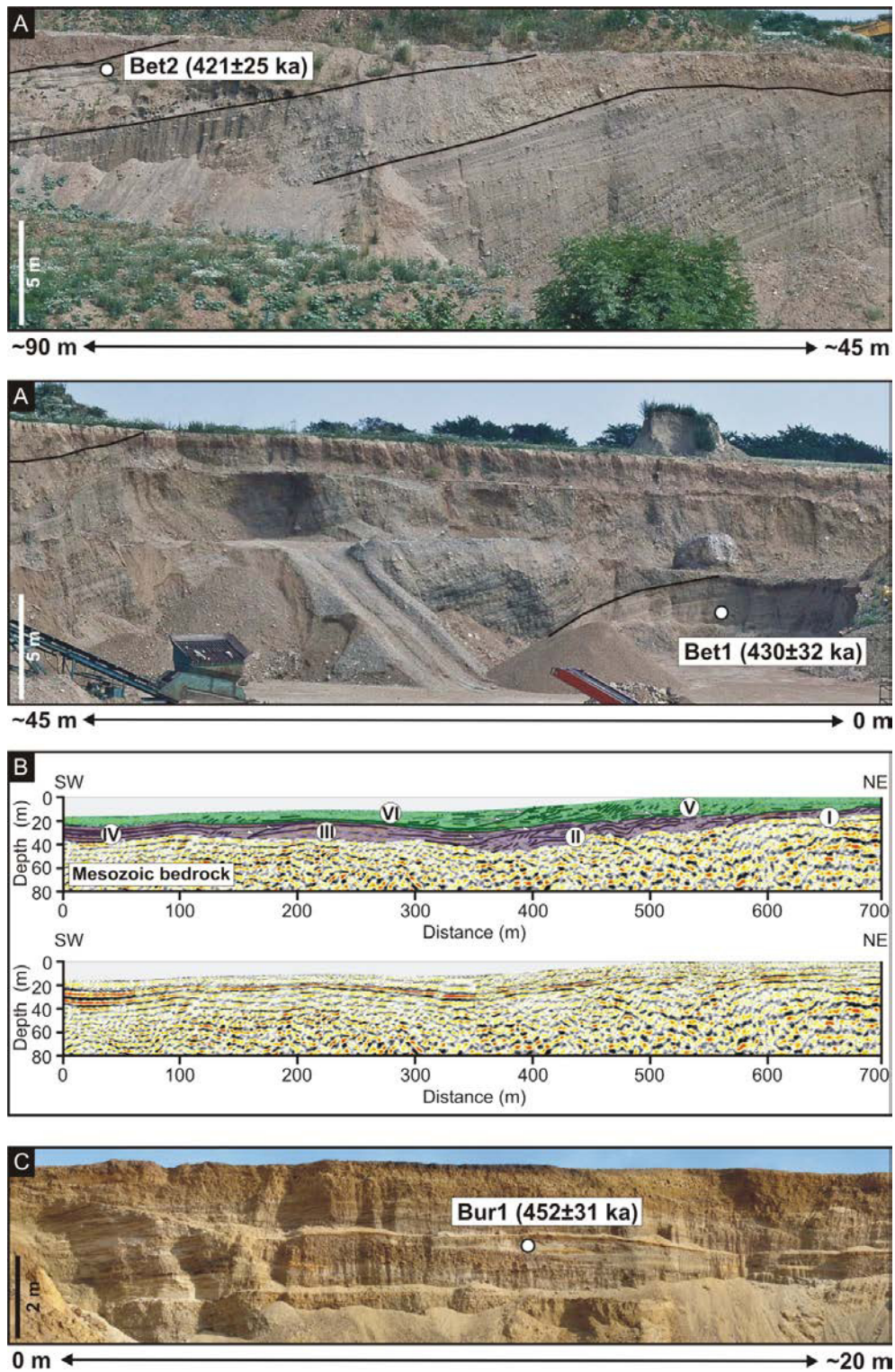


Fig. 6: Sedimentary facies and depositional architecture of the Betheln delta with sample location and luminescence age estimates. For location see **Fig. 1D**. **(A)** Coarse-grained delta-foreset deposits, unconformably overlying sand-rich delta-toeset deposits; Fischer pit. Photo courtesy of M. Wahle. **(B)** Shear wave seismic profile, measured south of the Fischer pit. For location see **Fig. 1D**. Seismic unit V can be correlated with the delta-foreset deposits exposed in the Fischer pit. **(C)** Coarse-grained delta mouth-bar deposits of the lower portion of the Betheln delta; Burgstemmen pit. Photograph courtesy of L. Pollok.

3.4.2.3 Shear wave seismic profile at the Fischer pit

A seismic profile was measured to determine the larger-scale architecture of the Betheln delta (**Figs 1D, 6B**). The Mesozoic bedrock is unconformably overlain by up to 40 m thick delta deposits. The lateral and vertical stacking pattern indicates two transgressive-regressive cycles. The oldest depositional units (I-IV) are laterally stacked and step basinwards. Seismic units I to IV are characterised by an internal continuous parallel, partly hummocky reflector pattern with an equidistant spacing. The external geometry is convex-up. These mound-shaped delta lobes are 190-290 m wide and 5-16 m thick. Seismic unit V rests on top of seismic units I, II and III and is up to 16 m thick. The internal reflector pattern is characterised by partly parallel continuous reflectors in the east that pass down-slope into westward dipping, inclined discontinuous reflectors. Seismic unit V is overlapped by seismic unit VI, which has a continuous, partly slightly transparent parallel or inclined reflector pattern.

Samples Bet1, Bet2 and Bur1 were taken from the upper (Fischer pit; **Figs 1D, 6A**) and lower portion (Burgstemmen pit; **Figs 1D, 6C**) of the Betheln delta complex, giving uncorrected IR₅₀ feldspar ages, ranging from 452±31 (Bur1) to 430±25 ka (Bet1) and 421±25 ka (Bet2; **Table 2A**).

3.4.2.4 Shear wave seismic profiles at Schliekum/Sarstedt

Seismic line 1 has been measured on different road surfaces (concrete and asphalt), which leads to a slightly different signal transfer function, influencing the shear wave propagation velocity (~1200 m s⁻¹ for concrete, 800 m s⁻¹ for asphalt) and therefore also the reflector pattern. Below the asphalt (profile sector ~275-600 m) the reflector pattern is relatively wide-spaced, whereas below the concrete the reflector pattern is smaller-spaced. The seismic profile 1 shows seven vertically and laterally stacked depositional units that represent time units, where seismic unit 1 is the oldest and seismic unit 7 the youngest (**Figs 1C, 7A**).

The Mesozoic bedrock is characterised by a high-amplitude continuous parallel reflector pattern and is unconformably overlain by seismic unit 1 (**Fig. 7A**). This unit is up to 8 m thick and characterised by a continuous to discontinuous subhorizontal, slightly convex-up and inclined-parallel reflector pattern. Seismic unit 2 has a concave-up external geometry, with a maximum thickness of 10.5 m and a maximum width of approximately 175 m (**Fig. 7A**). The internal basal reflectors are continuous parallel and partly concentric. The reflectors of the upper half of the seismic unit are discontinuous and more transparent. Seismic unit 1 is overlain by seismic unit 3, characterised by a continuous to partly discontinuous, slightly transparent, parallel re-

flector pattern that passes towards the east into an inclined reflector pattern. Seismic unit 3 is up to 5 m thick (**Fig. 7A**).

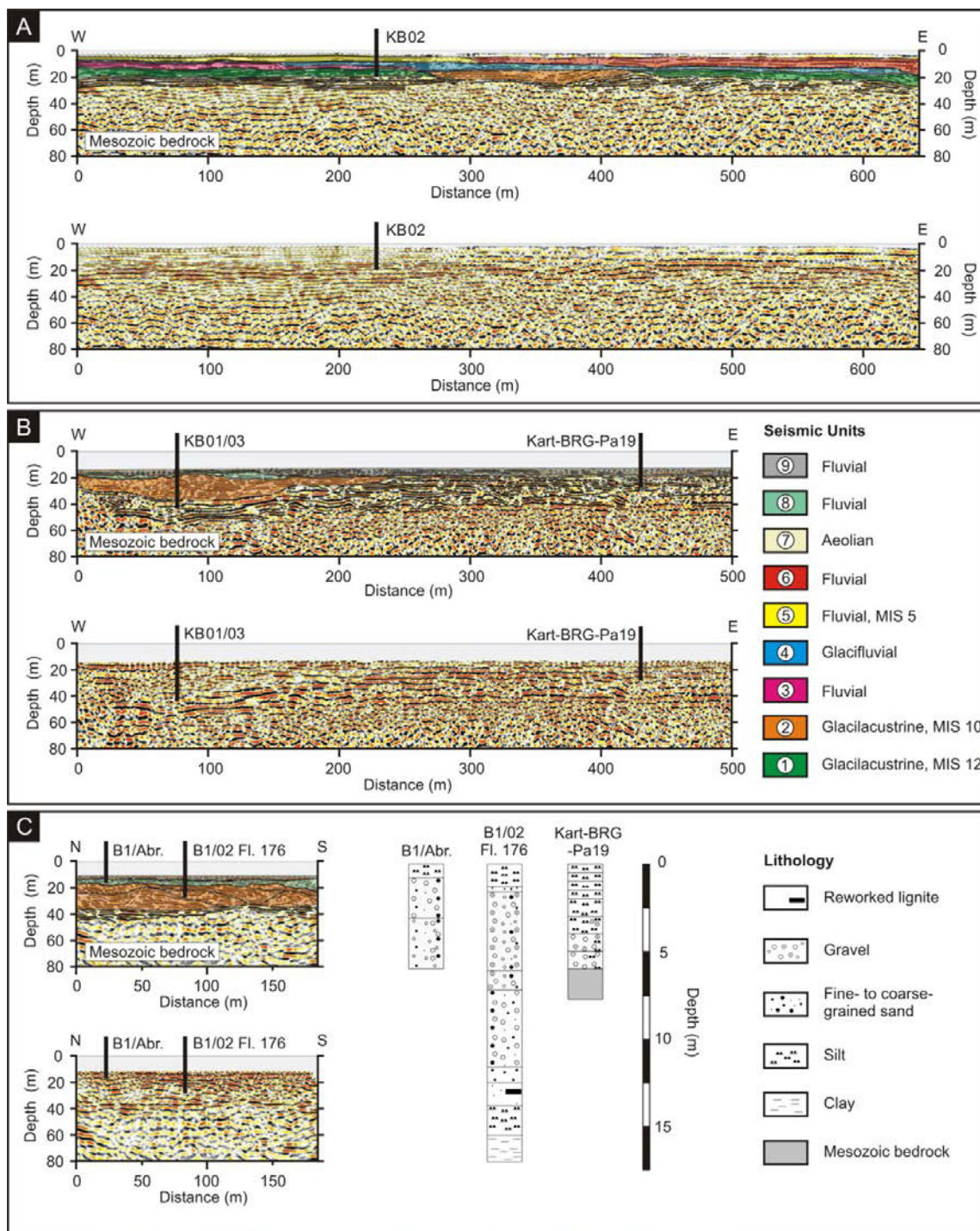


Fig. 7: Shear wave seismic profiles 1, 2 and 3, which were measured near Schliekum/Sarstedt. (A) Shear wave seismic line 1. (B) Shear wave seismic line 2. (C) Shear wave seismic line 3. For location see Fig. 1C.

Seismic unit 4 is laterally continuous and covers the whole section (**Fig. 7A**). It overlies unit 3 in the western part of the profile, in the central part it overlies seismic unit 2 and in the eastern part it directly rests on seismic unit 1 (**Fig. 7A**). In the western part, the reflector pattern is parallel, continuous to slightly discontinuous. In the central part of the section, it passes into an inclined, wider-spaced, slightly transparent reflector pattern. The thickness ranges from approximately 1-7 m. In the east, it is characterised by a discontinuous, moderately transparent reflector pattern (**Fig. 7A**). Seismic unit 5 is up to 4.7 m thick and pinches out towards the east. It has a parallel, continuous reflector pattern in the western part. In the very west, the reflector pattern is more discontinuous, more transparent and slightly inclined (**Fig. 7A**). Seismic unit 6 is only present on the eastern section, is up to 8 m thick and has a wide-spaced, discontinuous and partly transparent parallel reflector pattern (**Fig. 7A**). Seismic unit 7 has a very discontinuous, parallel partly transparent reflector pattern (**Fig. 7A**).

Seismic line 2 shows three vertically stacked depositional units (**Fig. 7B**). The Mesozoic bedrock is characterised by a high-amplitude continuous parallel reflector pattern and is unconformably overlain by seismic unit 2. Seismic unit 2 has a concave-up external geometry, is up to 21 m thick and approximately 250 m wide. The internal reflector pattern is discontinuous, hummocky and convex-up. The mound-shaped elements are 22-45 m wide and up to 8 m thick. These elements are shingled and vertically stacked. Seismic unit 2 is overlain by seismic unit 8, which is 1.5-6 m thick and laterally pinches out towards the east. The reflector pattern seems to be discontinuous parallel, but the low thickness of the unit makes it very difficult to define. Seismic unit 9 covers the whole section, is 1.5-7.7 m thick and characterised by a discontinuous, parallel, partly inclined reflector pattern.

As in seismic line 2, in seismic line 3, three seismic units are mapped, unconformably overlying Mesozoic bedrock (**Fig. 7C**). Seismic unit 2 is 18.5-20 m thick and characterised by a discontinuous, hummocky, convex-up reflector pattern. Individual mound-shaped elements are up to 100 m wide and up to 16.5 m thick. These elements are shingled. Seismic unit 2 is overlain by seismic unit 8, which is 2.3-7.5 m thick and displays a discontinuous, parallel, partly inclined reflector pattern. Seismic unit 9 is approximately 3 m thick and has a very discontinuous, diffuse reflector pattern.

Seismic unit 1 is interpreted as fine-grained glaciallacustrine delta deposits, based on the small-spaced, mound-shaped and inclined reflector pattern (Winsemann et al., 2009, 2011a), the sedimentary facies (core KB02, 11.60-16.75 m; **Fig. 8; Table S6**) and heavy mineral association (**Table S5**). The occurrence of an intercalated till (core KB02, 14.35-15.55 m; **Fig. 8**) may point to ice-margin oscillations (e.g., Lønne, 1995).

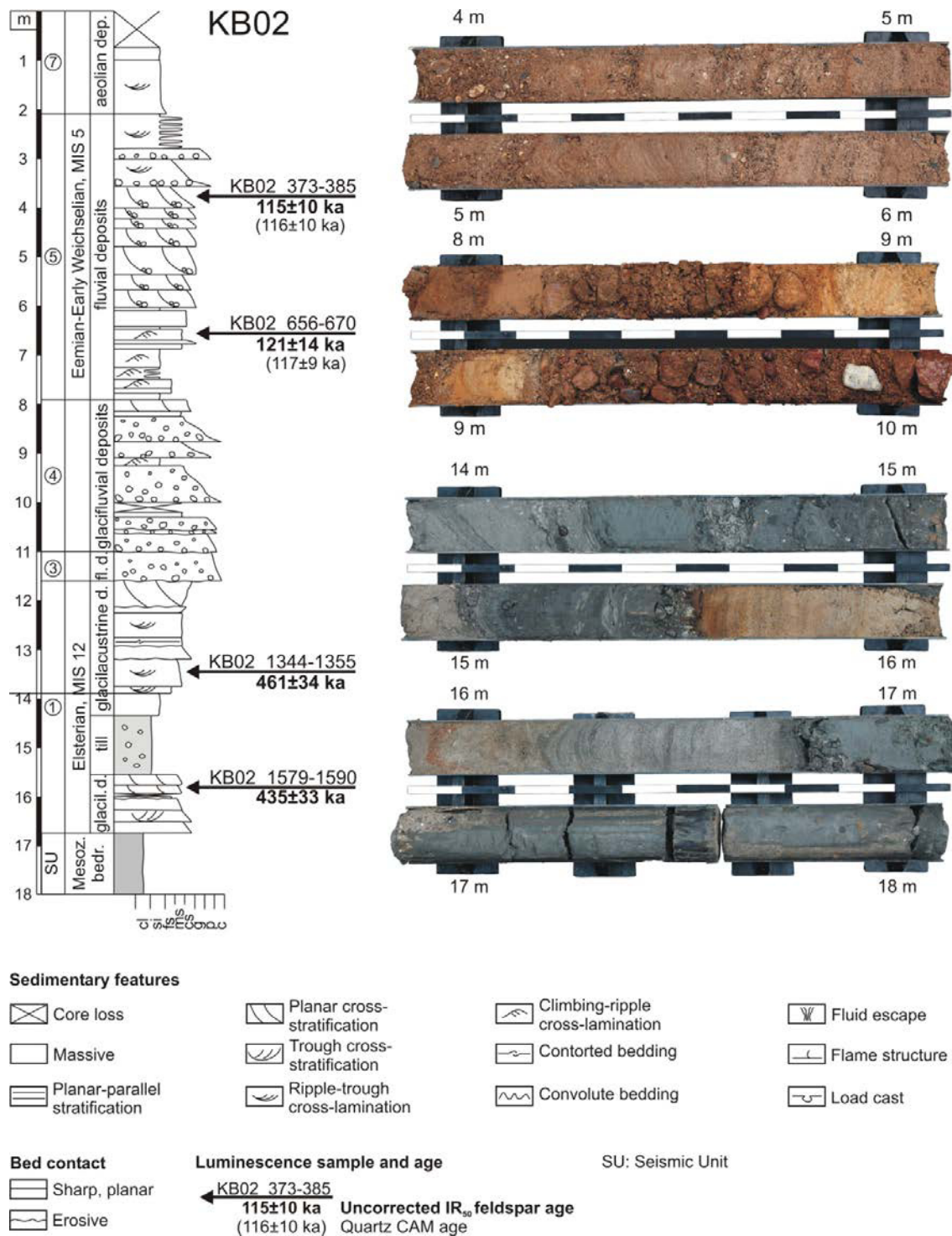


Fig. 8: Sedimentary log and photographs of core KB02. Location and estimated ages of luminescence samples are shown.

Seismic unit 2 is interpreted as a fill of a larger subglacial meltwater channel or subglacial basin, respectively (e.g., Rohde, 1983; Cook and Swift, 2012). The mound-shaped architectural elements in seismic lines 2 and 3 (**Fig. 7B, C**) indicate fine-grained prodelta and delta-lobe deposits (Correggiari et al., 2005; Winsemann et al., 2007, 2011a). The climbing-ripple cross-

laminated and cross-stratified delta slope deposits (**Table S6**) are partly rich in reworked organic material and lignite (core KB01, 6.22-16.89 m; **Fig. 9**), which has been eroded from older Early Pleistocene and Tertiary deposits (B. Urban, pers. comm., 2012). In combination with the southward palaeoflows, indicated by the lateral stacking pattern of delta lobes, seismic unit 2 is interpreted as a glaciallacustrine delta complex.

Seismic unit 3 is interpreted as a fluvial deposit of the River Leine with a high basal content of reworked glacialgenic material, based on the subhorizontal reflector pattern and the regional stratigraphic correlation (Rohde, 1983).

Seismic unit 4 represents glacialfluvial deposits, characterised by pebble- to cobble-gravel with a high amount of Scandinavian/Baltic material (**Fig. 8; Table S4**).

Seismic unit 5 is interpreted as a fluvial deposit of River Leine based on the subhorizontal reflector pattern, and clast and heavy mineral compositions (e.g., Rohde, 1983).

Seismic unit 6 has not been cored. Correlation with outcrop and borehole data further north (**Fig. 1C**) indicates that these deposits most probably consist of fluvial deposit of River Leine (Lüttig, 1960; Rohde, 1983).

Seismic unit 7 is interpreted as aeolian sand sheets and loess, partly deposited on wet surfaces (Schokker and Koster, 2004; Meinsen et al., 2014).

Seismic unit 8 and 9 consist of coarse-grained fluvial gravel (**Fig. 9; Table S4**) interpreted to represent deposits of the River Leine and Innerste (Rohde, 1983).

From seismic units 1, 2 and 5, seven luminescence samples were taken from glaciallacustrine and fluvial deposits of cores KB01 and KB02. For core KB01, uncorrected IR₅₀ feldspar ages are 376±27 ka (KB01_664-675), 365±24 ka (KB01_1060-1074) and 337±21 ka (KB01_1441-1453; **Table 2A**). For core KB02, uncorrected IR₅₀ feldspar ages are 461±34 ka (KB02_1579-1590), 435±33 ka (KB02_1344-1355), 121±14 ka (KB02_656-670) and 115±10 ka (KB02_373-385; **Table 2A**). Quartz CAM ages are 117±9 ka (KB02_656-670) and 116±10 ka (KB02_373-385; **Table 2B**).

The deposits of seismic units 3, 4, 6, 8 and 9 were not dated because either they were not cored or their grain size was inappropriate for luminescence dating.

3.5 Discussion

3.5.1 Reliability of the luminescence ages

The luminescence dating results and analysis of the stratigraphic architecture of the Leine-valley fill point to repeated glaciations during the Middle Pleistocene (MIS 12, MIS 10, MIS 8 and MIS 6; **Fig. 10**). However, the dating of glacialgenic sediments is generally considered to be

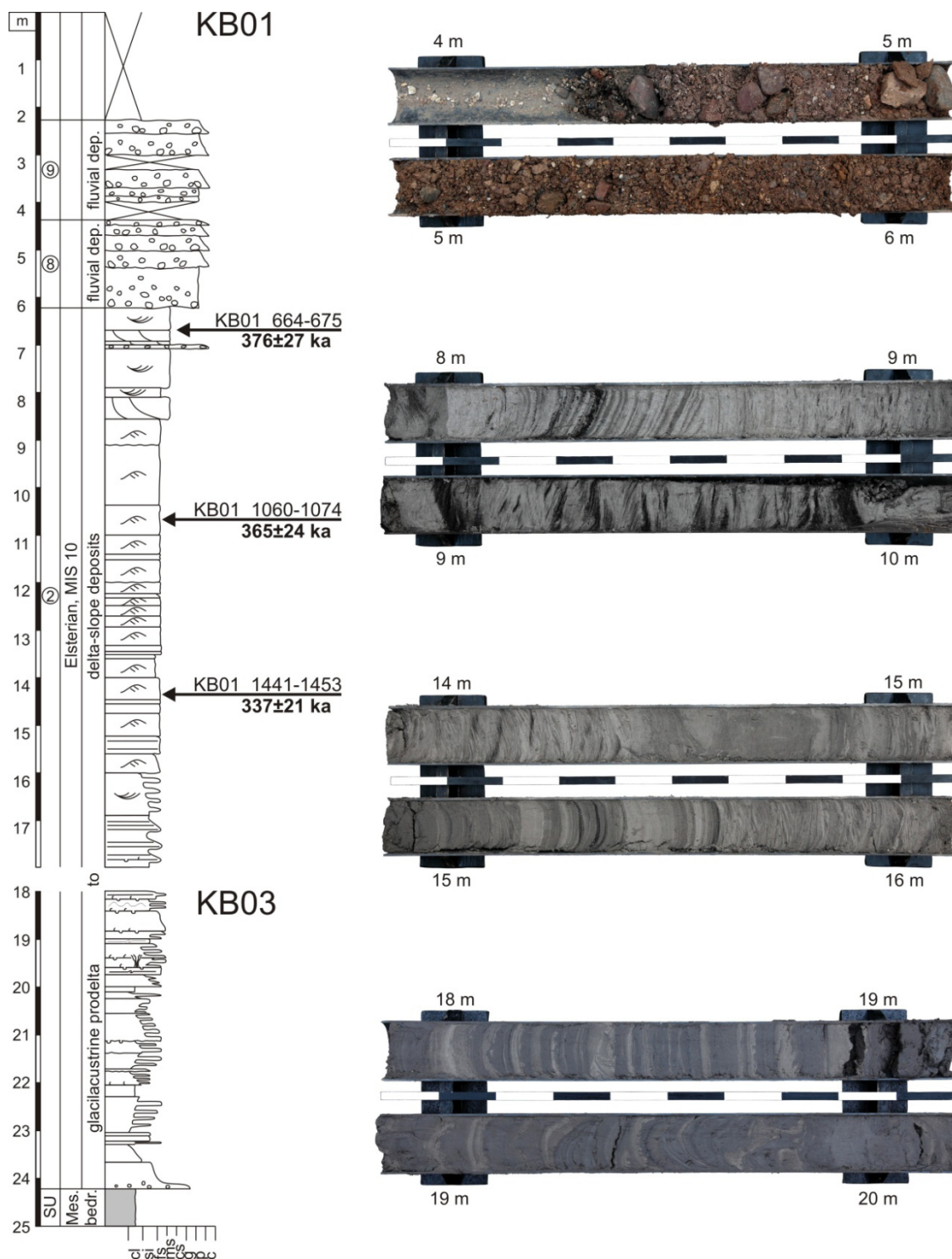


Fig. 9: Sedimentary log and photographs of core KB01/KB03. Location and estimated ages of luminescence samples are shown. For symbol explanations see Fig. II.8.

challenging because deposits may have been poorly bleached. Numerical age dating of glaciogenic sediments is sparse (Fuchs and Owen, 2008) but has successfully been applied to Anglian (Elsterian MIS 12) glaci-fluvial and glaci-lacustrine sediments in Great Britain (Pawley et al., 2008, 2010), early Saalian glaciogenic sediments in Denmark (Houmark-Nielsen, 2011), Saalian

glacifluvial sediments in northern Germany (Fehrentz and Radtke, 1998; Preusser, 1999), Saalian glacifluvial sediments in Finland (Pitkäranta et al., 2014) and modern glacifluvial sediments of the Svalbard archipelago in the Arctic Ocean (Alexanderson and Murray, 2012). However, in our case study, moderate feldspar dose rate values ($1.8\text{--}3.2\text{ mGy a}^{-1}$; **Table 2A**) and high feldspar D_e values (up to 1000 Gy; **Table 2A**) pushed us close to the limit of luminescence dating techniques. To check for the robustness of our data, we will discuss possible causes of age under- and overestimations.

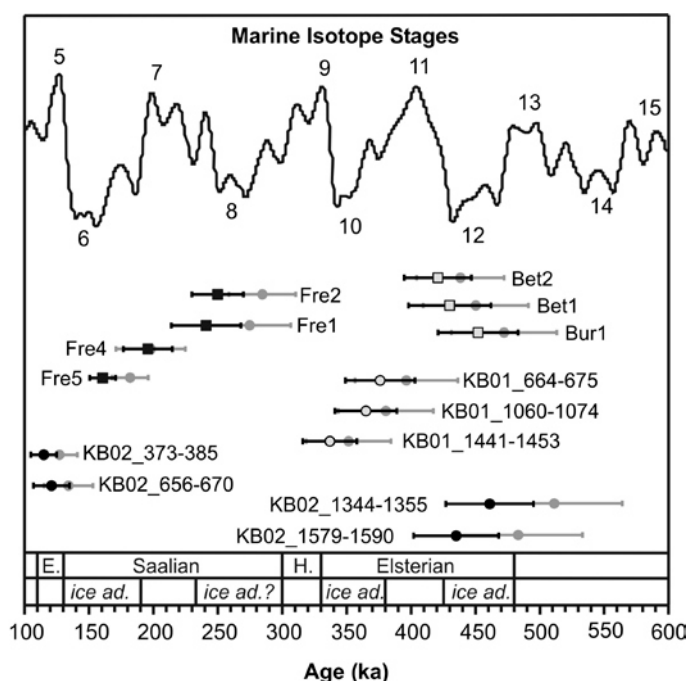


Fig. 10: Correlation of the determined uncorrected (black) and fading-corrected (grey) IR50 feldspar ages (ka) with the marine isotope stages (Lisiecki and Raymo, 2005). Error bars represent 1-sigma standard error. Chronostratigraphical units are based on this study.

3.5.1.1 Age underestimation

Age underestimation can occur if (i) anomalous fading is significant, and/or (ii) the natural signal is close to saturation. As for (i), an IRSL signal loss can result in age underestimation. As discussed above, the pulsed IRSL protocol was chosen to obtain a luminescence signal which is stable, more light-sensitive and less fading-dependent than other signals. The study of Buylaert et al. (2011) encouraged us to apply the fading correction model of Huntley and Lamothé (2001) to check for possible fading. The calculated fading rates were generally low ($\leq 1.4 \pm 0.2\%$ /decade; **Table 2A**) and consistently below the threshold of 1.5%/decade (Buylaert et al., 2011), therefore a fading correction was considered to be negligible. As shown in **Ta-**

ble 2A and **Fig. 10**, the fading-corrected feldspar ages lie in most cases within the same marine isotope stages as the fading-uncorrected ones.

As for (ii), underestimated depositional ages can be obtained when the natural signal is close to saturation. However, all of our mean D_e values were $<2 D_0$ (D_0 is the characteristic saturation dose) or 86% of the saturation level (**Table 2A**; Wintle and Murray, 2006; Buylaert et al., 2012). We assume that age underestimation caused by (nearly) saturated D_e values did not occur and can be excluded.

Consequently, we conclude that the effect of age underestimation for our samples, if any, is very small and will not affect our interpretation.

3.5.1.2 Age overestimation

The main possible cause for age overestimation is related to insufficient bleaching, which can be due to (i) insufficient bleaching of the sediment itself, and/or (ii) incorporation of subglacially eroded older material (Frechen et al., 2004; Fuchs and Owen, 2008; Houmark-Nielsen, 2008). As for (i), we were able to double-date two fluvial samples (KB02_373-385, KB02_656-670), whose quartz and feldspar ages agreed perfectly (**Table 2**). Interestingly, these samples had the highest overdispersion values (16.5 and 25.8%; **Table 2A**), suggesting insufficient bleaching to some extent. This observation, however, contradicts the good quartz and feldspar age agreement.

The overdispersion values for most of the glacial samples are low (0.0-7.1%; **Table 2A**), indicating that these deposits are likely to have been well bleached. Three samples (Fre2, Fre4, Fre5) had overdispersion values ranging from 11.9 to 17.4% (**Table 2A**), which might indicate poorer bleaching.

Evaluation of $D_e(t)$ plots can help to detect the bleaching characteristics (Bailey, 2003; Thomas et al., 2006; Fuchs and Owen, 2008), because a flat and plateau-like $D_e(t)$ plot is characteristic of good bleaching conditions. **Fig. 3C** shows a fairly flat $D_e(t)$ plot with D_e values slightly fluctuating around the mean D_e value. This is in accordance with luminescence dating results of glacial sediments from Arctic Russia, where a flat $D_e(t)$ -plot indicated sufficient bleaching, and quartz OSL ages were supported by independent age control (radiocarbon ages; Thomas et al., 2006). The study of Alexanderson and Murray (2012) showed that luminescence dating of glacial sediments is able to work although larger aliquots (2 mm) are used, when previously single-grain or small-sized aliquot measurements were conducted to extract only bleached grains of insufficiently bleached glacial samples. Given a certain transport distance to the ice-margin, glacial sediments can be sufficiently bleached (Fuchs and Ow-

en, 2008; Houmark-Nielsen, 2008; Alexanderson and Murray, 2012). Murray et al. (2012) found that ages based on both single-grain and large-sized aliquot measurements do not always agree with each other. Additional independent age control favoured the quartz OSL age derived from large aliquots. Based on previous studies and the analyses of our determined D_e values, we do not have strong indications for insufficient bleaching.

As for (ii), it is possible that older material was incorporated by subglacial erosion or slumping, resulting in age inversions (**Fig. 10**). A subsequent re-deposition of subglacially eroded sediment together with younger sediment, which has been bleached to a certain extent, can ultimately lead to insufficiently bleached grains, thus overestimated luminescence ages (Frechen et al., 2004; Fuchs and Owen, 2008; Houmark-Nielsen, 2008). Frechen et al. (2004) showed that such an age overestimation is displayed by a severe disagreement of luminescence and radiocarbon ages. In their case, sediment mixture is likely to have occurred due to subglacial erosion and re-deposition from plane-wall jets into a lake. We assume that the glacialfluvial delta systems of the Leine valley, characterised by subaerial delta plains, are likely to have been bleached to some extent (Fuchs and Owen, 2008; Houmark-Nielsen, 2008; Alexanderson and Murray, 2012).

A mixture of differently old sediments may also be caused by slope failure of e.g. steep delta systems and re-deposition of slumped material on the lower delta-slope or prodelta area. However, additional analysis of D_e histograms can help to identify this age overestimation by detecting a second prominent D_e peak. We were able to detect only very few outliers at higher doses (KB02_656-67, Fre4; **Fig. 4B, E**) but no significant second peak. However, our results are in accordance with the observations by Fuchs and Owen (2008) and Alexanderson and Murray (2012), indicating that the effect of age overestimation is likely to be small.

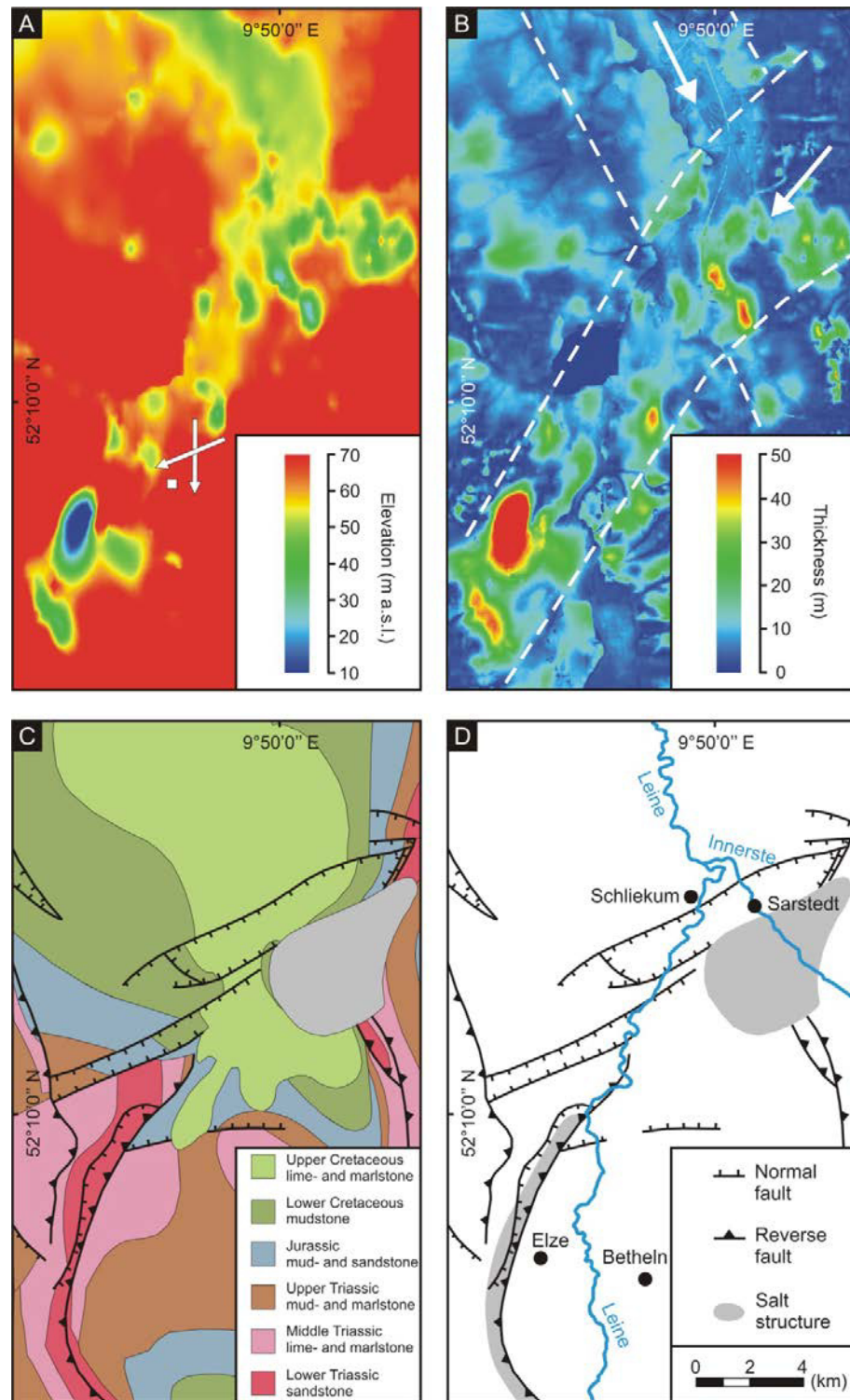
3.5.2 Evidence for repeated glaciations of the Leine valley during the Middle Pleistocene

From a geochronological point of view, the Leine-valley fill indicates repeated glaciations during the Middle Pleistocene (MIS 12 to MIS 6; **Fig. 10**). This is supported by our sedimentological and seismic data, which show a complex valley-fill architecture, which cannot be produced by a single ice advance-retreat cycle.

3.5.2.1 Glaciation during MIS 12 and MIS 10

During the Elsterian glaciation, at least two ice advances occurred into the study area, based on luminescence ages of ice-marginal deposits, ranging from 461 ± 34 to 421 ± 25 ka (MIS 12) and from 376 ± 27 to 337 ± 21 ka (MIS 10). The bedrock relief model and two different generations

Fig. 11: Bedrock relief model and modeled thickness and spatial distribution of Pleistocene deposits in the Leine valley, based on 1730 borehole logs. For location see **Fig. 1B**. **(A)** The bedrock relief model is characterized by a northeast-southwest trending erosional zone with local overdeepenings, interpreted to have formed by subglacial erosion during the MIS 10 ice advance. It cross-cuts a northwest-southeast trending erosional zone, which is interpreted to have formed during MIS 12. White arrows mark the direction of two different generations of striations (Jordan and Meyer, 1967). The older striations trend approximately north-south, the younger ones east-northeast-west-southwest. **(B)** Modelled thickness and spatial distribution of Pleistocene deposits. The dashed lines indicate two zones of increased sediment thickness, which are interpreted as the fill of subglacially eroded mini-basins. The inferred directions of ice advances during MIS 12 and MIS 10 are indicated by arrows. **(C)** Map of the Mesozoic and Cenozoic bedrock (modified after Baldschuhn and Kockel, 1987). **(D)** Structural map with the location of major salt structures (modified after Kockel, 1996).



(C) Map of the Mesozoic and Cenozoic bedrock (modified after Baldschuhn and Kockel, 1987). **(D)** Structural map with the location of major salt structures (modified after Kockel, 1996).

of striations (Jordan and Meyer, 1967) suggest an older ice advance from the north and a younger ice advance from the northeast (**Fig. 11A, B**). This is in accordance with data from northern and eastern Germany, where two Elsterian tills, separated by meltwater deposits, have

been mapped (Caspers et al., 1995; Eissmann, 2002; Litt et al., 2007; Ehlers et al., 2011; Lang et al., 2012). The clast composition of the older till is mainly derived from the Norwegian area, indicating an ice advance from the north for the older Elsterian glaciation (Meyer, 1970). From the Bay of Biscay, a significant input of terrigenous material has been recorded during both MIS 12 and MIS 10, also pointing to two separate ice advances during the Elsterian glaciation (Toucanne et al., 2009a, b). It is likely that during both ice advances glacial lakes were dammed in the Leine valley because of the northward blockage of river drainage systems (**Fig. 12**). During MIS 12, the lake level of glacial Lake Leine must have reached at least ~155 m a.s.l., as is indicated by the altitude of the foreset-topset transition of the Betheln delta (**Figs 6, 12A**). The Betheln ice-marginal delta complex is characterised by two transgressive-regressive cycles (**Fig. 6B**), which might either point to (i) local ice-margin oscillations, causing the repeated closure and opening of lake overflows; or (ii) two separate ice advances during MIS 12, which would be supported by data from the North Sea Basin (Stewart and Lonergan, 2011), Denmark (Houmark-Nielsen, 2011) and Schleswig-Holstein in northern Germany (Stephan, 2014). Alternatively, the older, not exposed delta deposits might be assigned to MIS 12, whereas the second delta complex might have been deposited during MIS 10. In this case, the depositional age would be overestimated, which is likely to be assigned to incomplete bleaching favoured by the combination of high-energy transport processes and a short delta plain. An indication for an age overestimation of the younger delta complex might come from the underlying bedrock with two different generations of striations (Jordan and Meyer, 1967).

The MIS 10 ice advance was associated with strong subglacial erosion, indicated by the formation of a ~4.0-6.5 km wide, northeast-southwest trending erosional zone with several local overdeepenings (**Fig. 11A**). The geometry and orientation of these overdeepenings were controlled by tectonic structures and lithological properties of the Mesozoic and Cenozoic bedrock (**Fig. 11C, D**). These mini-basins are 25-60 m deep, up to 3.5 km long and up to 2.5 km wide and correspond in size to many other subglacial basins (e.g., Cook and Swift, 2012). The deepest erosional features are developed above salt structures, where highly fractured rocks and an increased heat flow (cf. Grassmann et al., 2010) may have favoured bed coupling and plucking. Subglacial erosional processes partly included glacitectonic thrusting, as is indicated by displaced Cenozoic bedrock (Rohde, 1983). During rapid ice-margin retreat, overdeepenings were filled with fine-grained glacial-lacustrine deposits, partly rich in re-worked Tertiary lignite and amber (**Fig. 8**), which has also frequently been observed in late Elsterian tunnel valleys (Meyer, 2009; Stephan, 2014).

The maximum extent of the MIS 12 and MIS 10 ice-margins into the Leine valley is not exactly known. We assume that the ice-margin extended a few km further towards the south or southwest, respectively.

3.5.2.2 *Glaciation during MIS 8? and MIS 6*

During the Saalian glaciation, a renewed ice advance occurred, indicated by extensive till sheets and ice-marginal deposits near Freden, marking the maximum Middle Pleistocene ice advance into the study area. Luminescence dating of the Freden delta complex gave MIS 8 to MIS 7 (250 ± 20 to 241 ± 27 ka) and MIS 7 to MIS 6 (196 ± 19 to 161 ± 10 ka) ages. There are two possible explanations for this age difference of about 100 ka. (i) Samples Fre1 and Fre2 have been insufficiently bleached, leading to an overestimation of the depositional ages. However, insufficient bleaching seems to be unlikely because statistical results indicate Gaussian-like D_e distributions with low overdispersion values, pointing to relatively good bleaching conditions (**Fig. 4D**; **Table 2A**). Additionally, the relatively fine-grained sandy delta-foreset deposits require the presence of a larger delta plain, which would have allowed at least a certain bleaching degree (Fuchs and Owen, 2008; Houmark-Nielsen, 2008; Alexanderson and Murray, 2012). Therefore, we assume that the effect of incomplete bleaching is likely to be small. (ii) There have been two different ice advances into the study area and the ice-marginal delta complex consists of two different sediment bodies, one of them having a MIS 8 or early MIS 6 age, and the other one having a late MIS 6 age. **Fig. 1E** shows a digital elevation model of the Freden delta complex which has been reconstructed from old topographic maps. The oldest delta body (Fre1, Fre2) has been shed from a northeastern source (**Fig. 1E**). The determined luminescence ages imply a deposition during MIS 8 to MIS 7 (250 ± 20 to 241 ± 27 ka). We exclude a deposition during MIS 7 because no deep lake could have formed in the study area without ice-damming. In the northeastern pit, this delta body (**Fig. 5A, C**) is overlapped by fine-grained channelised delta or subaqueous fan deposits (delta body II), which differ in sedimentary facies and palaeocurrent directions (**Figs 1E, 5**). These sediments comprise flow till layers, are partly affected by glacetectonic deformation and are overlain by a basal till (**Fig. 5C**). Luminescence data of overlying younger delta deposits point to an early Saalian age (Fre4, 196 ± 19 ka). In the western pit, the sand-rich lowermost delta system is erosively overlain by coarse-grained channelised deposits (Fre5; **Fig. 5D**), which were shed from a western source (**Fig. 1E**) and gave a late Saalian age (161 ± 10 ka; **Table 2A**).

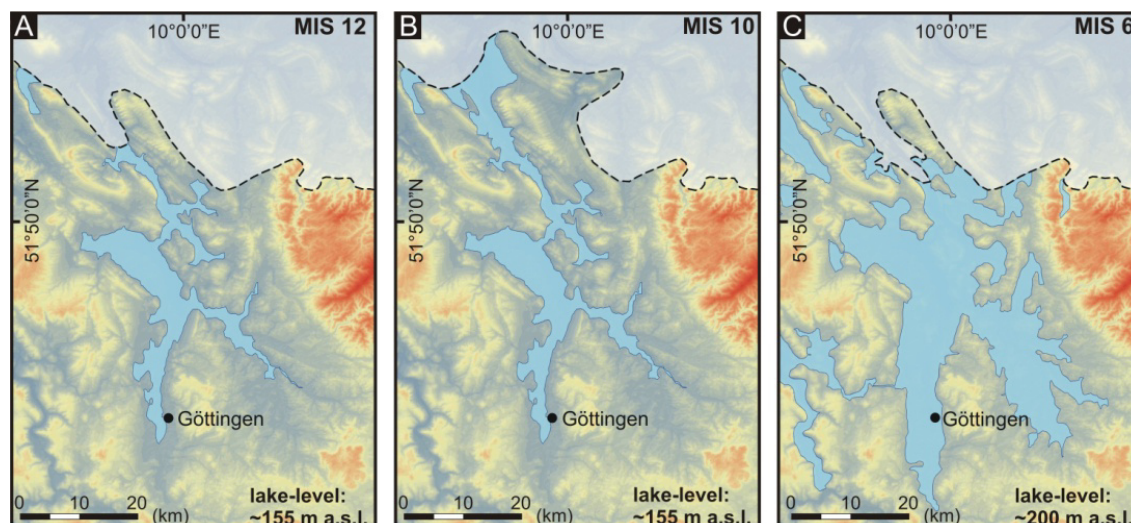


Fig. 12: Palaeogeographical reconstruction of glacial lakes (light blue areas) and inferred locations of the Middle Pleistocene ice-margins during (A) MIS 12, (B) MIS 10 and (C) MIS 6.

Based on the sedimentological and tectonic history and the luminescence data, we assume that the complex depositional architecture of the Freden delta complex is related to two ice advances that might have occurred during MIS 8 and MIS 6. This assumption would correspond with data from the Netherlands and Denmark, where amino acid racemization and luminescence ages cluster at around ~250 ka, thus pointing to an early Saalian glaciations during MIS 8 (Beets et al., 2005; Houmark-Nielsen, 2011; Kars et al., 2012). High values of terrigenous input are also reported for MIS 8 and MIS 6 from the Bay of Biscay (Toucanne et al., 2009a, b). These assumed two Saalian ice advances may correlate with the deposition of the two different tills of the older Saalian Drenthe glaciation in northern Germany (cf. Litt et al., 2007; Stephan, 2014).

3.6 Conclusions

- The Middle Pleistocene Leine-valley fill south of the North German lowlands bears evidence for repeated glaciations during MIS 12, MIS 10, MIS 8 and MIS 6. During these glaciations, ice-dammed lakes formed in the Leine valley and its tributaries. Based on detailed sedimentological data and the sensitivity analysis of the luminescence data, we assume that the estimated luminescence ages are reliable. Age underestimation can most probably be ruled out. The effect of age overestimation for most of the samples is assumed to be small.
- Luminescence dating of ice-marginal deposits point to a deposition between 461 ± 34 to 421 ± 25 ka (MIS 12) and between 376 ± 27 to 337 ± 21 ka (MIS 10), indicating at least two

ice advances into the Leine valley. The MIS 12 advance occurred from a northern and the MIS 10 advance from a northeastern direction, indicated by subglacial erosional structures, deeply incised into Mesozoic and Cenozoic bedrock. These separate ice advances are correlated with the deposition of two Elsterian tills in northern Germany and are consistent with the MIS 9 age of interglacial deposits preserved in tunnel valleys.

- Luminescence dating of the Freden delta complex bears evidence for two separate Saalian ice advances into the study area that might have occurred during MIS 8 and MIS 6. Estimated luminescence ages range from 250 ± 20 to 161 ± 10 ka. These two Saalian ice advances may correlate with the deposition of the two tills of the older Saalian Drenthe glaciation in northern Germany.
- The Elsterian and Saalian ice sheets approximately reached the same position in the Leine valley and were probably controlled by the formation of deep proglacial lakes in front of the advancing glaciers, which prevented a further southward advance.

Acknowledgements

Financial support by MWK Niedersachsen Project (11.2-76202-17-7/08) is gratefully acknowledged. We are grateful to Editor-in-Chief Jan A. Piotrowski, Lewis A. Owen and an anonymous reviewer for constructive comments, which helped to improve the manuscript. We thank LBEG (State Authority of Mining, Energy and Geology) and Hermann Wegener GmbH and Co. KG for providing borehole data, Fugro Consult GmbH for providing GeODin software for data management, BGR (Federal Institute for Geosciences and Natural Resources) and LIAG (Leibniz Institute for Applied Geophysics) for the permission to use the facilities at Grubenhagen for core description and sampling. Many thanks are due to the owners of the open-pit Ulrich at Freden and of the open-pits Fischer and Burgstemmen for permitting us to work on their properties, and Hermann Wegener GmbH and Co. KG and M. Büsse for the permission to drill on their properties. Celler Brunnenbau GmbH and Co. KG carried out the drilling and helped with core handling. S. Cramm, S. Grüneberg, W. Rode and D. Vogel (LIAG) carried out the seismic survey and K. Bußmann, T. Fandré, J. Meier, L. Pollok, M. Wahle, T. Wixwat, M. Zillmer helped with field work. Many thanks are also due to S. Mischke and S. Voges (Einbeck) for core photographs, S. Riemenschneider for technical support in the luminescence laboratory, D. Steinmetz for assistance in creating the GOCAD model, F. Busch for GIS work, B. Urban for determination of organic material and J. Lang for discussion.

References

- Adamiec, G., Aitken, M.J., 1998. Dose-rate conversion factors: update. *Ancient TL* 16, 37-50.
- Alexanderson, H., Murray, A.S., 2012. Luminescence signals from modern sediments in a glaciated bay, NW Svalbard. *Quaternary Geochronology* 10, 250-256.
- Allen, J.R.L., 1984. Sedimentary structures: their character and physical basis. *Developments in Sedimentology* 30, Part A, 1-663.
- Bailey, R.M., 2003. The use of measurement-time dependent single-aliquot equivalent-dose estimates from quartz in the identification of incomplete signal resetting. *Radiation Measurements* 37, 673-683.
- Baldschuhn, R., Kockel, F., 1987. Geologische Karte von Hannover und Umgebung 1: 100 000 – Quartär und Tertär abgedeckt. Niedersächsisches Landesamt für Bodenforschung, Bundesanstalt für Geowissenschaften und Rohstoffe.
- Balescu, S., Lamothe, M., 1994. Comparison of TL and IRSL age estimates of feldspar coarse grains from waterlain sediments. *Quaternary Science Reviews* 13, 437-444.
- Beets, D.J., Meijer, T., Beets, C.J., Cleveringa, P., Laban, C., van der Spek, A.J.F., 2005. Evidence for a Middle Pleistocene glaciation of MIS 8 age in the southern North Sea. *Quaternary International* 133-134, 7-19.
- Blair, T.C., McPherson, J.G., 1994. Alluvial fans and their natural distinction from rivers based on morphology, hydraulic processes, sedimentary processes, and facies assemblages. *Journal of Sedimentary Research* 64, 450-489.
- Brown, L.F., Fisher, W.L., 1977. Seismic-stratigraphic interpretation of depositional systems: examples from Brazilian rift and pull-apart basins. In: Payton, C.E. (ed.), *Seismic Stratigraphy – Applications to Hydrocarbon Exploration*. AAPG Memoir 26, 117-133.
- Busschers, F.S., Weerts, H.J.T., Wallinga, J., Cleveringa, P., Kasse, C., de Wolf, H., Cohen, K.M., 2005. Sedimentary architecture and optical dating of Middle and Late Pleistocene Rhine-Meuse deposits – fluvial response to climate change, sea-level fluctuation and glaciation. *Geologie en Mijnbouw* 84, 25-41.
- Busschers, F.S., van Balen, R.T., Cohen, K.M., Kasse, C., Weerts, H.J.T., Wallinga, J., Bunnik, F.P.M., 2008. Response of the Rhine-Meuse fluvial system to Saalian ice-sheet dynamics. *Boreas* 37, 377-398.
- Buylaert, J.-P., Huot, S., Murray, A.S., Van den Haute, P., 2011. Infrared stimulated luminescence dating of an Eemian (MIS 5e) site in Denmark using K-feldspar. *Boreas* 40, 46-56.

- Buylaert, J.-P., Jain, M., Murray, A.S., Thomsen, K.J., Thiel, C., Sohbati, R., 2012. A robust feldspar luminescence dating method for Middle and Late Pleistocene sediments. *Boreas* 41, 435-451.
- Caspers, G., Jordan, H., Merkt, J., Meyer K.-D., Müller, H., Streif, H., 1995. III. Niedersachsen. In Benda, L. (ed.), *Das Quartär von Deutschland*. Gebrüder Borntraeger, Berlin, 23-58.
- Clemmensen, L.B., Houmark-Nielsen, M., 1981. Sedimentary features of a Weichselian glaciolacustrine delta. *Boreas* 10, 229-245.
- Cohen, K.M., Gibbard, P., 2010. Global chronostratigraphical correlation table for the last 2.7 million years. Subcommission on Quaternary Stratigraphy, International Commission on Stratigraphy, Cambridge.
- Correggiari, A., Cattaneo, A., Trincardi, F., 2005. The modern Po delta system: lobe switching and asymmetric prodelta growth. *Marine Geology* 222-223, 49-74.
- Cook, S.J., Swift, D.A., 2012. Subglacial basins: Their origin and importance in glacial systems and landscapes. *Earth-Science Reviews* 115, 332-372.
- Crawford, J.M., Doty, W.E.N., Lee, M.R., 1960. Continuous signal seismograph. *Geophysics* 25, 95-105.
- Cunningham, A.C., Wallinga, J., 2010. Selection of integration time intervals for quartz OSL decay curves. *Quaternary Geochronology* 5, 657-666.
- Ehlers, J., Grube, A., Stephan, H.J., Wansa, S., 2011. Chapter 13 – Pleistocene Glaciations of North Germany - new results. In: Ehlers, J., Gibbard, P.L., Hughes, P.D. (eds.), *Quaternary Glaciations - Extent and Chronology – A closer look*. *Developments in Quaternary Science* 15, Elsevier, Amsterdam, 149-162.
- Eissmann, L., 2002. Quaternary geology of eastern Germany (Saxony, Saxon-Anhalt, South Brandenburg, Thuringia), type area of the Elsterian and Saalian Stages in Europe. *Quaternary Science Reviews* 21, 1275-1346.
- Fehrentz, M., Radtke, U., 1998. Lumineszenzdatierung an pleistozänen Schmelzwassersanden der Senne (östliches Münsterland). *Kölner Geographische Arbeiten* 70, 103-115.
- Frechen, M., Schwab, M.J., Sutter, I., 2004. Luminescence and radiocarbon dating of lake sediments from east Antarctica. In: Higham, T., Bronk Ramsey, C., Owen, C. (eds.), *Radiocarbon and archaeology: fourth international symposium St. Catherine's College, Oxford, 9-14 April 2002; conference proceedings*, Oxbow Books, 17-34.

- Frechen, M., Sierralta, M., Oezen, D., Urban, B., 2007. Uranium-series dating of peat from Central and Northern Europe. In: Sirocko, F., Claussen, M., Sánchez Goñi, M.F., Litt, T. (eds.), *The Climate of Past Interglacials. Developments in Quaternary Science 7*, Elsevier, Amsterdam, 93-117.
- Fuchs, M., Owen, L.A., 2008. Luminescence dating of glacial and associated sediments: review, recommendations and future directions. *Boreas* 37, 636–659.
- Galbraith, R.F., Roberts, R.G., Laslett, G.M., Yoshida, H., Olley, J.M., 1999. Optical dating of single and multiple grains of quartz from Jinmium rock shelter, Northern Australia: part I, experimental design and statistical models. *Archaeometry* 41, 339-364.
- Geyh, M.A., Müller H., 2005. Numerical $^{230}\text{Th}/\text{U}$ dating and a palynological review of the Holsteinian/Hoxnian Interglacial. *Quaternary Science Reviews* 24, 1861-1872.
- Gibbard, P.L., Clark, C.D. 2011. Chapter 7 - Pleistocene Glaciation Limits in Great Britain. In: Ehlers, J., Gibbard, P.L., Hughes, P.D. (eds.), *Quaternary Glaciations - Extent and Chronology - A Closer Look. Developments in Quaternary Science 15*, Elsevier, Amsterdam, 75-93.
- Ghose, R., Brouwer, J., Nijhof, V. 1996. A portable S-wave vibrator for high-resolution imaging of the shallow subsurface. *Proceedings of the 58th Annual Meeting, European Association of Geoscientists and Engineers, Expanded Abstracts*, MO37.
- Grassmann, S., Cramer, B., Delisle, G., Hantschel, T., Messner, J., Winsemann, J., 2010. pT-effects of Pleistocene glacial periods on permafrost, gas hydrate stability zones and reservoir of the Mittelplate oil field, northern Germany. *Marine and Petroleum Geology* 27, 298-306.
- Hall, A.M., Migoń, P., 2010. The first stages of erosion by ice sheets: Evidence from central Europe. *Geomorphology* 123, 349-363.
- Henningsen, D., 1983. Der Schwermineral-Gehalt der Drenthe-zeitlichen Schmelzwassersande in Niedersachsen. *E&G Quaternary Science Journal* 33, 133-140.
- Hilgers, A., 2007. The chronology of Late Glacial and Holocene dune development in the northern Central European lowland reconstructed by optically stimulated luminescence (OSL) dating. Ph.D. thesis, University of Cologne, 318 pp.
- Houmark-Nielsen, M. 2008. Testing OSL failures against a regional Weichselian glaciation chronology from southern Scandinavia. *Boreas* 37, 660-677.
- Houmark-Nielsen, M., 2011. Chapter 5 - Pleistocene Glaciations in Denmark: A Closer Look at Chronology, Ice Dynamics and Landforms. In: Ehlers, J., Gibbard, P.L., Hughes, P.D.

- (eds.), Quaternary Glaciations - Extent and Chronology – A closer look. Developments in Quaternary Science 15, Elsevier, Amsterdam, 47-58
- Huntley, J.D., Baril, M.R., 1997. The K content of the K-feldspars being measured in optical dating or in thermoluminescence dating. *Ancient TL* 15, 11-13.
- Huntley, J.D., Lamothe, M. 2001. Ubiquity of anomalous fading in K-feldspars and the measurement and correction for it in optical dating. *Canadian Journal of Earth Sciences* 38, 1093-1106.
- Huuse, M., Lykke-Andersen, H., 2000. Overdeepened Quaternary valleys in the eastern Danish North Sea: morphology and origin. *Quaternary Science Reviews* 19, 1233-1253.
- Jordan, H., Meyer, K.-D., 1967. Gletscherschrammen bei Burgstemmen südlich von Hannover. *E&G Quaternary Science Journal* 18, 198-203.
- Kaltwang, J., 1992. Die pleistozäne Vereisungsgrenze im südlichen Niedersachsen und im östlichen Westfalen. *Mitteilungen des Geologischen Instituts der Universität Hannover* 33, 1-161.
- Kars, R.H., Wallinga, J., Cohen, K.M., 2008. A new approach towards anomalous fading correction for feldspar IRSL dating - tests on samples in field saturation. *Radiation Measurements* 43, 786-790.
- Kars, R.H., Busschers, F.S., Wallinga, J., 2012. Validating post IR-IRSL dating on K-feldspars through comparison with quartz OSL ages. *Quaternary Geochronology* 12, 74-86.
- Kockel, F., 1996. *Geotektonischer Atlas von NW-Deutschland – 1: 300 000*. Bundesanstalt für Geowissenschaften und Rohstoffe, Hannover.
- Krbetschek, M.R., Degering, D., Alexowsky, W., 2008. Infrarot-Radiofluoreszenz-Alter (IR-RF) unter-saalezeitlicher Sedimente Mittel- und Ostdeutschlands. *Zeitschrift der Deutschen Gesellschaft für Geowissenschaften* 159, 133-140.
- Laban, C., van der Meer, J.J.M., 2011. Chapter 20 – Pleistocene Glaciation in the Netherlands. In: Ehlers, J., Gibbard, P.L., Hughes, P.D. (eds.), *Quaternary Glaciations - Extent and Chronology – A closer look*. Developments in Quaternary Science 15, Elsevier, Amsterdam, 247-260.
- Lamothe, M., Auclair, M., Hanazaoui, C., Huot, S., 2003. Towards a prediction of long-term anomalous fading of feldspar IRSL. *Radiation Measurements* 37, 493-498.
- Lang, J., Winsemann, J., Steinmetz, D., Polom, U., Pollok, P., Böhner, U., Serangeli, J., Brandes, C., Hampel, A., Winghart, S., 2012. The Pleistocene of Schöningen, Germany: a

complex tunnel valley fill revealed from 3D subsurface modelling and shear wave seismics. *Quaternary Science Reviews* 39, 86-105.

- Lee, J.R., Rose, J., Hamblin, R.J.O., Moorlock, B.S.P., Riding, J.B., Phillips, E., Barendregt, R.W., Candy, I., 2011. Chapter 6 – The Glacial History of the British Isles during the Early and Middle Pleistocene: Implications for the long-term development of the British Ice Sheet. In: Ehlers, J., Gibbard, P.L., Hughes, P.D. (eds.), *Quaternary Glaciations - Extent and Chronology – A closer look. Developments in Quaternary Science 15*, Elsevier, Amsterdam, 59-74.
- Lemons, M.A., Chan, M.A., 1999. Facies Architecture and Sequence Stratigraphy of Fine-Grained Deltas Along the Eastern Margin of Late Pleistocene Lake Bonneville, Northern Utah and Southern Idaho. *AAPG Bulletin* 83, 635-665.
- Lepper, J., 1984. Elster-Kaltzeit. In: Lepper, J. (ed.), *Erläuterungen zu Blatt Nr. 3725 Sarstedt. Geologische Karte von Niedersachsen 1: 25 000*. Niedersächsisches Landesamt für Bodenforschung, Hannover, 95-98.
- Lisiecki, L.E., Raymo, M.E., 2005. A Pliocene-Pleistocene stack of 57 globally distributed benthic $\delta^{18}O$ records. *Paleoceanography* 20, 1–17.
- Litt, T., Behre, K.-E., Meyer, K.-D., Stephan, H.-J., Wansa, S., 2007. Stratigraphische Begriffe für das Quartär des norddeutschen Vereisungsgebietes. *E&G Quaternary Science Journal* 56, 7-65.
- Lønne, I., 1995. Sedimentary facies and depositional architecture of ice-contact glaciomarine systems. *Sedimentary Geology* 98, 13-43.
- Lüthgens, C., Böse, M., Lauer, T., Krbetschek, M., Strahl, J., Wenske, D., 2011. Timing of the last interglacial in Northern Europe derived from Optically Stimulated Luminescence (OSL) dating of a terrestrial Saalian-Eemian-Weichselian sedimentary sequence in NE Germany. *Quaternary International* 241, 79-96.
- Lüttig, G., 1960. Neue Ergebnisse quartärgeologischer Forschung im Raume Alfeld – Hameln – Elze. *Geologisches Jahrbuch* 77, 337-390.
- Lutz, R., Kalka, S., Gaedicke, C., Reinhardt, L., Winsemann, J., 2009. Pleistocene tunnel valleys in the German North Sea: spatial distribution and morphology. *Zeitschrift der Deutschen Gesellschaft für Geowissenschaften* 160, 225-235.
- Marks, L., 2011. Chapter 23 – Quaternary Glaciation in Poland. In: Ehlers, J., Gibbard, P.L., Hughes, P.D. (eds.), *Quaternary Glaciations - Extent and Chronology – A closer look. Developments in Quaternary Science 15*, Elsevier, Amsterdam, 299-303.

- Meinsen, J., Winsemann, J., Roskosch, J., Brandes, C., Frechen, M., Dultz, S., Böttcher, J., 2014. Climate control on the evolution of Late Pleistocene alluvial-fan and aeolian sand-sheet systems in NW Germany. *Boreas* 43, 42-66.
- Meyer, K.-D., 1970. Zur Geschiebeführung des Ostfriesisch-Oldenburgischen Geestrückens. *Abhandlungen des Naturwissenschaftlichen Vereins zu Bremen* 37, 227-246.
- Meyer, K.-D., 2009. Bernstein-Vorkommen in Niedersachsen – Alter, Herkunft und Transport. Amber deposits in Lower Saxony - Age, origin and transport. *Die Kunde N.F.* 60, 39-47.
- Miall, A.D., 1985. Architectural-element analysis: a new method of facies analysis applied to fluvial deposits. *Earth-Science Reviews* 22, 261-308.
- Mitchum, R.M., Vail, P.R., Sangree, J.B., 1977. Seismic stratigraphy and global changes of sea-level, Part 6: stratigraphic interpretation of seismic reflection patterns in depositional sequences. In: Payton, C.E. (ed.), *Seismic Stratigraphy – Applications to Hydrocarbon Exploration*. AAPG Memoir 26, 117-133.
- Murray, A.S., Wintle, A.G., 2000. Luminescence dating of quartz using an improved single-aliquot regenerative-dose protocol. *Radiation Measurements* 32, 57-73.
- Murray, A.S., Wintle, A.G., 2003. The single aliquot regenerative dose protocol potential form improvements in reliability. *Radiation Measurements* 37, 377-381.
- Murray, A.S., Thomsen, K.J., Masuda, N., Buylaert, J.-P., Jain, M., 2012. Identifying well-bleached quartz using the different bleaching rates of quartz and feldspar luminescence signals. *Radiation Measurements* 47, 688-695.
- Olley, J.M., Caitcheon, G.G., Roberts, R.G., 1999. The origin of dose distributions in fluvial sediments, and the prospect of dating single grains from fluvial deposits using optically stimulated luminescence. *Radiation Measurements* 30, 207-217.
- Pawley, S.M., Bailey, R.M., Rose, J., Moorlock, B.S.P., Hamblin, R.J.O., Booth, S.J., Lee, J.R., 2008. Age limits on Middle Pleistocene glacial sediments from OSL dating, north Norfolk, UK. *Quaternary Science Reviews* 27, 1363-1377.
- Pawley, S.M., Toms, P., Armitage, S.J., Rose, J., 2010. Quartz luminescence dating of Anglian Stage (MIS 12) fluvial sediments: comparison of SAR age estimates to the terrace chronology of the Middle Thames valley, UK. *Quaternary Geochronology* 5, 569-582.
- Pitkäranta, R., Lunkka, J.-P., Eskola, K., 2014. Lithostratigraphy and Optically Stimulated Luminescence age determinations of pre-Late Weichselian deposits in the Suupohja area, western Finland. *Boreas* 43, 193-207.

- Polom, U., 2006. Vibration Generator for Seismic Applications. United States Patent No. US 7,136,325 B2.
- Polom, U., Bagge, M., Wadas, S., Winsemann, J., Brandes, C., Binot, F., Krawczyk, C.M., 2013. Surveying near-surface depocentres by means of shear wave seismics. *First Break* 31, 63-75.
- Posamentier, H.W., Vail, P.R., 1988. Eustatic controls on clastic deposition II – sequence and system tract models. In: Wilgus, C.K., Hastings, B.S., Kendall, C.G.St.C., Posamentier, H.W., Ross, C.A., Van Wagoner, J.C. (eds.), *Sea Level Changes – An Integrated Approach*. SEPM Special Publication 42, 125-154.
- Prescott, J.R., Hutton, J.T., 1994. Cosmic ray contribution to dose rates for luminescence and ESR dating: large depths and long-term time variations. *Radiation Measurements* 23, 497-500.
- Preusser, F., 1999. Lumineszenzdatierung fluviatiler Sedimente: Fallbeispiele aus der Schweiz und Norddeutschland. *Kölner Forum für Geologie und Paläontologie* 3, 1-62.
- Rausch, M., 1977. Fluß-, Schmelzwasser- und Solifluktuationsablagerungen im Terrassengebiet der Leine und der Innerste. *Mitteilungen des Geologischen Instituts der Technischen Universität Hannover* 14, 1-84.
- Rohde, P., 1983. Erläuterungen zu Blatt Nr. 3742 Pattensen. *Geologische Karte von Niedersachsen – 1: 25 000*. 192 pp. Niedersächsisches Landesamt für Bodenforschung, Hannover.
- Rohde, P., 1994. Weser und Leine am Berglandrand zur Ober- und Mittelterrassen-Zeit. *E&G Quaternary Science Journal* 44, 106-133.
- Schokker, J., Koster, E.A., 2004. Sedimentology and facies distribution of Pleistocene cold-climate aeolian and fluvial deposits in the Roer Valley Graben (Southeastern Netherlands). *Permafrost and Periglacial Processes* 15, 1-20.
- Sejrup, H.P., Hjelstuen, B.O., Bahlgren, K.I.T., Haflidason, H., Kuijpers, A., Nygård, A., Praeg, D., Stoker, M.S., Vorren, T.O., 2005. Pleistocene glacial history of the NW European continental margin. *Marine and Petroleum Geology* 22, 1111-1129.
- Sierralta, M., Frechen, M., Urban, B., 2011. $^{230}\text{Th}/\text{U}$ dating results from opencast mine Schöningen. In: Behre, K.-E. (ed.), *Die chronologische Einordnung der paläolithischen Fundstellen von Schöningen*. *Forschungen zur Urgeschichte im Tagebau von Schöningen*. Schriftenreihe Forschungen im Tagebau Schöningen 1. Verlag des Römisch-Germanischen Zentralmuseums, Mainz, 143-154.

- Spooner, N.A., 1994. The anomalous fading of infrared-stimulated luminescence from feldspars. *Radiation Measurements* 23, 625-632.
- Stephan, H.-J., 2014. Climato-stratigraphic subdivision of the Pleistocene in Schleswig-Holstein, Germany and adjoining areas. *E&G Quaternary Science Journal* 63, 3-18.
- Stewart, M.A., Lonergan, L., 2011. Seven glacial cycles in the middle-late Pleistocene of northwest Europe: Geomorphic evidence from buried tunnel valleys. *Geology* 39, 283-286.
- Thiel, C., Buylaert, J.P., Murray, A., Terhorst, B., Hofer, I., Tsukamoto, S., Frechen, M., 2011. Luminescence dating of the Stratzing loess profile (Austria) – Testing the potential of an elevated temperature post-IR IRSL protocol. *Quaternary International* 234, 23–31.
- Thomas, P.J., Murray, A.S., Kjær, K.H., Funder, S., Larsen, E., 2006. Optically Stimulated Luminescence (OSL) dating of glacial sediments from Arctic Russia – depositional bleaching and methodological aspects. *Boreas* 35, 587-599.
- Toucanne, S., Zaragosi, S., Bourillet, J.F., Cremer, M., Eynaud, F., Van Vliet-Lanoë, B., Penaud, A., Fontanier, C., Turon, J.L., Cortijo, E., Gibbard, P.L., 2009a. Timing of massive „Fleuve Manche“ discharges over the last 350 kyr: insights into the European ice-sheet oscillations and the European drainage network from MIS 10 to 2. *Quaternary Science Reviews* 28, 1238–1256.
- Toucanne, S., Zaragosi, S., Bourillet, J.F., Gibbard, P.L., Eynaud, F., Giraudeau, J., Turon, T.L., Cremer, M., Cortijo, E., Martinez, P., Rossignol, L., 2009b. A 1.2 Ma record of glaciation and fluvial discharge for the west European Atlantic margin. *Quaternary Science Reviews* 28, 2974-2981.
- Tsukamoto, S., Denby, P.M., Murray, A.S., Bøtter-Jensen, L., 2006. Time-resolved luminescence from feldspars: New insight into fading. *Radiation Measurements* 41, 790-795.
- Urban, B., Sierralta, M., Frechen, M., 2011. New evidence for vegetation development and timing of Upper Middle Pleistocene interglacials in Northern Germany and tentative correlations. *Quaternary International* 241, 125-142.
- Vollbrecht, A., Tanner, D.C., 2011. Der Leinetalgraben als Teil einer regionalen Pull-Apart-Struktur. In: Leiss, B., Tanner, D.C., Vollbrecht, A., Arp, G. (eds.), *Neue Untersuchungen zur Geologie der Leinetalgrabenstruktur. Bausteine zur Erkundung des geothermischen Potentials der Region*. Universitätsdrucke Göttingen, Göttingen, 9-15.

- Wallinga, J., Törnqvist, T.E., Busschers, F.S., Weerts, H.J.T., 2004. Allogenic forcing of the late Quaternary Rhine-Meuse fluvial record: the interplay of sea-level change, climate change and crustal movements. *Basin Research* 16, 535-547.
- Winsemann, J., Asprion, U., Meyer, T., Schramm, C., 2007. Facies characteristics of Middle Pleistocene (Saalian) ice-margin subaqueous fan and delta deposits, glacial Lake Leine, NW Germany. *Sedimentary Geology* 193, 105-129.
- Winsemann, J., Brandes, C., Polom, U., 2011a. Response of a proglacial delta to rapid high-magnitude lake-level change: an integration of outcrop data and high-resolution shear-wave seismics. *Basin Research* 23, 22-52.
- Winsemann, J., Brandes, C., Polom, U., Weber, C., 2011b. Depositional architecture and palaeogeographic significance of Middle Pleistocene glaciolacustrine ice marginal deposits in northwestern Germany: a synoptic overview. *E&G Quaternary Science Journal* 60, 212-235.
- Winsemann, J., Hornung, J.J., Meinsen, J., Asprion, U., Polom, U., Brandes, C., Bußmann, M., Weber, C., 2009. Anatomy of a subaqueous ice-contact fan and delta complex, Middle Pleistocene, north-west Germany. *Sedimentology* 56, 1041-1076.
- Wintle, A.G., Murray, A.S., 2006. A review of quartz optically stimulated luminescence characteristics and their relevance in single-aliquot regeneration dating protocols. *Radiation Measurements* 41, 369-391.

Online supplementary data to publication 2
Table S1: Information about luminescence samples.

Sample	Lab. number	Location	Longitudes and latitudes	Depth b.s. (m)	Altitude (m a.s.l.)	Grain size (μm)
Bet1	2597	Betheln	E 9°47'49.40" N 52°07'45.84"	2.90	133.00	100-150
Bet2	2662	Betheln	E 9°47'47.39" N 52°07'44.69"	1.80	150.00	150-200
Bur1	2663	Burgstemmen	E 9°45'57.65" N 52°07'30.76"	2.00	112.00	150-200
Fre1	2598	Freden	E 9°51'42.69" N 51°56'13.83"	6.30	142.00	100-200
Fre2	2599	Freden	E 9°51'50.25" N 51°56'09.31"	5.40	149.00	100-150
Fre4	2826	Freden	E 9°52'9.20" N 51°56'15.12"	1.80	151.00	150-200
Fre5	2827	Freden	E 9°51'45.9" N 51°56'10.48"	9.00	159.00	150-200
KB01_664-675	2600	Sarstedt	E 9°49'26.35" N 52°14'1.23"	6.69	54.35	100-150
KB01_1060-1074	2601	Sarstedt	E 9°49'26.35" N 52°14'1.23"	10.67	50.37	100-150
KB01_1441-1453	2602	Sarstedt	E 9°49'26.35" N 52°14'1.23"	14.47	46.75	100-150
KB02_373-385	2621	Schliekum	E 9°48'52.78" N 52°14'03.99"	3.79	70.33	150-200
KB02_656-670	2622	Schliekum	E 9°48'52.78" N 52°14'03.99"	6.63	67.49	150-200
KB02_1344-1355	2623	Schliekum	E 9°48'52.78" N 52°14'03.99"	13.50	60.63	150-200
KB02_1579-1590	2624	Schliekum	E 9°48'52.78" N 52°14'03.99"	15.85	58.73	150-200

Table S2: Seismic acquisition parameters.

Shear wave reflection recording parameters	
Recording system	Geometrics Geode, 123 channels (Geometrics Inc., Tulsa OK, U.S.A.), 5 modules of 24 channels each (data), 1 module of 8 channels (aux)
Geophone type	Single geophone SM6-H 10 Hz (horizontal), SH configuration
Receiver interval	1 m
Recording time	12 s (non-correlated)
Sampling interval	1 ms
Recording filter	---
Polarity	SEG convention
File format	SEG2
Data storage type	Unstacked, non-correlated
Source	ELVIS SH shear wave vibrator, electrodynamic, wheelbarrow mounted
Source interval	4 m
Source signal	20-160 Hz linear Sweep, 10 s duration, 100 ms cos-taper
Recording time after correlation	2 s
Vibration count/location	2 ([+Y] – [-Y] alternating vibrations)

Table S3: (A) Pulsed IRSL SAR protocol for coarse-grained potassium-rich feldspar measurements; (B) pIRIR protocol for coarse-grained quartz measurements (KB02_373-385 and KB02_656-670).

Run	(A) Feldspar treatment
1	Dose
2	Preheat, 60 s @ 250°C
3	Pulsed IR stimulation, 400 s @ 50°C (on: 50 μ s; off: 200 μ s)
4	Test dose
5	Cutheat, 60 s @ 250°C
6	Pulsed IR stimulation, 400 s @ 50°C (on: 50 μ s; off: 200 μ s)
7	Pulsed IR stimulation, 100 s @ 200°C
8	Return to step 1

Run	(B) Quartz treatment
1	Dose
2	Preheat, 10 s @ 260°C
3	IR stimulation, 100 s @ 50°C
4	OSL stimulation, 40 s @ 125°C
5	Test dose
6	Cutheat 0 s @ 240°C
7	IR stimulation, 100 s @ 50°C
8	OSL stimulation, 40 s @ 125°C
9	Return to step 1

Table S4: Clast composition of gravel samples from cores KB01 and KB02. Pebble-sized clasts were divided into three groups, regarding their provenance: (1) clasts with a Scandinavian/Baltic provenance, (2) clasts derived from the adjacent Mesozoic bedrock and river catchments and (3) clasts derived from the Palaeozoic bedrock of the river catchments.

	Depth b.s. (m)	(1) Sc./Ba. (%)	(2) Mesozoic (%)	(3) Palaeozoic (%)
KB01	2.00-2.33	1	66	33
	2.33-2.66	1	63	37
	2.66-3.00	1	62	37
	3.35-3.66	+	75	25
	3.66-4.00	1	66	33
	4.40-4.70	4	71	25
	4.70-5.00	0	50	50
	5.00-5.33	5	39	56
	5.33-5.66	4	40	56
	5.66-6.00	2	34	64
KB02	3.35-3.41	11	55	34
	9.25-9.50	31	55	14
	9.50-9.75	31	59	9
	9.75-10.00	29	55	16
	10.20-10.45	33	52	14
	10.45-10.70	21	72	7
	10.70-11.00	25	60	15
	11.00-11.60	14	83	3
Freden		16	70	14
		13	72	15
		14	67	19
Betheln/ Burgstemmen		9 ¹	89 ¹	2 ¹
		14 ²	70 ²	5 ²

¹Data from Lüttig (1960).

²Data from Rausch (1977).

Table S5: Transparent heavy mineral association of sand samples (cf. Henningsen, 1983). Grt = garnet; Hbl, gr./br. = hornblende, green-/brown-coloured; Ep = epidote group; St = staurolite; Ky = kyanite; Sil = sillimanite; And = andalusite; Aug = augite; Opx = orthopyroxene; Tur = tourmaline; Zrn = zircon; Ap = apatite; + = ≤1%; (1) Scandinavian/Baltic provenance; (2) southern provenance of the river catchment area; *term is descriptive because minerals of this group may predominantly be associated with philipstadite.

(%)	Bet1	Bet2	Bur1	Fre1	Fre2	KB01			KB02			
	2661	2662	2663	2598	2599	2600	2601	2602	2621	2622	2623	2624
(1) Grt	25	37	46	26	21	26	10	11	28	34	37	50
(1) Hbl, gr.	23	19	14	23	31	26	37	31	19	23	19	14
(1) Ep	28	26	21	24	29	27	35	42	22	21	26	16
(1) St	2	2	2	3	3	1	1	1	3	3	2	3
(1) Ky	1	2	0	2	2	3	1	1	1	0	2	2
(1) Sil	1	1	0	2	1	1	1	0	1	2	1	1
(1) And	+	+	0	0	1	+	0	1	0	1	+	1
(2) Aug	1	1	+	3	1	0	+	+	8	2	1	1
(2) Opx	0	0	0	0	0	1	1	+	3	2	0	0
(2) Hbl, br.*	8	7	12	4	3	8	10	4	4	3	7	8
(2) Tur	2	3	2	3	4	2	1	4	6	6	3	1
(2) Zrn	6	2	3	7	3	3	1	4	3	2	2	1
(2) Ap	1	0	0	+	0	0	+	1	1	0	0	0
Rest	≤2	-	-	≤3	1	≤2	<2	-	1	1	-	2

Table S6: Core description and interpretation (continued on the next page).

Core	Description	Interpretation
KB01		
0.00-2.27 m	Core loss	-
2.27-6.22 m	Normally graded pebble to cobble gravel with a coarse-grained sand matrix. Bed contacts are erosive. Individual beds are 40-120 cm thick.	Fluvial bedload. The normally graded gravel probably represents migrating 3D dunes (Allen, 1984).
6.22-8.55 m	Large-scale planar cross-stratified medium-grained sand, alternating with ripple-trough cross-laminated medium-grained sand. Beds are 40-80 cm thick and bed contacts are sharp. Very characteristic is the occurrence of reworked lignite in foreset beds.	Lower to upper delta-slope deposits. The large-scale planar cross-stratified medium-grained sand is interpreted to represent downslope migrating 2D dunes (Clemmensen and Houmark-Nielsen, 1981; Winsemann et al., 2007).
8.55-16.00 m	Climbing-ripple cross-laminated fine-grained sand and silt. In the lower succession, climbing-ripple cross-laminated beds form 65-145 cm thick fining-upward successions. Upsection climbing-ripple cross-laminated beds form 140 cm thick thickening and coarsening-upward sequences. Very characteristic is the occurrence of reworked lignite in ripple foreset beds.	Lower delta-slope deposits. Thick beds with climbing-ripple cross-lamination indicate high sedimentation rates and deposition from sustained waning and waxing turbulent flows (Clemmensen and Houmark-Nielsen, 1981; Winsemann et al., 2007).
16.00-18.00 m	Very thin- to thin-bedded (0.1-4 cm) alternations of fine-grained sand, silt and clay. Individual beds commonly consist of intervals of normally graded or massive sand that fines upwards into planar-parallel laminated and/or ripple cross-laminated sand and silt, and finally into laminated or massive mud. Beds are commonly normally graded and show planar-parallel and ripple trough-cross lamination. Ripples partly form climbing bed sets. Bed contacts are sharp or gradual. Soft-sediment deformation structures, such as load casts and flame structures are common. Deposits are characterized by metre-scale thickening- and fining-upward successions. Towards the top, 1-5 mm thick layers with reworked lignite are intercalated.	Lower delta-slope deposits (Lemons and Chan, 1999; Winsemann et al., 2007). Normal grading and fining of individual beds reflect deposition from waning low-density turbidity currents. The frequent soft-sediment deformation structures indicate high sedimentation rates.
KB03		
18.00-24.22 m	Very thin- to thin-bedded (0.2-7 cm) alternations of fine-grained sand, silt and clay. Beds are commonly normally graded and/or planar-parallel laminated. Bed contacts are sharp, erosive or gradual. Soft-sediment deformation structures, such as load casts, flame structures, fluid escape structures, convolute and contorted bedding are common. Deposits are characterized by an overall coarsening- and thickening-upward trend.	Prodelta or lower delta-slope deposits (Lemons and Chan, 1999). The normally graded and/or planar-parallel laminated sand, silt and clay is interpreted to have been deposited from waning low density turbidity currents. The frequent soft-sediment deformation structures indicate high sedimentation rates.
≥24.22 m	Structureless marlstone.	Upper Cretaceous bedrock (Rohde, 1983).

Table S6: Core description and interpretation.

Core	Description	Interpretation
KB02		
0.00-0.75 m	Core loss	-
0.75-2.08 m	Massive, planar-parallel and ripple-trough cross-laminated silt. The deposits show an overall fining-upward trend.	Wind ripple cross-lamination, partly deposited on a wet surface (Schokker and Koster, 2004; Meinsen et al., 2014).
2.08-7.90 m	Ripple-trough cross-laminated silt and planar cross-stratified sand and pebbly sand. Bed contacts are sharp. Individual cross-sets are 10-75 cm thick.	Fluvial bedload. The large-scale cross-stratified pebbly sand and sand represents migrating 2D or 3D dunes (Allen, 1984).
7.90-11.00 m	Normally graded pebble to cobble gravel with a coarse- to fine-grained sand matrix, interbedded with ripple cross-laminated sand and silt. Components have a high proportion of material derived from Scandinavia and/or the Baltic area. Bed contacts are sharp. Individual gravel beds are 50-75 cm thick, sand and silt beds are 10-25 cm thick.	Glacifluvial bedload. The normally graded gravel probably represents migrating 3D dunes (Allen, 1984)
11.00-11.60 m	Normally graded pebble to cobble gravel. The matrix consists of coarse- to fine-grained sand. Bed contacts are erosive. Individual gravel beds are 10-60 cm thick.	Fluvial bedload. The normally graded gravel probably represents migrating 3D dunes (Allen, 1984).
11.60-14.35 m	Normally graded and ripple-trough cross-laminated coarse- to fine-grained sand and silt. Contorted bedding. Individual beds are 40-70 cm thick and bed contacts are mainly sharp.	Glacilacustrine subaqueous fan or delta deposits (Lønne, 1995; Winsemann et al., 2009).
14.35-15.55 m	Massive diamiction. The matrix consists of a poorly sorted mixture of clay, silt and fine- to coarse-grained sand. Components have a high proportion of material derived from Scandinavian and/or the Baltic area. One quartzite clast is striated.	The striated clast and high content of components with a Scandinavian and/or Baltic provenance are indicative for a till (Rausch 1977).
15.55-16.75 m	Massive, normally graded, planar and trough cross-stratified coarse- to medium-grained sand. Beds are 30-45 cm thick. Bed contacts are sharp.	Glacilacustrine subaqueous fan or delta deposits (Lønne 1995; Winsemann et al., 2009).
≥16.75 m	Structureless marlstone.	Upper Cretaceous bedrock (Rohde, 1983).

Chapter 4

Publication 3

This chapter has been submitted to *Geochronometria* (in review).

Luminescence dating of fluvial deposits from the Weser valley, Germany: a comparison with independent age control

Julia Roskosch¹⁾, Sumiko Tsukamoto²⁾, Manfred Frechen²⁾

- 1) Institut für Geologie, Leibniz Universität Hannover, Callinstraße 30, D-30167 Hannover, Germany
- 2) Leibniz Institute for Applied Geophysics (LIAG), Geochronology and Isotope Hydrology, Stilleweg 2, D-30655 Hannover, Germany

Abstract

Luminescence dating was applied on coarse-grained monomineralic potassium-rich feldspar and polymineralic fine-grained minerals of five samples derived from fluvial deposits of the River Weser in northwestern Germany. We used a pulsed infrared stimulated luminescence (IRSL) single aliquot regenerative (SAR) dose protocol with an IR stimulation at 50°C for 400 s (50 μs on-time and 200 μs off-time). In order to obtain a stable luminescence signal, only off-time IRSL signal was recorded. Anomalous fading was intended to be reduced by using the pulsed IRSL signal measured at 50°C (IR₅₀), but fading correction was still necessary due to moderate fading rates. Performance tests gave solid results. Fading corrected pulsed IR₅₀ ages revealed two major fluvial aggradation phases during the Middle and Late Pleistocene, namely during marine isotope stage (MIS) 5 (100±5 ka) and from late MIS 5b to MIS 4 (77±6 ka to 68±5 ka). Our data is consistent with and supported by ²³⁰Th/U dating results from underlying interglacial deposits of the same pit, which are correlated with MIS 7c to early MIS 6.

4.1 Introduction

Optically stimulated luminescence (OSL) dating has been applied to fluvial deposits in order to give new insights into the timing of fluvial aggradation and degradation (e.g., Wallinga, 2002; Busschers et al., 2008; Cordier et al., 2010; Lauer et al., 2010). The major difficulty in dating fluvial sediments by means of luminescence is mainly caused by the occurrence of insufficient bleaching of the luminescence signal, which, if left undetected, can lead to overestimated depositional ages (e.g., Murray et al., 1995; Gemmell, 1997; Olley et al., 1999; Stokes et al., 2001). In a fluvial environment, insufficient bleaching can be caused by different environmental conditions, such as water depth, transport distance and the mode of transport. In the water column, sunlight is being attenuated and therefore generally hampers the probability for the transported minerals to be sufficiently bleached. Furthermore, rapid erosion and transport due to storm, high-discharge and flooding events may also limit the time needed for resetting the luminescence signal (cf. Wallinga, 2002; Jain et al., 2004; Rittenour, 2008).

In order to check if the problem related to insufficient bleaching exists, one can perform both feldspar and quartz measurement on the fluvial deposits (e.g., Wallinga et al., 2001; Frechen et al., 2008; Cordier et al., 2010; Roskosch et al., 2015). Since the signals of both minerals are reset at different rates, an age agreement indicates good bleaching conditions prior to deposition (Murray et al., 2012). However, the use of quartz minerals for luminescence measurements is often restricted to younger deposits (e.g., Fuchs and Lang, 2001; Lewis et al., 2001; Wallinga, 2002; Briant et al., 2006; Busschers et al., 2008) due to its comparably lower saturation level. In some rare cases, Middle and Late Pleistocene fluvial deposits could be dated (e.g., Lewis et al., 2001; Briant et al., 2006; Busschers et al., 2008), which benefited from relatively low dose rates (less than 1 Gy ka^{-1} ; Briant et al., 2006; Busschers et al., 2008).

The quartz luminescence signal is much more light-sensitive, thus faster to bleach than the feldspar luminescence signal, but feldspar minerals allow for dating comparably older (fluvial) sediments (infrared-radiofluorescence used by e.g., Krbetschek et al., 2008; Lauer et al., 2011) due to the higher saturation limit of the luminescence signal. Yet, they may suffer from a certain signal loss over time, referred to as anomalous fading (Wintle, 1973; Aitken, 1985; Spooner, 1994). However, in order to identify the limits of different dating methods, including their uncertainties, and to calibrate the chronological framework, independent age control can be substantially helpful. Independent age control can be provided e.g. by additional radiocarbon (^{14}C) dating, electron spin resonance (ESR) dating, amino acid racemization (AAR) or uranium-thorium ($^{230}\text{U}/\text{Th}$) dating of (i) the sediment itself or of (ii) the under- and/or overlying deposits, depending on the availability of appropriate dating material (e.g., organic matter).

Given the fact that results of all applied dating methods are consistent with each other and in stratigraphic order, the accuracy and reliability of the performed dating techniques can be proven.

In this study, we present new feldspar luminescence ages of fluvial deposits in northwestern Germany, which are tested against independent age control based on $^{230}\text{U}/\text{Th}$ dating of underlying interglacial deposits.

4.2 Study area and previous research

4.2.1 Study area

The study area is located in the southern Weser valley in northwestern Germany (**Fig. 1A**) and is characterised by up to 530 m high mountain ridges of the Central German Uplands and the broad valley of the River Weser (**Fig. 1B**). Here, the folded Variscan basement is unconformably overlain by Lower Permian (Rotliegend) red beds, Upper Permian (Zechstein) marine evaporites and carbonates, Lower Triassic (Buntsandstein) sandstones and Middle Triassic (Muschelkalk) shallow marine sediments (Lepper and Mengeling, 1990; Lepper, 1991). From the late Cretaceous to Neogene, these sediments experienced uplift, which led to a subsequent incision of the River Weser that formed its isoclinal valley between the Buntsandstein anticlinal at its west and the outcropping and steep cuestas of the Lower Muschelkalk at its east during the subsequent Neogene to Late Pleistocene (Grupe, 1912, 1929).

The Nachtigall pit is located at the western flank of the Buntsandstein anticlinal about 5 km southwest of Holzminden (**Fig. 1B**). Its sedimentary record comprises Middle Pleistocene (Saalian) fluvial deposits of the River Weser (Winsemann et al., *subm.*), which are referred to as Older and Younger Middle Terraces (e.g., Rohde et al., 2012), and are intercalated with interglacial limnic and fen peat of the so-called Nachtigall-Complex (Kleinmann et al., 2011; Waas et al., 2011). Based on Rohde et al. (2012), the fluvial deposits are overlain by Late Pleistocene slope sediments and loess. Winsemann et al. (*subm.*) interpreted the upper part of the sedimentary record of the Nachtigall pit as fine-grained floodplain and loess deposits.

4.2.2 Previous research

Reconstruction of the fluvial terrace architecture of the River Weser is largely based on lithostratigraphy and topographic height (Rohde, 1983, 1989, 1994). Rohde (1989, 1994) mapped up to 11 terrace levels, recording about 170 m of fluvial incision during the



Fig. 1: (A) Map of northern central Europe. The black box marks the study area. The hill-shaded relief model is based on SRTM data. (B) Close-up view of the study area of Weser valley with location of the Nachtigall pit. The hill-shaded relief model is based on SRTM data.

Pleistocene. The fluvial terrace architecture is recently being re-examined by Winsemann et al. (subm.).

Studies regarding the deposits of the Nachtigall pit go back to the 19th century (e.g., Dechen, 1884; Carthaus, 1886; Koken, 1901). Deposition of the interglacial deposits has been assigned to the Holsteinian, based on pollen analysis (Grupe, 1929), and to the Eemian, based on their stratigraphic position towards the Middle Terrace deposits (Siegert, 1912, 1921; Soergel, 1927, 1939). Much later, Mangelsdorf (1981) performed detailed palynological analysis on the interglacial deposits and proposed a late Comerian age (Bilshausen/Rhume interglacial). The late Cromerian age was not supported by Müller (mentioned in Waas et al., 2011), who performed pollen analysis of the interglacial sediments of the Nachtigall pit in 1998 (mentioned in Lepper, 1998) and tentatively assumed a Saalian deposition. Recently, $^{230}\text{U}/\text{Th}$ datings and palynological studies on the interglacial limnic sediments support these findings and refer to a deposition during marine isotope stages (MIS) 7c to early MIS 6 (227 +9/-8 ka to 177±8 ka; Kleinmann et al., 2011; Waas et al., 2011). Based on these ages, the overlying fluvial

al deposits were interpreted to have been deposited during MIS 6 and form part of the Middle Terraces that accumulated prior to the Saalian Drenthe glaciation (~155 ka; Kleinmann et al., 2011; Waas et al., 2011; Rohde et al., 2012).

4.3 Methods

4.3.1 Sampling and preparation

Five luminescence samples were taken in 2012 from the fluvial sediments of the Nachtigall pit, overlying the 13-25 m thick interglacial deposits (**Fig. 2**). $^{230}\text{U}/\text{Th}$ ages were derived from these interglacial deposits (Waas et al., 2011) about 175 m northwest of sample NG1. The western part of the pit is characterised by up to 8 m thick deposits, which consist of about 5 m thick gravel sheet deposits, that are overlain by up to 1 m thick fine-grained overbank deposits, consisting mainly of ripple cross-laminated and planar-parallel laminated silt and silty sand (Winsemann et al., *subm.*). From here, sample NG5 was taken (**Fig. 2**). These overbank deposits are truncated and overlain by about 2 m thick gravel sheet deposits.

From the eastern part of the pit, samples NG1, NG 2, NG3 and NG4 were taken from up to 55 cm thick sandy bedforms, comprising planar-parallel stratified, planar or trough cross-stratified or ripple cross-laminated medium- to fine-grained sand (Winsemann et al., *subm.*). These sandy deposits are embedded into up to 15 m thick gravel sheet deposits, lateral and downstream accretion macroforms. Locally, deposits are overlain by fine-grained floodplain deposits and draped by loess. The deposits are characterised by a major bounding surface, separating the western from the eastern part (**Fig. 2**). For further details on the large-scale depositional architecture and sedimentology of the Nachtigall deposits, see Winsemann et al. (*subm.*).

Sampling and preparation procedures of the luminescence samples can be found in detail in Roskosch et al. (2015). For luminescence measurements, monomineralic coarse-grained (150-200 μm) potassium-rich feldspar minerals and polymineralic fine-grained (4-11 μm) minerals were used (**Table 1**). Aliquots were created by mounting coarse-grained minerals on 9.8 mm stainless steel discs using silicone spray as an adhesive (2.5 mm aliquots), and by mounting fine-grained minerals on 9.8 mm aluminum discs from a suspension in acetone.

Sample preparation and luminescence measurements were performed in 2012 and 2013 at the Leibniz Institute for Applied Geophysics (Hannover, Germany), using an automated Risø TL/OSL reader (DA-20) with a calibrated $^{90}\text{Sr}/^{90}\text{Y}$ beta source (1.48 GBq = 40 mCi). Feldspar signals were stimulated by pulsing by infrared (IR) light-emitting diodes (LED). A

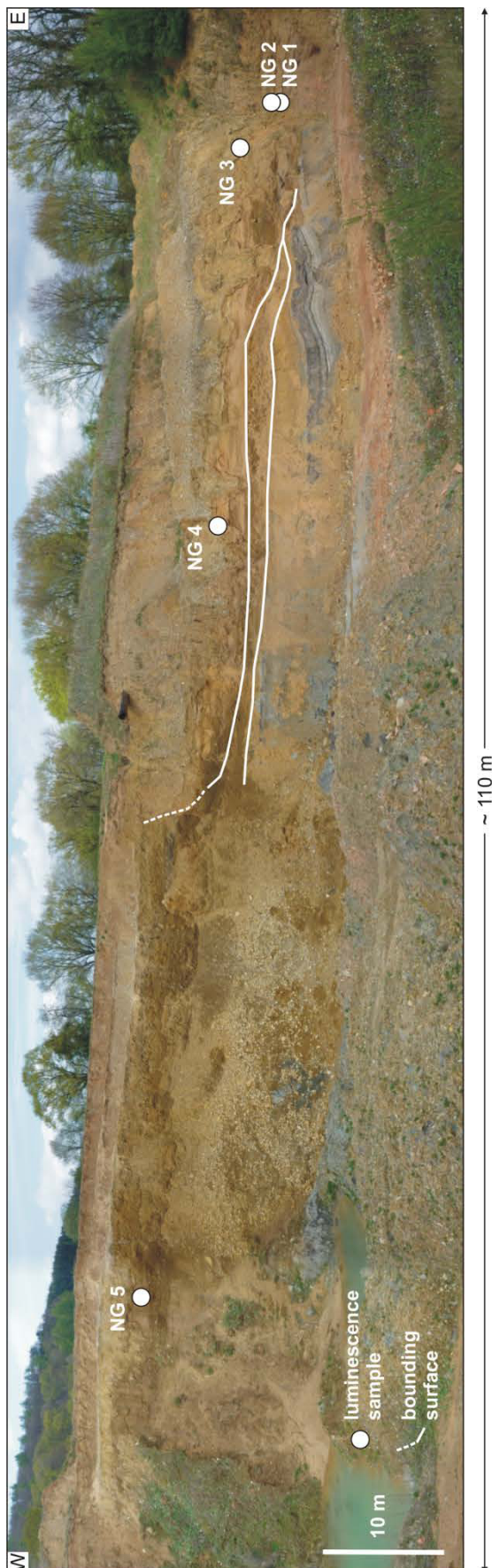


Fig. 2: Photo panel of the Nachtigall pit. Location of luminescence samples and major bounding surfaces are shown. The $^{230}\text{U}/\text{Th}$ samples by Waas et al. (2011) were taken from below the lower major bounding surface about 175 m northwest from sample NG1. Note that dimensions may be distorted due to panorama view.

Schott BG39/Corning 7-59 filter combination was used and the feldspar signals were detected in the blue-violet (320-460 nm) during the off-periods of each pulse cycle.

4.3.2 Equivalent dose and dose rate determination

A pulsed infrared stimulated luminescence (IRSL) single aliquot regenerative (SAR) dose protocol was used for feldspar equivalent dose (D_e) determination (Table 2), measuring at least 10 aliquots per sample (see Roskosch et al., 2015). In order to reduce possible anomalous fading, we chose to measure the pulsed IRSL signal at 50°C (IR_{50}) because it has been shown to be faster bleachable than the elevated temperature post-IR IRSL signal (Roskosch et al., 2015). During measurement, IR stimulation was carried out at 50°C for 400 s (on-time: 50 μs ; off-time: 200 μs) and only off-time signal was recorded because it was found to give a stable luminescence signal (Tsukamoto et al., 2006). The net feldspar luminescence signal was then calculated from the middle part of the decay curve (21-60 s) after subtracting a late background of the last 50 s (see Roskosch et al., 2015). Aliquots were accepted when the passed the

Table 1: Basic information on fluvial samples that were taken for luminescence dating using feldspar minerals.

Sample	Lab number	Longitudes and latitudes		Depth b.s. (m)	Altitude a.s.l. (m)	Grain size (μm)
NG1	2665	E 9°24'11.16"	N 51°48'30.83"	9.50	94.00	150-200
NG2	2666	E 9°24'11.16"	N 51°48'30.83"	9.00	94.50	150-200
NG3	2667	E 9°24'10.90"	N 51°48'31.9"	6.70	96.80	150-200
NG4	2668	E 9°24'9.13"	N 51°48'31.49"	6.30	98.70	150-200
NG5	2828	E 9°24'7.9"	N 51°48'31.69"	2.50	99.00	4-11

following criteria: recycling ratio limit within 10% of unity; maximal test dose error 10%; signal intensity larger than 3 sigma above background. We assumed a measurement error of $\pm 2.0\%$. In order to calculate D_e values, dose response curves were fitted with a saturating exponential function.

For dose rate determination, the radionuclide concentration of uranium (^{238}U), thorium (^{232}Th) and potassium (^{40}K) was determined by high-resolution gamma spectrometry. For coarse-grained feldspar minerals, an internal potassium content of $12.5 \pm 0.5\%$ was assumed (Huntley and Baril, 1997). The a -value was set to 0.15 ± 0.05 for monomineralic coarse-grains (Balescu and Lamothe, 1994) and 0.08 ± 0.02 for polymineralic fine-grains (cf. Lang et al., 2003), respectively. Cosmic radiation was corrected for altitude and sediment thickness after Prescott and Hutton (1994). Water content was measured and set to an average value of $10 \pm 5\%$. Dosimetry results are provided in **Table 3**.

Table 2: Pulsed IRSL SAR protocol for feldspar measurements.

Run	Treatment
1	Dose
2	Preheat, 60 s @ 250°C
3	Pulsed IR stimulation, 400 s @ 50°C
4	Test dose
5	Cutheat, 60 s @ 250°C
6	Pulsed IR stimulation, 400 s @ 50°C
7	Pulsed IR stimulation, 100 s @ 200°C
8	Return to step 1

4.3.3 Dose recovery and recycling ratio tests

Dose recovery experiments on three aliquots of each sample were performed prior to D_e measurements to check for the suitability of the applied SAR protocol under laboratory conditions. Within the Risø TL/OSL reader, aliquots were bleached by IR diodes and then given a similar beta dose that was close to the natural expected one (2000 s or 271 Gy for samples

Table 3: Dosimetry results, dose rates and total dose rate of coarse-grained monomineralic potassium-rich feldspar and polyminerally fine-grained minerals. The a -value was 0.15 ± 0.05 for monomineralic coarse-grains (Balescu and Lamothe, 1994) and 0.08 ± 0.02 for polyminerally fine-grains (cf. Lang et al., 2003). The average water content for all samples was $10 \pm 5\%$.

Sample	Dosimetry			Dose rates					Total dose rate (mGy a ⁻¹)
	Uranium (ppm)	Thorium (ppm)	Potassium (%)	D _α (mGy a ⁻¹)	D _β (mGy a ⁻¹)	D _γ (mGy a ⁻¹)	D _{internal} (mGy a ⁻¹)	D _{cosmic} (mGy a ⁻¹)	
NG1	1.20±0.01	4.91±0.03	1.97±0.01	0.11±0.06	1.49±0.06	0.71±0.05	0.69±0.09	0.05±0.01	3.04±0.13
NG2	1.73±0.01	7.04±0.03	2.08±0.01	0.14±0.07	1.65±0.06	0.86±0.05	0.69±0.09	0.06±0.01	3.39±0.14
NG3	2.16±0.01	8.98±0.03	2.57±0.01	0.17±0.07	2.04±0.06	1.07±0.05	0.69±0.09	0.08±0.01	4.06±0.14
NG4	2.43±0.02	8.03±0.03	2.23±0.01	0.17±0.07	1.83±0.06	0.99±0.05	0.69±0.09	0.08±0.01	3.77±0.14
NG5	2.65±0.02	11.04±0.04	2.49±0.01	0.85±0.18	2.33±0.09	1.25±0.09	-	0.16±0.02	4.58±0.22

Table 4: Results of luminescence measurements, including number of measured aliquots (n_m) and number of aliquots taken for age calculation (n_c), mean recycling ratios, overdispersion (σ_{OD}), dose recovery ratios, total dose rates, CAM D_e values and ages, fading rates (g-values), mean IR₅₀ D_e values, fading uncorrected and fading corrected pulsed IR₅₀ ages. Final ages are written in bold.

Sample	n_m/n_c	Mean re-cycling ratio	σ_{OD} (%)	Dose recovery ratio	Total dose rate (mGy a ⁻¹)	CAM D _e (Gy)	CAM age (ka)	g-value (% per decade)	Mean IR ₅₀ D _e (Gy)	Uncorr. IR ₅₀ age (ka)	Corr. IR ₅₀ age (ka)
NG1	10/10	1.04±0.04	0.00	0.95±0.00	3.04±0.13	176±4	58±3	2.5±0.1	177±3	58±3	73±3
NG2	10/10	1.03±0.04	0.00	0.95±0.00	3.39±0.14	201±4	59±3	2.7±0.4	202±4	59±3	77±6
NG3	10/10	1.03±0.04	0.00	0.94±0.04	4.06±0.14	227±5	56±2	2.1±0.4	227±3	56±2	68±5
NG4	10/10	1.03±0.04	0.00	0.94±0.02	3.77±0.14	215±5	57±2	2.6±0.2	216±2	57±2	73±4
NG5	10/9	1.02±0.04	0.00	1.01±0.01	4.58±0.22	455±11	99±5	0.6±0.2	456±5	100±5	105±6

NG1, NG2, NG3 and NG4; 3000 s or 401 Gy for sample NG5). Afterwards, the same SAR protocol was applied to check if the given dose could be accurately recovered.

Additionally, recycling ratio tests were conducted by applying the same dose twice, i.e. at the beginning and at the end of the D_e measurement. A recycling ratio value that is within 10% of unity (0.9-1.1; Wintle and Murray, 2006) indicates that sensitivity changes which might occur during measurement were successfully corrected. Dose recovery and recycling ratios are presented in **Table 4** and **Fig. 3**.

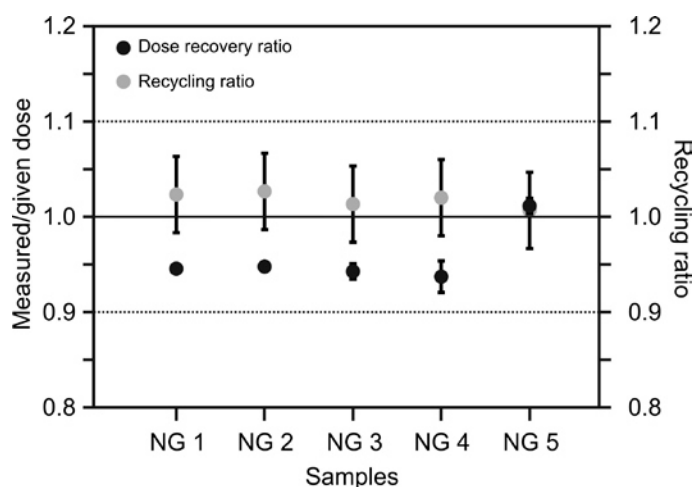


Fig. 3: Results of dose recovery and recycling ratio tests.

4.3.4 Fading tests and age calculations

Feldspar minerals have been observed to show an instability of the luminescence signal, which is also known as anomalous fading (Wintle, 1973; Aitken, 1985; Spooner, 1994). This signal loss over time results in (significantly) lower, thus severely underestimated IRSL ages. Huntley and Lamothe (2001) proposed a fading correction model, which was applied to three aliquots of each of our samples to obtain fading rates (g-values). Based on Thiel et al. (2011) and Buylaert et al. (2012), g-values below the threshold of ~1.5% per decade were considered to be laboratory artefacts, thus samples with g-values above this threshold called for fading corrections. Fading uncorrected and corrected pulsed IR_{50} ages are shown in **Table 4**.

Final ages were calculated taking into account the mean D_e values of all accepted aliquots. In addition to this, the central age model (CAM; Galbraith et al., 1999) was applied, giving weighted means and assuming a natural D_e distribution. The standard deviation of this distribution represents statistically unaccounted variations and is referred to as overdispersion (σ_{OD}).

4.4. Results

For all luminescence samples, dose response curves and frequency- D_e histograms were created based on the accepted aliquots (**Fig. 4**). Dose response curves are characterised by a saturating exponential growth. Histograms are characterised by very narrow and tight D_e distributions, suggesting generally good bleaching conditions. Results of dose recovery and recycling ratio tests are all satisfying and in the acceptable range of 10% of unity (0.9-1.1; **Fig. 3**; Wintle and Murray, 2006). Dose recovery ratios range between 0.94 ± 0.04 (NG3) to 1.01 ± 0.01 (NG5; **Table 4**). These results indicate that the applied SAR protocol is able to recover a given dose reliably and creates consistent D_e values. Recycling ratios range between 1.02 ± 0.04 (NG5) and 1.04 ± 0.04 (NG1; **Table 4**). Sensitivity changes that might occur during measurements were successfully corrected by the chosen SAR protocol. We therefore believe that our samples have experienced good bleaching conditions during transport, which is also reflected by the obtained σ_{OD} values that were consistently 0.00 % for all samples (**Table 4**).

Dose rate results gave values ranging from 3.04 ± 0.13 mGy a⁻¹ (NG1) to 4.58 ± 0.22 mGy a⁻¹ (NG5; **Table 3**). Fading uncorrected and corrected pulsed IR₅₀ ages are presented in **Table 4**. The obtained g-values for all samples were between $2.1 \pm 0.4\%$ per decade (NG3) and $2.7 \pm 0.04\%$ per decade (NG2) for monomineralic coarse-grains and $0.6 \pm 0.2\%$ per decade (NG5) for polymineralic fine-grains and thus clearly above the threshold of 1.5% per decade (Thiel et al., 2011; Buylaert et al., 2012), implying that anomalous fading occurred and determined fading uncorrected pulsed IR₅₀ ages needed correction. The fading corrected pulsed IR₅₀ ages are younger than the proposed ²³⁰U/Th ages of the underlying interglacial deposits (Waas et al., 2011) and point to two major depositional phases. Sample NG5 gave a fading uncorrected pulsed IR₅₀ age of 100 ± 5 ka, indicating a Late Pleistocene deposition which can be correlated with MIS 5d. Samples NG1 to NG4 gave fading corrected pulsed IR₅₀ ages ranging from 77 ± 6 ka (NG2) to 68 ± 5 ka (NG3), pointing to a Late Pleistocene (Early Weichselian to Early Pleniglacial) deposition which can be correlated with late MIS 5b to MIS 4.

The final depositional ages reveal a chronological gap of about 12 ka. This gap seems to coincide with a major bounding surface (Winsemann et al., *subm.*).

4.5 Discussion

Feldspar luminescence dating of fluvial samples overlying the interglacial sediments of the Nachtigall pit indicate a deposition during MIS 5d and from late MIS 5b to MIS 4. Interpretation of the large-scale terrace architecture led to the assumption that the fluvial deposits

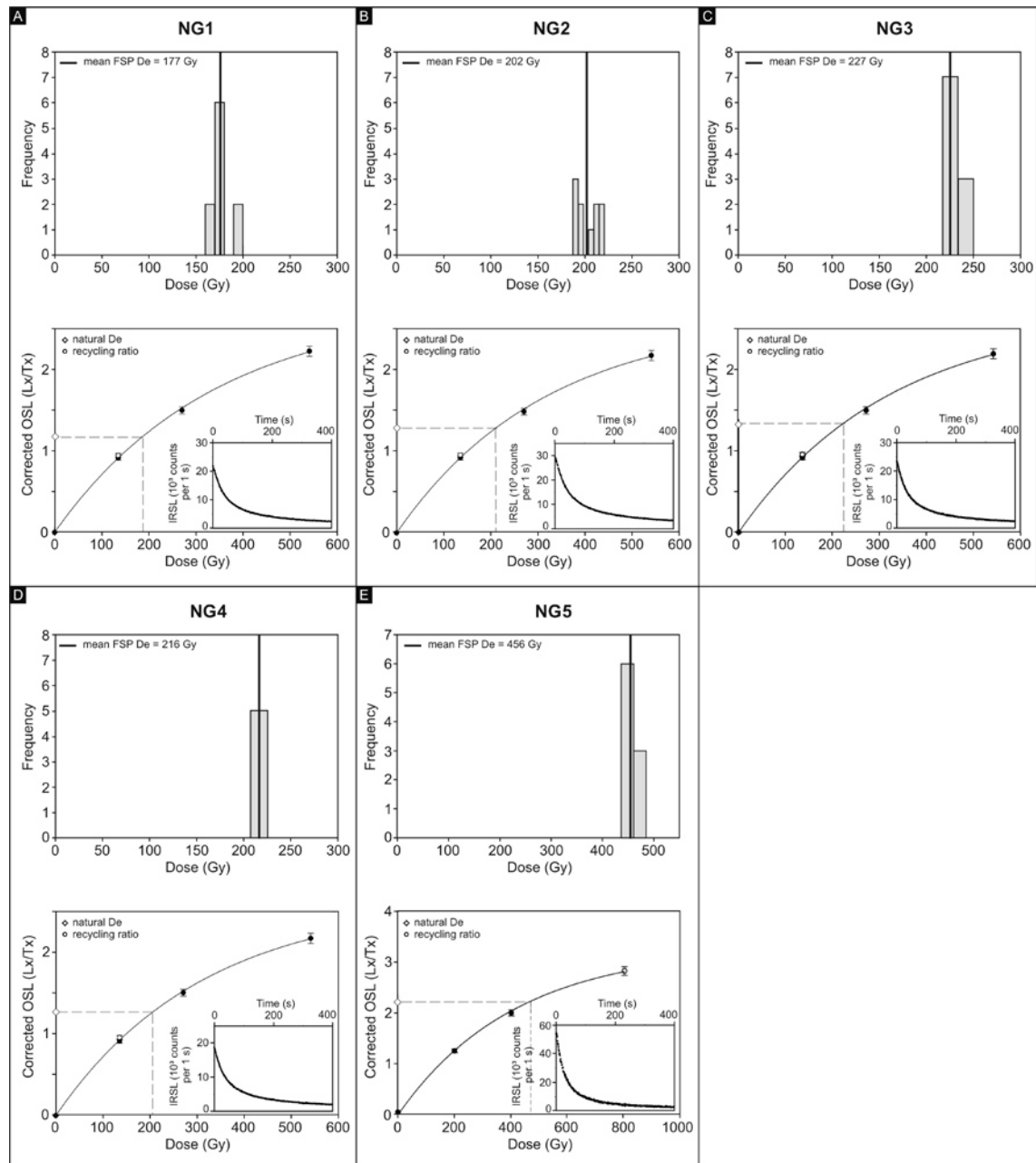


Fig. 4: Representative frequency- D_e histograms (top) including mean feldspar D_e values (solid line), dose response curves (bottom) and decay curves (inset) of luminescence samples NG1, NG2, NG3, NG4 and NG5.

display laterally attached terraces (Winsemann et al., *subm.*), which form when both rates of fluvial aggradation and degradation are balanced (Archer et al., 2011).

As mentioned before, numerical dating of fluvial deposits is often referred to as a challenging task (e.g., Wallinga, 2002). Therefore, a well-considered SAR protocol can be of great help in order to minimize anomalous fading in feldspar minerals and to obtain a stable luminescence signal. Anomalous fading was intended to be reduced by using the much more light-sensitive pulsed IR₅₀ signal for measurements but calculated fading rates were clearly above

the threshold of 1.5 % per decade for samples NG1-4 (Thiel et al., 2011; Buylaert et al., 2012) and fading correction was considered necessary. **Table 4** shows that fading uncorrected pulsed IR₅₀ ages were up to about 18 ka younger (NG2) than the fading corrected pulsed IR₅₀ ages.

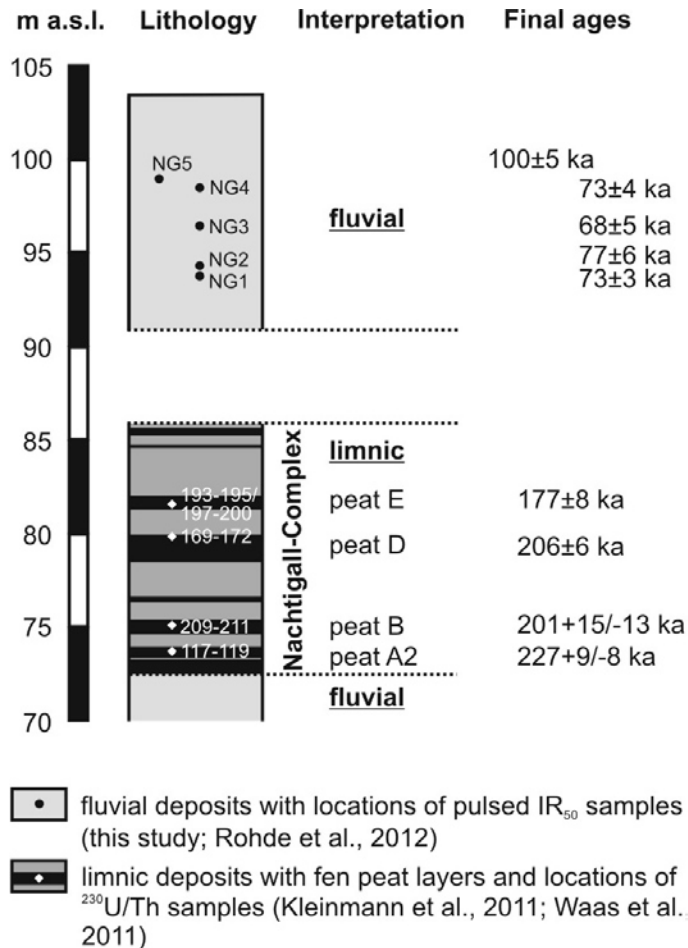


Fig. 5: Schematic log of the investigated deposits of the Nachtigall pit, showing lithology, interpretation and final pulsed IR₅₀ and ²³⁰U/Th ages. The transition zone marks the transition from fluvial to limnic deposits. Note that this zone of about 5 m exists due to the fact that the ²³⁰U/Th samples of the Nachtigall-Complex were derived from a core drilled about 175 m northwest of sample NG1. Here, altitude of the surface during drilling was 108.55 m a.s.l. For these limnic deposits, lithology boundaries were taken from Kleinmann et al. (2011) and Waas et al. (2011). For sample NG1, surface altitude was 103.5 m a.s.l. For better comparison, we provide altitude data.

However, the major problem in luminescence dating (of fluvial deposits) is assigned to the occurrence of insufficient bleaching, resulting in overestimated depositional ages (e.g., Murray et al., 1995; Gemmill, 1997; Olley et al., 1999; Stokes et al., 2001). In order to cope with the effect and influence of insufficient bleaching, several approaches were proposed. Small-sized aliquots or even single grain measurements allow for the detection and extraction of only bleached grains of insufficiently bleached samples (e.g., Olley et al., 1998; Duller et al., 1999; Duller, 2000, 2008). Nevertheless, we chose to use 2.5 mm-sized aliquots, which have been shown to give satisfactory luminescence results from sediments that were prone to insufficient bleaching as well (Roskosch et al., 2015). Moreover, based on the very satisfying results of the applied performance tests and the evaluation of the frequency-D_e histograms (**Table 4; Fig. 4**), we are confident that the obtained fading corrected pulsed IR₅₀ ages are reliable and D_e distributions do not show major detectable and obvious signs of insufficient bleaching. Unfortunately,

ly, we were not able to date both feldspar and quartz minerals due to the fact that the quartz minerals were very likely to be in or close to saturation and thus were useless for age determination and comparison. However, agreeing feldspar IRSL and quartz OSL ages are considered a useful method for identifying the bleaching degree of a sediment (cf. Murray et al., 2012). Since the luminescence signals of both minerals are reset at different rates, an age agreement points good bleaching conditions. This has been reported from other European sites where fluvial sediments had numerically been dated using both feldspar and quartz minerals (e.g., Wallinga et al., 2001; Frechen et al., 2008; Cordier et al., 2010; Roskosch et al., 2015). Moreover, it has been shown that the impact of incomplete bleaching on comparably older sediments is (very) small and often considered to be negligible (Duller, 2008) and can be seen as an advantage over younger sediments where the detection of incomplete bleaching is of major importance and can lead to severe age overestimation is left undetected.

Comparison with the results of other dating techniques (^{14}C , AAR, ESR, $^{230}\text{U}/\text{Th}$), used as independent age control, is another effective approach to evaluate and verify the results (e.g., Mol, 1997; Busschers et al., 2007; Schulte et al., 2008; Cordier et al., 2013). The $^{230}\text{U}/\text{Th}$ ages of the interglacial deposits of the so-called Nachtigall-Succession (cf. Kleinmann et al., 2011; Rohde et al., 2012), which were correlated with MIS 7c to early MIS 6 (Waas et al., 2011), and our pulsed IR_{50} ages are in excellent accordance regarding their stratigraphic order, proving the reliability and accuracy of both dating methods. However, the luminescence ages both confirm and reject the previously established Middle to Late Pleistocene fluvial depositional model (e.g., Rohde et al., 2012) and are therefore of considerable value. On the one hand, the occurrence of fluvial sediments, which had been deposited after the interglacial MIS 7 and prior to the Saalian Drenthe glaciation, could not be verified based on the luminescence dating results. On the other hand, the occurrence of Late Pleistocene (Weichselian) fluvial deposits was expected to occur only in the floodplain area of River Weser (cf. Rohde et al., 2012). The previous depositional model has to be revised due to the obtained luminescence ages of samples NG1 to NG4, pointing to an Early Weichselian to Early Pleniglacial deposition for this part of the pit. It is, however, likely that the adjacent valley area is characterised by gravelly and sandy fluvial sediments (referred to as Lower Terrace deposits; cf. Rohde et al., 2012), which had been deposited afterwards and which are probably underlain by Saalian fluvial deposits, as has been described by Rohde et al. (2012). Therefore, the Late Pleistocene sedimentary complex seems to have been subdivided into two fluvial sediment bodies (**Fig. 5**). However, for further details on the fluvial terrace architecture, we kindly refer to Winsemann et al. (subm.).

The luminescence dating results have shown that comparison with independent age control is of great importance. Given the considerable value of the obtained luminescence ages, additional numerical dating approaches may be performed and thus complement the chronostratigraphic framework of the deposits of the Nachtigall pit.

4.6 Conclusions

We present new luminescence ages from five fluvial samples of the Nachtigall pit in the southern Weser valley in northwestern Germany. Luminescence measurements on monomineralic feldspar coarse-grains and polymineralic fine-grains were performed using a pulsed IRSL SAR protocol. Independent age control is given by $^{230}\text{U}/\text{Th}$ ages of underlying interglacial deposits (Waas et al., 2011).

- Numerical dating results point two phases of fluvial aggradation, which occurred during the Late Pleistocene (Early Weichselian to Early Pleniglacial). One polymineralic fine-grained sample was derived from fine-grained overbank deposits from the western part of the succession and gave a feldspar age of 100 ± 5 ka, correlating with MIS 5d. Four coarse-grained samples were derived from medium- to fine-grained sandy deposits, interbedded into gravel sheet deposits, lateral and downstream accretion macroforms in the eastern part of the succession, giving feldspar ages ranging from 77 ± 6 ka to 68 ± 5 ka. These ages point to a depositing during late MIS 5b to MIS 4.
- Luminescence samples passed required performance tests, and results of both dose recovery and recycling ratio tests were satisfyingly acceptable. Overdispersion values are all 0.00%. Frequency- D_e histograms are characterised by tight and narrow D_e distributions. Consequently, the effect of insufficient bleaching of our samples, if any, should be negligible.
- Correlation with $^{230}\text{U}/\text{Th}$ results of underlying interglacial sediments, which gave ages ranging from MIS 7c to early MIS 6 (Waas et al., 2011) supports the assumption that the overlying fluvial deposits are stratigraphically younger, proving the accuracy and reliability of our luminescence data.

Acknowledgements

We gratefully acknowledge financial support by the Leibniz Universität Hannover. Many thanks are due to J.-U. Müller of Bauunternehmen Jens Müller GmbH for permitting us to work on his property at the Nachtigall pit. Sincere thanks are given to P. Rohde for drawing our attention to the Nachtigall pit, for assistance during field work, for fruitful discussions and

personal comments on the draft version of the manuscript. J. Lang, J. Lepper, A. Osman, L. Pollok, A. Weitkamp and J. Winsemann are thanked for field work and helpful discussion, and S. Riemenschneider is thanked for technical support in the luminescence laboratory.

References

- Aitken, M.J., 1985. Thermoluminescence Dating. Academic Press, London, 359pp.
- Archer, S.G., Reynisson, R.F., Schwab, A.M., 2011. River terraces in the rock record: An overlooked landform in geological interpretation. In: Davidson, S.K., Leleu, S., North, C.P., (eds.), From River to Rock Record: The Preservation of Fluvial Sediments and their Subsequent Interpretation. SEPM, Special Publication, 97, 63-85.
- Balescu, S., Lamothe, M., 1994. Comparison of TL and IRSL age estimates of feldspar coarse grains from waterlain sediments. Quaternary Science Reviews 13, 437-444.
- Busschers, F.S., Kasse, C., van Balen, R.T., Vandenberghe, J., Cohen, K.M., Weerts, H.J.T., Wallinga, J., Johns, C., Cleveringa, P., Bunnik, F.P.M., 2007. Late Pleistocene evolution of the Rhine-Meuse system in the southern North Sea basin: imprints of climate change, sea-level oscillation and glacio-isostasy. Quaternary Science Reviews 26, 3216-3248.
- Busschers, F.S., van Balen, R.T., Cohen, K.M., Kasse, C., Weerts, H.J.T., Wallinga, J., Bunnik, F., 2008. Response of the Rhine-Meuse fluvial system to Saalian ice-sheet dynamics. Boreas 37, 377-398.
- Briant, R.M., Bates, M.R., Schwenninger, J.-L., Wenban-Smith, F., 2006. An optically stimulated luminescence dated Middle to Late Pleistocene fluvial sequence from the western Solent Basin, southern England. Journal of Quaternary Science 21, 507-523.
- Buylaert, J.-P., Jain, M., Murray, A.S., Thomsen, K.J., Thiel, C., Sohbati, R., 2012. A robust feldspar luminescence dating method for Middle and Late Pleistocene sediments. Boreas 41, 435-451.
- Carthaus, E., 1886. Mitteilungen über die Triasformation im nordöstlichen Westfalen und in einigen angrenzenden Gebieten. PhD thesis, University of Würzburg, 69pp.
- Cordier, S., Frechen, M., Tsukamoto, S., 2010. Methodological aspects on luminescence dating of fluvial sands from the Moselle Basin, Luxembourg. Geochronometria 35, 67-74.
- Cordier, S., Frechen, M., Harmand, D., 2013. Dating fluvial erosion: fluvial response to climate change in the Moselle catchment (France, Germany) since the Late Saalian. Boreas 43, 450-468.

- Dechen, H. von, 1884. Erläuterung zur geologischen Karte der Rheinprovinz und der Provinz Westfalen sowie einiger angrenzenden Gegenden. Bonn, Henry, 933pp.
- Duller, G.A.T., Bøtter-Jensen, L., Murray, A.S., Truscott, A.J., 1999. Single grain laser luminescence (SGLL) measurements using a novel automated reader. *Nuclear Instruments and Methods in Physics Research B: Beam Interactions with Materials and Atoms* 155, 506–514.
- Duller, G.A.T., 2000. Optical dating of single sand-sized grains of quartz: Sources of variability. *Radiation Measurements* 32, 453–457.
- Duller, G.A.T., 2008. Single-grain optical dating of Quaternary sediments: why aliquot size matters in luminescence dating. *Boreas* 37, 589–612.
- Frechen, M., Ellwanger, D., Rimkus, D., Techmer, A., 2008. Timing of Medieval Fluvial Aggradation at Bremgarten in the Southern Upper Rhine Graben – a Test for Luminescence Dating. *E&G Quaternary Science Journal* 57, 411–432.
- Fuchs, M., Lang, A., 2001. OSL dating of coarse-grain fluvial quartz using single-aliquot protocols on sediments from NE Peloponnese, Greece. *Quaternary Science Reviews* 20, 783–787.
- Galbraith, R.F., Roberts, R.G., Laslett, G.M., Yoshida, H., Olley, J.M., 1999. Optical dating of single and multiple grains of quartz from Jinmium rock shelter, Northern Australia: part I, experimental design and statistical models. *Archaeometry* 41, 339–364.
- Gemmell, A.M.D., 1997. Fluctuations in the thermoluminescence signal of suspended sediment in an alpine glacial meltwater stream. *Quaternary Science Reviews* 16, 281–290.
- Grupe, O., 1912. Erläuterungen zur Geologischen Karte von Preußen und benachbarten Bundesstaates 1:25 000, Blatt 4122 Holzminden. Königlich Preußische Geologische Landesanstalt, Berlin, 95pp.
- Grupe, O., 1929. Erläuterungen zur Geologische Karte von Preußen und benachbarten deutschen Ländern 1:25 000, Blatt 4122 Holzminden. Preußische Geologische Landesanstalt, Berlin, 71pp.
- Huntley, J.D., Baril, M.R., 1997. The K content of the K-feldspars being measured in optical dating or in thermoluminescence dating. *Ancient TL* 15, 11–13.
- Huntley, J.D., Lamothe, M., 2001. Ubiquity of anomalous fading in K-feldspars and the measurement and correction for it in optical dating. *Canadian Journal of Earth Sciences* 38, 1093–1106.

- Jain, M., Murray, A.S., Bøtter-Jensen, L., 2004. Optically stimulated luminescence dating: how significant is incomplete light exposure in fluvial environments? *Quaternaire* 15, 143-157.
- Kleinmann, A., Müller, H., Lepper, J., Waas, D., 2011. Nachtigall: A continental sediment and pollen sequence of the Saalian Complex in NW-Germany and its relationship to the MIS-framework. *Quaternary International* 241, 97-110.
- Koken, E., 1901. Beiträge zur Kenntnis des schwäbischen Diluviums. *Neues Jahrbuch für Mineralogie, Geologie und Paläontologie* 14, 120-170.
- Krbetschek, M.R., Degering, D., Alexowsky, W., 2008. Infrarot-Radiofluoreszenz-Alter (IR-RF) unter-saalezeitlicher Sedimente Mittel- und Ostdeutschlands. *Zeitschrift der Deutschen Gesellschaft für Geowissenschaften* 159, 133–140.
- Lang, A., Hatte, C., Rousseau, D.-D., Antoine, P., Fontugne, M., Zöller, L., Hambach, U., 2003. High-resolution chronologies for loess: comparing AMS ^{14}C and optical dating results. *Quaternary Science Reviews* 22, 953-959.
- Lauer, T., Frechen, M., Hoselmann, C., Tsukamoto, S., 2010. Fluvial aggradation phases in the Upper Rhine Graben – new insights by quartz OSL dating. *Proceedings of Geologists Association* 121, 154-161.
- Lauer, T., Krbetschek, M., Frechen, M., Tsukamoto, S., Hoselmann, C., Weidenfeller, M., 2011. Infrared radiofluorescence (IR-RF) dating of Middle Pleistocene fluvial archives of the Heidelberg Basin (southwest Germany). *Geochronometria* 38, 23-33.
- Lepper, J., 1991. Beiheft zur Geologischen Wanderkarte, Mittleres Weserbergland mit Naturpark Solling-Vogler 1:100 000. *Bericht der Naturhistorischen Gesellschaft Hannover* 10, 58pp.
- Lepper, J., 1998. Tongrube Nachtigall des Ziegelwerkes Buch bei Albaxen. In: Feldmann, L., Meyer, K.-D. (eds.), *Quartär in Niedersachsen. Deuqua-Exkursionsführer*, Hannover, 205pp.
- Lepper, J., Mengeling, H., 1990. Geologische Wanderkarte, Mittleres Weserbergland mit Naturpark Solling-Vogler 1:100 000. *Zweckverband Naturpark Soling-Vogler in Zusammenarbeit mit dem Niedersächsischen Landesamt für Bodenforschung*.
- Lewis, S.G., Maddy, D., Scaife, R.G., 2001. The fluvial system response to abrupt climate change during the last cold stage: the Upper Pleistocene River Thames fluvial succession at Ashton Keynes, UK. *Global Planetary Change* 28, 341-359.

- Mangelsdorf, P., 1981. Quartärgeologische und paläobotanische Untersuchungen in der Tongrube „Nachtigall“ N Höxter/Weser. Unpublished diploma thesis, University of Hannover, 63pp.
- Mol, J., 1997. Fluvial response to Weichselian climate changes in the Niederlausitz (Germany). *Journal of Quaternary Science* 12, 43-60.
- Murray, A.S., Olley, J.M., Caitcheon, G.G., 1995. Measurement of equivalent doses in quartz from contemporary water-lain sediments using optically stimulated luminescence. *Quaternary Science Reviews* 14, 365-371.
- Murray, A.S., Thomsen, K.J., Masuda, N., Buylaert, J.-P., Jain, M., 2012. Identifying well-bleached quartz using the different bleaching rates of quartz and feldspar luminescence signals. *Radiation Measurements* 47, 688–695.
- Olley J.M., Caitcheon G.G., Murray A.S., 1998. The distribution of apparent dose as determined by optically stimulated luminescence in small aliquots of fluvial quartz: implications for dating young sediments. *Quaternary Science Reviews* 17, 1033-1040.
- Olley J.M., Caitcheon G.G., Roberts R.G., 1999. The origin of dose distributions in fluvial sediments, and the prospect of dating single grains from fluvial deposits using optically stimulated luminescence. *Radiation Measurements* 30, 207-217.
- Prescott, J.R., Hutton, J.T., 1994. Cosmic ray contribution to dose rates for luminescence and ESR dating: large depths and long-term time variations. *Radiation Measurements* 23, 497-500.
- Rittenour, T.M., 2008. Luminescence dating of fluvial deposits: applications to geomorphic, palaeoseismic and archaeological research. *Boreas* 37, 613-635.
- Rohde, P., 1983. Geologische Karte von Niedersachsen 1:25 000, Erläuterung zu Blatt Nr. 3724 Pattensen. Niedersächsisches Landesamt für Bodenforschung Hannover, 192pp.
- Rohde, P., 1989. Elf pleistozäne Sand-Kies-Terrassen der Weser: Erläuterungen eines Gliederungsschemas für das obere Weser-Tal. *E&G Quaternary Science Journal* 39, 42-56.
- Rohde, P., 1994. Weser und Leine am Berglandrand zur Ober- und Mittelterrassen-Zeit. *E&G Quaternary Science Journal* 44, 106-133.
- Rohde, P., Lepper, J., Thiem, W., 2012. Younger Middle Terrace - Saalian pre-Drenthe deposits overlying MIS 7 Nachtigall interglacial strata near Höxter/Weser, NW-Germany. *E&G Quaternary Science Journal* 61, 133-145.

- Roskosch, J., Winsemann, J., Polom, U., Brandes, C., Tsukamoto, S., Weitkamp, A., Bartholomäus, W.A., Henningsen, D., Frechen, M., 2015. Luminescence dating of ice-marginal deposits in northern Germany: evidence for repeated glaciations during the Middle Pleistocene (MIS 12 to MIS 6). *Boreas* 44, 103-126.
- Schulte, L., Juliá, R., Burjachs, F., Hilgers, A., 2008. Middle Pleistocene to Holocene geochronology of the River Aguas terrace sequence (Iberian Peninsula): Fluvial response to Mediterranean environmental change. *Geomorphology* 98, 13-33.
- Siegert, L., 1912. Über die Entwicklung des Wesertales. *Zeitschrift der Deutschen Geologischen Gesellschaft* 64, 233-264.
- Siegert, L., 1921. Beiträge zur Kenntnis des Pliocäns und der diluvialen Terrassen im Flußgebiet der Weser. *Abhandlungen der Preußischen Geologischen Landesanstalt, Neue Folge* 90, Berlin, 130pp.
- Soergel, W., 1927. Zur Talentwicklung des Weser-Werra- und des Ilm-Systems. *Geologische Rundschau* 18, 103-120.
- Soergel, W., 1939. Das diluviale System. *Fortschritte der Geologie und Paläontologie* 12, 155-292.
- Spooner, N.A., 1994. The anomalous fading of infrared-stimulated luminescence from feldspars. *Radiation Measurements* 23, 625-632.
- Stokes, S., Bray, H.E., Blum, M.D., 2001. Optical resetting in large drainage basins: Tests of zeroing assumptions using single-aliquot procedures. *Quaternary Science Reviews* 20, 879-885.
- Thiel, C., Buylaert, J.-P., Murray, A., Terhorst, B., Hofer, I., Tsukamoto, S., Frechen, M., 2011. Luminescence dating of the Stratzing loess profile (Austria) – Testing the potential of an elevated temperature post-IR IRSL protocol. *Quaternary International* 234, 23-31.
- Tsukamoto, S., Denby, P.M., Murray, A.S., Bøtter-Jensen, L., 2006. Time-resolved luminescence from feldspars: new insight into fading. *Radiation Measurements* 41, 790–795.
- Waas, D., Kleinmann, A., Lepper, J., 2011. Uranium-thorium dating of fen peat horizons from pit Nachtigall in northern Germany. *Quaternary International* 241, 111-124.
- Wallinga, J., 2002. Optically stimulated luminescence dating of fluvial deposits: a review. *Boreas* 31, 303-322.

- Wallinga, J., Murray, A.S., Duller, G.A.T., Törnqvist, T.E., 2001. Testing optically stimulated luminescence dating of sand-sized quartz and feldspar from fluvial deposits. *Earth and Planetary Science Letters* 193, 617–630.
- Winsemann, J., Lang, J., Böhner, U, Polom, U., Brandes, C., Roskosch, J., Glotzbach, C., Frechen, M., submitted to *Quaternary Science Reviews*. Terrace styles and timing of terrace formation in the Weser and Leine Valley, northern Germany: response of a fluvial system to climate change and glaciation.
- Wintle, A.G., 1973. Anomalous fading of thermoluminescence in minerals. *Nature* 245, 143–144.
- Wintle, A.G., Murray, A.S., 2006. A review of quartz optically stimulated luminescence characteristics and their relevance in single-aliquot regeneration dating protocols. *Radiation Measurements* 41, 369–391.

Chapter 5

Summarising discussion

Discussions of the results of each paper have been provided in detail in the corresponding sections of this thesis. In order to gain a final overall picture of the findings of this thesis, the geochronological approaches and geological implications will be discussed and evaluated on a broader and summarising basis.

5.1 Geochronological discussion

The deposits under study were primarily derived from depositional environments which are considered to be difficult in terms of resetting the luminescence clock prior to deposition. Therefore, the main and major challenge was to detect and evaluate the effect of bleaching of mostly glacial, alluvial and fluvial deposits. Before doing so, the optimal mineral, aliquot-size and method for D_e determination had to be found and tested with regard to producing and re-producing consistent, robust and reliable luminescence ages.

In this thesis, monomineralic coarse-grained potassium-rich feldspar minerals were used when the expected depositional age was assumed to be relatively old (Chapters 2, 3 and 4). In case of low D_e values, additional monomineralic coarse-grained quartz measurements were performed (Münsterland Embayment, Leine valley; Chapters 2 and 3). Polymineralic fine-grains were used once because this sample was derived from fine-grained (silty) overbank deposits (Weser valley; Chapter 4).

As stated in Chapter 1.3.4.2, feldspar minerals are characterised by a brighter luminescence signal and a higher saturation level when compared to quartz minerals, which makes it the ideal choice for dating older deposits (e.g., Buylaert et al., 2011). The chosen SAR protocols for feldspar measurements on medium-sized aliquots (2.5 mm diameter with about 100–120 grains) were (i) an elevated temperature pIRIR protocol using a preheat at 320°C for 60 s, IR stimulation at 50°C for 100 s and a post-IR stimulation at 290°C for 210 s (Chapter 2; Thiel et al., 2011), or (ii) a pulsed IRSL SAR protocol using IR stimulation at 50°C for 400 s with 50 μ s on-time and 200 μ s off-time (Chapters 3 and 4; Tsukamoto et al., 2006). These protocols were chosen because they had either been proved to show negligible anomalous fading (Thiel et al., 2011; Buylaert et al., 2012) or used a less-fading dependent and more stable luminescence signal (Tsukamoto et al., 2006). Although several fading correction models exist (e.g., Huntley and Lamothe, 2001; Lamothe et al., 2003; Kars et al., 2008), they all incorporate untestable assumptions. It is therefore recommended to use the less fading-dependent or even non-fading-dependent parts of the IRSL signal, as has been done in all feldspar measurements (Chapters 2, 3 and 4). Nevertheless, fading rates were calculated and determined D_e values were corrected in case of fading rates above a threshold of 1.5% per decade (Thiel et al., 2011;

Buylaert et al., 2012). Such small fading rates could be laboratory artefacts and were therefore considered negligible (Thiel et al., 2011; Buylaert et al., 2012). For the upper Senne deposits of the Münsterland Embayment (Chapter 2), mean IR_{50} g-values were $2.2 \pm 0.5\%$ per decade (Oerlinghausen) and $2.8 \pm 0.4\%$ per decade (Augustdorf), and mean $pIRIR_{290}$ g-values were $0.8 \pm 0.3\%$ per decade (Oerlinghausen) and $1.2 \pm 0.3\%$ per decade (Augustdorf), respectively. Only IR_{50} D_e values were corrected and used for interpretation. For the Leine valley deposits, g-values were between $0.5 \pm 0.4\%$ per decade and $1.4 \pm 0.2\%$ per decade and no fading correction was performed (Chapter 3). For the Weser valley deposits, g-values were between $0.6 \pm 0.2\%$ per decade and $2.7 \pm 0.4\%$ per decade. D_e values were mostly fading corrected to avoid underestimated depositional ages (Chapter 4).

Monomineralic coarse-grained quartz measurements were conducted on 14 alluvial, aeolian and fluvial samples (Chapters 2 and 3) using a double SAR protocol (Murray and Wintle, 2000, 2003), which includes an IR stimulation to reduce the feldspar signal prior to stimulation of the aliquots with blue LEDs. For the quartz samples of the Münsterland Embayment (Chapter 2), small-sized aliquots (1 mm diameter with about 20-45 grains) were measured. For the quartz samples of the Leine valley (Chapter 3), medium-sized aliquots (2.5 mm diameter with about 100-120 grains) were measured.

After measurements, evaluation of the bleaching characteristics of each sample was performed by means of (i) comparison of the obtained luminescence ages with independent age control, and/or (ii) double-dating using both feldspar and quartz minerals, and/or (iii) creation of $D_e(t)$ plots, and/or (iv) D_e histograms, and/or (v) radial plots. As for (i), which had been described in publication 3 (Chapter 4), comparison with independent age control is the easiest way to identify possible age overestimation and thus poor bleaching conditions (e.g., Murray and Olley, 2002; Rhodes et al., 2003; Frechen et al., 2004; Olley et al., 2004; Busschers et al., 2007; Rittenour, 2008). A significant age disagreement of ages obtained from sediment over- or underlying the luminescence dated deposits points to unreliable, inaccurate and imprecise ages. However, independent age control for the fluvial deposits of the Nachtigall pit (Chapter 4) were only available for the underlying interglacial sediments dated by means of $^{230}U/Th$ (Waas et al., 2011). The obtained luminescence ages were consequently interpreted as maximum depositional ages and further (luminescence) dating approaches were recommended.

As for (ii), if double dating using both dosimeters is possible, comparison of quartz and feldspar ages can be indicative of the bleaching conditions prior to deposition (e.g., Wallinga et al., 2001; Frechen et al., 2008; Buylaert et al., 2011; Murray et al., 2012). The reason for this is that quartz and feldspar minerals have different bleaching behaviours, where quartz bleaches

more rapidly than feldspar (Godfrey-Smith et al., 1988). An age agreement can therefore only occur when the dated minerals were sufficiently bleached before burial. In the course of this thesis, out of 14 double-dated samples, five samples gave agreeing quartz and feldspar ages. These samples were derived from an aeolian environment (Sen5, Aug3, Aug4; Chapter 2) or of fluvial character (KB02_373-385, KB02_656-670; Chapter 3). The nine remaining double-dated alluvial samples (Sen10, Sen1, Sen2, Sen3, Sen4, Sen8, Sen9, Aug1, Aug2; Chapter 2) were considered to be less well bleached due to the quartz and feldspar age disagreement.

As for (iii), plotting D_e values as a function of simulation time and thus creating $D_e(t)$ plots may be of great help in order to evaluate the bleaching characteristics (Huntley et al., 1985; Bailey, 2003; Vandenberghe, 2003; Thomas et al., 2006; Fuchs and Owen, 2008; Preusser et al., 2008). For insufficiently bleached samples, D_e values are expected to increase with simulation time, while a flat and plateau-like $D_e(t)$ plot is considered to be characteristic for good bleaching conditions. This has successfully been performed on glacial sediments from Russia, where a flat $D_e(t)$ plot was interpreted to represent sufficiently bleached samples and obtained D_e values were in accordance with ^{14}C ages (Thomas et al., 2006). Contrary to this, Fiebig and Preusser (2007) demonstrated that analyses of $D_e(t)$ plots were not able to fully identify the bleaching degree of the dated fluvial deposits. Preusser et al. (2008) therefore suggested that analyses of $D_e(t)$ plots should not be seen as 'hard proof' of sufficient bleaching. They may, however, give evidence for the bleaching degree.

As for (iv) and (v), evaluation of the scatter of D_e values in histograms and radial plots may also be indicative of the sample's bleaching characteristics (e.g., Galbraith, 1990; Murray et al., 1995; Olley et al., 1999; Wallinga, 2002a). Tight, narrow and Gaussian-like D_e distributions (bin width = median of the standard errors of the obtained D_e values), as shown in publications 2 and 3 (Chapters 3 and 4), have often been interpreted to represent sufficiently bleached samples. The same applies to radial plots, when measured aliquots are mostly within the 2-sigma level of the average D_e value (Chapter 2). D_e histogram and radial plot evaluation supported the assumption that the alluvial deposits of the upper Senne area (Chapter 2) were not fully bleached, as had been suggested by the disagreeing quartz and feldspar ages. D_e histograms of the glacial deposits derived from the Leine valley (Chapter 3) also pointed to a certain degree of insufficient bleaching, as they showed some outlier at higher doses. Contrary to this, the fluvial deposits from the Nachtigall pit (Chapter 4) were characterised by very tight and narrow D_e distributions, indicating good bleaching conditions. However, the amount of grains on each aliquot is to be kept small to avoid averaging effects that may occur and conceal the true burial dose (Olley et al., 1999; Wallinga, 2002a).

It is therefore mostly recommended to use single-grains or small-sized aliquots with only a few tens of grains when dating deposits derived from depositional environments that are prone to insufficient bleaching (e.g., Duller, 2008). However, luminescence dating of glacial deposits from the Arctic has successfully been conducted by using medium-sized aliquots (Alexanderson and Murray, 2012). Furthermore, Murray et al. (2012) measured single-grains and large-sized aliquots and found that only the luminescence ages derived from large-sized aliquots were in good agreement with independent age control. Therefore, the consistent use of medium-sized feldspar aliquots was considered to be suitable and final feldspar ages were calculated using the mean D_e values of all accepted aliquots.

Unlike most feldspar grains, quartz minerals derived from the Münsterland Embayment (Chapter 2) did not give a bright luminescence signal which would have made a final age calculating simply based on mean D_e values of all accepted quartz aliquots somewhat difficult. At last, quartz CAM ages were taken for interpretation because MAM-3 D_e distributions were very broad and characterised by a very low precision, suggesting that MAM-3 ages were derived from very few and imprecise aliquots. Quartz CAM ages seemed to be very precise and most reliable for the uppermost aeolian sediments. They may, however, be slightly overestimated for the rest of the dated sediments due to the occurrence of insufficient bleaching conditions.

Conclusively, well-considered and adequate measurement procedures and careful analysis of the determined D_e values showed that although samples of all three studied areas were clearly prone to insufficient bleaching due to their depositional environment, good bleaching conditions seem to have occurred for most of the glacial deposits of the Leine valley (Chapter 3). Here, the glacial delta systems were likely to be characterised by subaerial delta plains that favoured adequate bleaching to some extent (e.g., Fuchs and Owen, 2008; Houmark-Nielsen, 2008, Alexanderson and Murray, 2012). The fluvial deposits of the Weser valley (Chapter 4) are also likely to have experienced some sort of light exposure although insufficient bleaching has often been detected from these depositional environments (e.g., Wallinga, 2002b; Rittenour, 2008; Lauer et al., 2010; Popov et al., 2012). Less well bleaching conditions seemed to have occurred for the alluvial deposits of the upper Senne, which is probably due to periodically occurring high-energy floods (Chapter 2).

5.2 Geological implications

In combination with detailed sedimentological, seismic and borehole data, the obtained luminescence ages clearly prove that the Middle and Late Pleistocene glaciation history of northern

Germany is much more complex than has long been assumed. For the first time, at least two separate ice advances could be reconstructed for the Middle Pleistocene Elsterian glaciation during MIS 12 (461 ± 34 to 421 ± 25 ka) and MIS 10 (376 ± 27 to 337 ± 21 ka; Chapter 3). These findings may not agree with data from Poland and Great Britain, where only one Elsterian ice advance was reconstructed (e.g., Gibbard and Clark, 2011; Marks, 2011). Yet, they are in accordance with data from the North Sea area, Denmark and northern Germany, where up to three ice advances were assumed (e.g., Cohen and Gibbard, 2010; Houmark-Nielsen, 2011; Caspers et al., 1995; Eissmann, 2002; Litt et al., 2007; Ehlers et al., 2011; Stephan, 2014). However, solely based on the luminescence ages from the Betheln pit in the Leine valley that gave uncorrected IR_{50} ages ranging from 452 ± 31 to 421 ± 25 ka (Chapter 3), it is difficult to assign both ice advances to MIS 12 or one occurring during MIS 12 and the other one occurring during MIS 10. This is due to the fact that insufficient bleaching has been considered to have only had a negligible impact but it could not be fully excluded. Based on the geochronological and seismic results from the Sarstedt/Schliekum area of the Leine valley (Chapter 3), both MIS 12 and MIS 10 glaciations were reconstructed. The MIS 10 ice advance was associated with strong subglacial erosion, indicated by the formation of an erosional northeast-southwest trending zone with local overdeepenings. These formations correspond well with similar Elsterian subglacial features in northern Central Europe, such as tunnel valleys (Stackebrandt, 2009) and subglacial mini-basins (Cook and Swift, 2012).

During the Middle Pleistocene Saalian glaciation, a renewed ice advance was reconstructed, as was indicated by the ice-marginal deposits near Freden in the Leine valley (Chapter 3). Luminescence dating gave ages correlating with MIS 8 to MIS 7 (250 ± 20 to 241 ± 27 ka) and MIS 7 to MIS 6 (196 ± 19 to 161 ± 10 ka). So far, an MIS 8 glaciation has only been reported from a few sites in the Netherlands, Denmark and Poland (Beet et al., 2005; Hall and Migón, 2010; Houmark-Nielsen, 2011; Laban and van der Meer, 2011; Marks, 2011; Kars et al., 2012). Radiofluorescence data from eastern Germany, however, point to a long period without glaciations during MIS 9 to early MIS 6 (Krbetschek et al., 2008), disagreeing with the obtained MIS 8 ages in this thesis. If the obtained MIS 8 ages of samples Fre1 and Fre2 had suffered from insufficient bleaching, only one single ice advance could have been reconstructed. However, due to the negligible effect of insufficient bleaching, two separate glaciations were assumed to have occurred either during MIS 8 and MIS 6 or during early and late MIS 6. The former would correspond nicely to data from the Netherlands and Denmark (Beets et al., 2005; Houmark-Nielsen, 2011; Kars et al., 2012) as well as from northern Germany where two different tills of the older Saalian Drenthe glaciation were found (Litt et al., 2007; Stephan, 2014).

The MIS 12, MIS 10, MIS 8? and MIS 6 dated glacial deposits studied in the Leine valley therefore provide a first geochronological evidence for the occurrence of two Elsterian and two Saalian glaciations in northern Germany. Detailed sedimentological analyses furthermore point to the occurrence of deep proglacial lakes in front of the advancing ice sheets, as is indicated by glacial lacustrine sediments. These proglacial lakes probably prevented the glaciers from advancing further towards the south.

During climatic changes, fluvial systems have to adapt not only to altered drainage pathways but also to changes in vegetation cover, sediment supply, and water discharge. Major fluvial aggradation is commonly assigned to cold stages when the absence of vegetation cover leads to an increase in sediment supply. Prior to the advancing MIS 6 Drenthe ice sheet, River Weser deposited thick braided river deposits on top of interglacial sediments (publication 3, Chapter 4). These interglacial limnic and fen peat deposits were correlated with MIS 7c to early MIS 6 (Waas et al., 2011). Fading corrected IR₅₀ ages pointed to two major aggradational phases, occurring during the Late Pleistocene MIS 5d (100±5 ka) and during the Late Pleistocene (Early Weichselian to Early Pleniglacial) MIS 5b to MIS 4 (77±6 to 68±5 ka). The major chronological gap of about 12 ka seems to coincide with a major bounding (erosional) surface, which was probably incised during MIS 5c (Winsemann et al., *subm.*). The geochronological results are not generally in accordance with previous interpretations (Rohde, 1989, Rohde, 1994, Rohde et al., 2012). Although the fluvial deposits overlying the interglacial sediments have been proved to be stratigraphically younger (Rohde et al., 2012), they cannot be interpreted as Younger Middle Terrace deposits (Rohde et al., 2012) based on the obtained luminescence ages. Additional numerical datings need to be performed to verify the determined ages and to be able to establish a detailed fluvial depositional model.

The sedimentary succession of the upper Senne in the Münsterland Embayment was found to have been deposited during the Late Pleistocene to Late Glacial, recording climate changes for the past about 30 ka. Quartz CAM ages ranged from 29.3±3.2 ka (alluvial plain deposits) to 25.4±3.6 to 18.7±1.9 ka (alluvial fan deposits) to 19.6±2.1 to 13.1±1.5 ka (aeolian deposits), contradicting the results reported by Fehrentz and Radtke (1998, 2001) and Lang and Fehrentz (1998). In combination with detailed sedimentological analysis performed by Meinsen et al. (2014), the sedimentary succession of the upper Senne resembles fluvial-aeolian deposits from the Netherlands and Poland (e.g., Kasse et al., 2007; Zieliński, et al., 2011). Its depositional history may have occurred as follows: The warm-cold transition at the end of MIS 3 (~30 ka) was marked by the deposition of alluvial plain deposits (Middle to Late Pleniglacial, 29.3±3.2 ka) which were overlain by alluvial fan deposits, reflecting an overall decrease in

water and sediment supply during MIS 2 (Late Pleniglacial, 25.4 ± 3.6 to 18.7 ± 1.9 ka). The alluvial fan deposits were bounded by an unconformity which may be correlated with the Beuningen Gravel event that is assumed to result from deflation under polar desert-like conditions at the end of the Late Pleniglacial (~ 17 to 15 ka; Kasse et al., 2007). The uppermost aeolian sandsheet deposits indicate rapidly increasing aridity during the Late Glacial (19.6 ± 2.1 to 13.1 ± 1.5 ka). Results showed that the alluvial fan systems of the upper Senne quickly responded to rapidly changing climatic conditions and even small-scale climate variations could be reconstructed.

Chapter 6

Conclusions

- Luminescence dating results of this thesis have shown that the glaciation history of north-western Germany and northern Central Europe is much more complex and cannot be broken down into three major ice advances having occurred during the Middle and Late Pleistocene. One-directional approaches based on solely lithostratigraphy or geomorphology are not able to trace and reconstruct climate changes associated with glaciation events in terms of (geological) time. For this thesis, the geochronological framework is based on monomineralic coarse-grained potassium-rich feldspar and quartz minerals as well as polymineralic fine-grains derived from ice-marginal and alluvial depositional systems in northern Germany. Adequate measurement procedures using different signals and protocols for D_e determination (pIRIR₂₉₀, conventional IR₅₀, pulsed IR₅₀; double SAR protocol) and careful analysis of the determined D_e values (histograms, radial plots, $D_e(t)$ plots; CAM, MAM-3) gave mostly reliable and robust depositional ages which were systematically discussed in terms of possible causes for age under- and overestimation. It has successfully been shown that luminescence dating is applicable to deposits which may have experienced insufficient bleaching conditions prior to deposition, giving final ages that reach back the Middle Pleistocene (MIS ≤ 12). However, some effect of insufficient bleaching and thus overestimated ages may not be fully excludable.
- The Leine valley: Luminescence ages of ice-marginal and fluvial deposits using mostly feldspar but also quartz minerals pointed to repeated glaciations during the Middle Pleistocene, which were accompanied by the formation of large proglacial lakes in front of the advancing ice sheets. For both the Elsterian and Saalian glaciations, at least two ice advances each were reconstructed, occurring during MIS 12 (461±34 to 421±25 ka) and MIS 10 (376±27 to 337±21 ka), and probably during MIS 8? (250±20 to 241±27 ka) and MIS 6 (196±19 to 161±10 ka). The finding of a possible Saalian MIS 8 ice advance is of remarkable significance because it has not been described before in northern Germany and corresponding dating results have only been reported from Denmark and the Netherlands (Beets et al., 2005; Houmark-Nielsen, 2011; Kars et al., 2012).
- The Weser valley: Maximum depositional ages derived from monomineralic feldspar coarse-grains and polymineralic fine-grains pointed to two phases of fluvial aggradation, explicitly during the Late Pleistocene MIS 5d (100±5 ka) and during the Late Pleistocene (Early Weichselian to Early Pleniglacial) MIS 5b to MIS 4 (77±6 to 68±5 ka). A major bounding surface may coincide with the chronological gap of about 12 ka (Winsemann et al., *subm.*). Independent age control, provided by ²³⁰U/Th ages reported by Waas et al.

(2011), was of tremendous significance and acted as a possible lower age limit for the overlying fluvial deposits.

- The Senne of the Münsterland Embayment: The sedimentary succession under study consists of alluvial fan and aeolian sandsheet deposits (Meinsen et al., 2014), whose geochronological framework was based on both feldspar and quartz minerals. Quartz CAM results gave the most reliable and precise depositional ages. Alluvial plain deposition started at the warm-cold transition at the end of MIS 3 (29.3 ± 3.2 ka) and was followed by an alluvial fan deposition during MIS 2 (25.4 ± 3.6 to 18.7 ± 1.9 ka), reflecting an overall decrease in water and sediment supply. Polar desert-like conditions at the end of the Late Pleniglacial were proved by an unconformity correlated with the Beuningen Gravel event (e.g., Kasse et al., 2007) underlying the aeolian sandsheet deposits of Late Glacial age (19.6 ± 2.1 to 13.1 ± 1.5 ka). High-resolution datings of the upper Senne deposits showed that the alluvial fan systems quickly responded to rapidly changing climatic conditions and are therefore excellent terrestrial climate archives for the past about 30 ka.
- The obtained numerical dating results of this thesis can subsequently be considered to form part of the basic chronological framework for the glaciation history of northern Germany. They need to be supported by additional multidisciplinary studies, at best comprising detailed sedimentological and seismic analyses, carefully handled borehole and outcrop data, which are complemented with and chronologically framed by high-resolution luminescence datings of the studied successions.

References

- Alexanderson, H., Murray, A.S., 2012. Luminescence signals from modern sediments in a glaciated bay, NW Svalbard. *Quaternary Geochronology* 10, 250-256.
- Bailey, R.M., 2003. The use of measurement-time dependent single-aliquot equivalent-dose estimates from quartz in the identification of incomplete signal resetting. *Radiation Measurements* 37, 673-683.
- Beets, D.J., Meijer, T., Beets, C.J., Cleveringa, P., Laban, C., van der Spek, A.J.F., 2005. Evidence for a Middle Pleistocene glaciation of MIS 8 age in the southern North Sea. *Quaternary International* 133-134, 7-19.
- Busscher, F.S., Kasse, C., van Balen, R.T., Vandenberghe, J., Cohen, K.M., Weerts, H.J.T., Wallinga, J., Johns, C., Cleveringa, P., Bunnik, F.P.M., 2007. Late Pleistocene evolution

- of the Rhine-Meuse system in the southern North Sea basin: imprints of climate change, sea-level oscillation and glacio-isostasy. *Quaternary Science Reviews* 26, 3216-3248.
- Buylaert, J.-P., Huot, S., Murray, A.S., Van den Haute, P., 2011. Infrared stimulated luminescence dating of an Eemian (MIS 5e) site in Denmark using K-feldspar. *Boreas* 40, 46-56.
- Buylaert, J.-P., Jain, M., Murray, A.S., Thomsen, K.J., Thiel, C., Sohbati, R., 2012. A robust feldspar luminescence dating method for Middle and Late Pleistocene sediments. *Boreas* 41, 435-451.
- Caspers, G., Jordan, H., Merkt, J., Meyer K.-D., Müller, H., Streif, H., 1995. III. Niedersachsen. In Benda, L. (ed.), *Das Quartär von Deutschland*. Gebrüder Borntraeger, Berlin, 23-58.
- Cohen, K.M., Gibbard, P., 2010. Global chronostratigraphical correlation table for the last 2.7 million years. Subcommission on Quaternary Stratigraphy, International Commission on Stratigraphy, Cambridge.
- Cook, S.J., Swift, D.A., 2012. Subglacial basins: Their origin and importance in glacial systems and landscapes. *Earth-Science Reviews* 115, 332-372.
- Duller, G.A.T., 2008. Single-grain optical dating of Quaternary sediments: why aliquot size matters in luminescence dating. *Boreas* 37, 589-612.
- Ehlers, J., Grube, A., Stephan, H.J., Wansa, S., 2011. Chapter 13 – Pleistocene Glaciations of North Germany - new results. In: Ehlers, J., Gibbard, P.L., Hughes, P.D. (eds.), *Quaternary Glaciations - Extent and Chronology – A closer look*. *Developments in Quaternary Science* 15, Elsevier, Amsterdam, 149-162.
- Eissmann, L., 2002. Quaternary geology of eastern Germany (Saxony, Saxon-Anhalt, South Brandenburg, Thuringia), type area of the Elsterian and Saalian Stages in Europe. *Quaternary Science Reviews* 21, 1275-1346.
- Fehrentz, M., Radtke, U., 1998. Lumineszenzdatierung an pleistozänen Schmelzwassersanden der Senne (östliches Münsterland). *Kölner Geographische Arbeiten* 70, 103-115.
- Fehrentz, M., Radtke, U., 2001. Luminescence dating of Pleistocene outwash sediments of the Senne area (Eastern Münsterland, Germany). *Quaternary Science Reviews* 20, 725-729.
- Fiebig, M., Preusser, F., 2007. Investigating the amount of zeroing in modern sediments of River Danube, Austria. *Quaternary Geochronology* 2, 143-149.
- Frechen, M., Schwab, M.J., Sutter, I. 2004. Luminescence and radiocarbon dating of lake sediments from east Antarctica. In: Higham, T., Bronk Ramsey, C., Owen, C. (eds.), *Radio-*

- carbon and Archaeology: Fourth International Symposium St. Catherine's College, Oxford, 9–14 April 2002; Conference Proceedings, 17-34. Oxbow Books, Oxford.
- Frechen, M., Ellwanger, D., Rimkus, D., Techmer, A., 2008. Timing of Medieval Fluvial Aggradation at Bremgarten in the Southern Upper Rhine Graben – a Test for Luminescence Dating. *E&G Quaternary Science Journal* 57, 411-432.
- Fuchs, M., Owen, L.A., 2008. Luminescence dating of glacial and associated sediments: review, recommendations and future directions. *Boreas* 37, 636–659.
- Galbraith, R.G., 1990. The radial plot: graphical assessment of spread in ages. *Nuclear Tracks and Radiation Measurements* 17, 207-214.
- Gibbard, P.L., Clark, C.D. 2011. Chapter 7 - Pleistocene Glaciation Limits in Great Britain. In: Ehlers, J., Gibbard, P.L., Hughes, P.D. (eds.), *Quaternary Glaciations - Extent and Chronology - A Closer Look*. *Developments in Quaternary Science* 15, Elsevier, Amsterdam, 75-93.
- Godfrey-Smith, D.I., Huntley, D.J., Chen, W.H., 1998. Optical dating studies of quartz and feldspar sediment extracts. *Quaternary Science Reviews* 7, 373-380.
- Hall, A.M., Migoń, P., 2010. The first stages of erosion by ice sheets: Evidence from central Europe. *Geomorphology* 123, 349-363.
- Houmark-Nielsen, M. 2008. Testing OSL failures against a regional Weichselian glaciation chronology from southern Scandinavia. *Boreas* 37, 660-677.
- Houmark-Nielsen, M., 2011. Chapter 5 - Pleistocene Glaciations in Denmark: A Closer Look at Chronology, Ice Dynamics and Landforms. In: Ehlers, J., Gibbard, P.L., Hughes, P.D. (eds.), *Quaternary Glaciations - Extent and Chronology – A closer look*. *Developments in Quaternary Science* 15, Elsevier, Amsterdam, 47-58.
- Huntley, J.D., Lamothe, M. 2001. Ubiquity of anomalous fading in K-feldspars and the measurement and correction for it in optical dating. *Canadian Journal of Earth Sciences* 38, 1093-1106.
- Huntley, D.J., Godfrey-Smith, D.I., Thewalt, M.L.W., 1985. Optical dating of sediments. *Nature* 313, 105-107.
- Kars, R.H., Wallinga, J., Cohen, K.M., 2008. A new approach towards anomalous fading correction for feldspar IRSL dating - tests on samples in field saturation. *Radiation Measurements* 43, 786-790.

- Kars, R.H., Busschers, F.S., Wallinga, J., 2012. Validating post IR-IRSL dating on K-feldspars through comparison with quartz OSL ages. *Quaternary Geochronology* 12, 74-86.
- Kasse, C., Vandenberghe, D., De Corta, F., Van den Haute, P., 2007. Late Weichselian fluvio-aeolian sands and coversands of the type locality Grubbenvorst (southern Netherlands): sedimentary environments, climate record and age. *Journal of Quaternary Science* 22, 695-708.
- Krbetschek, M.R., Degering, D., Alexowsky, W., 2008. Infrarot-Radiofluoreszenz-Alter (IR-RF) unter-saalezeitlicher Sedimente Mittel- und Ostdeutschlands. *Zeitschrift der Deutschen Gesellschaft für Geowissenschaften* 159, 133-140.
- Laban, C., van der Meer, J.J.M., 2011. Chapter 20 – Pleistocene Glaciation in the Netherlands. In: Ehlers, J., Gibbard, P.L., Hughes, P.D. (eds.), *Quaternary Glaciations - Extent and Chronology – A closer look. Developments in Quaternary Science* 15, Elsevier, Amsterdam, 247-260.
- Lamothe, M., Auclair, M., Hanazaoui, C., Huot, S., 2003. Towards a prediction of long-term anomalous fading of feldspar IRSL. *Radiation Measurements* 37, 493-498.
- Lang, M., Fehrentz, M., 1998. GR-OSL- und IR-OSL-Datierungen an spätpleistozänen und holozänen Dünensanden der Senne (östliches Münsterland). *Kölner Geographische Arbeiten* 70, 47-58.
- Lauer, T., Frechen, M., Hoselmann, C., Tsukamoto, S., 2010. Fluvial aggradation phases in the Upper Rhine Graben – new insights by quartz OSL dating. *Proceedings of the Geologists' Association* 121, 154-161.
- Litt, T., Behre, K.-E., Meyer, K.-D., Stephan, H.-J., Wansa, S., 2007. Stratigraphische Begriffe für das Quartär des norddeutschen Vereisungsgebietes. *E&G Quaternary Science Journal* 56, 7-65.
- Marks, L., 2011. Chapter 23 – Quaternary Glaciation in Poland. In: Ehlers, J., Gibbard, P.L., Hughes, P.D. (eds.), *Quaternary Glaciations - Extent and Chronology – A closer look. Developments in Quaternary Science* 15, Elsevier, Amsterdam, 299-303.
- Meinsen, J., Winsemann, J., Roskosch, J., Brandes, C., Frechen, M., Dultz, S., Böttcher, J., 2014. Climate control on the evolution of Late Pleistocene alluvial-fan and aeolian sand-sheet systems in NW Germany. *Boreas* 43, 42-66.
- Murray, A.S., Wintle, A.G., 2000. Luminescence dating of quartz using an improved single-aliquot regenerative-dose protocol. *Radiation Measurements* 32, 57-73.

- Murray, A.S., Olley, J.M., 2002. Precision and accuracy in the optically stimulated luminescence dating of sedimentary quartz: a status review. *Geochronometria* 21, 1-16.
- Murray, A.S., Wintle, A.G., 2003. The single aliquot regenerative dose protocol potential form improvements in reliability. *Radiation Measurements* 37, 377-381.
- Murray, A.S., Olley, J.M., Caitcheon, G.C., 1995. Measurement of equivalent dose in quartz from contemporary water-lain sediments using optically stimulated luminescence. *Quaternary Science Reviews* 14, 365-371.
- Murray, A.S., Thomsen, K.J., Masuda, N., Buylaert, J.-P., Jain, M., 2012. Identifying well-bleached quartz using the different bleaching rates of quartz and feldspar luminescence signals. *Radiation Measurements* 47, 688-695.
- Olley, J.M., Caitcheon, G.G., Roberts, R.G., 1999. The origin of dose distributions in fluvial sediments, and the prospect of dating single grains from fluvial deposits using optically stimulated luminescence. *Radiation Measurements* 30, 207-217.
- Olley, J.M., Pietsch, T., Roberts, R.G., 2004. Optical dating of Holocene sediments from a variety of geomorphic settings using single grains of quartz. *Geomorphology* 60, 337-358.
- Popov, D., Vendenberghe, D.A.G., Marković, S.B., 2012. Luminescence dating of fluvial deposits in Vojvodina, N Serbia: First results. *Quaternary Geochronology* 13, 42-51.
- Preusser, F., Degering, D., Fuchs, M., Hilgers, A., Kadereit, A., Klasen, N., Krbetschek, M., Richter, D., Spencer, J.Q.G., 2008. Luminescence dating: basics, methods and applications. *E&G Quaternary Science Journal* 57, 95-149.
- Rhodes, E.J., Bronk-Ramsey, C., Outram, Z., Batt, C., Willis, L., Dockrill, S., Bond, J., 2003. Bayesian methods applied to the interpretation of multiple OSL dates: high precision sediment age estimates from Old Scatness Broch excavations, Shetland Isles. *Quaternary Science Reviews* 22, 1231-1244
- Rittenour, T.M., 2008. Luminescence dating of fluvial deposits: applications to geomorphic, palaeoseismic and archaeological research. *Boreas* 37, 613-635.
- Rohde, P., 1989. Elf pleistozäne Sand-Kies-Terrassen der Weser: Erläuterungen eines Gliederungsschemas für das obere Weser-Tal. *E&G Quaternary Science Journal* 39, 42-56.
- Rohde, P., 1994. Weser und Leine am Berglandrand zur Ober- und Mittelterrassen-Zeit. *E&G Quaternary Science Journal* 44, 106-133.

- Rohde, P., Lepper, J., Thiem, W., 2012. Younger Middle Terrace - Saalian pre-Drenthe deposits overlying MIS 7 Nachtigall interglacial strata near Höxter/Weser, NW-Germany. *E&G Quaternary Science Journal* 61, 133-145.
- Stakebrandt, W., 2009. Subglacial channels of Northern Germany – a brief review. *Zeitschrift der Deutschen Gesellschaft für Geowissenschaften* 60, 203-210.
- Stephan, H.-J., 2014. Climato-stratigraphic subdivision of the Pleistocene in Schleswig-Holstein, Germany and adjoining areas. *E&G Quaternary Science Journal* 63, 3-18.
- Thiel, C., Buylaert, J.P., Murray, A., Terhorst, B., Hofer, I., Tsukamoto, S., Frechen, M., 2011. Luminescence dating of the Stratzing loess profile (Austria) – Testing the potential of an elevated temperature post-IR IRSL protocol. *Quaternary International* 234, 23-31.
- Thomas, P.J., Murray, A.S., Kjær, K.H., Funder, S., Larsen, E., 2006. Optically Stimulated Luminescence (OSL) dating of glacial sediments from Arctic Russia – depositional bleaching and methodological aspects. *Boreas* 35, 587-599.
- Tsukamoto, S., Denby, P.M., Murray, A.S., Bøtter-Jensen, L., 2006. Time-resolved luminescence from feldspars: New insight into fading. *Radiation Measurements* 41, 790-795.
- Vandenbergh, D., 2003. Investigation of the optically stimulated luminescence dating method for application to young geological sediments. PhD thesis, University Gent, 298 pp.
- Waas, D., Kleinmann, A., Lepper, J., 2011. Uranium-thorium dating of fen peat horizons from pit Nachtigall in northern Germany. *Quaternary International* 241, 111-124.
- Wallinga, J., 2002a. On the detection of OSL age overestimation using single aliquot techniques. *Geochronometria* 21, 17-26.
- Wallinga, J., 2002b. Optically stimulated luminescence dating of fluvial deposits: a review. *Boreas* 31, 303-322.
- Wallinga, J., Murray, A.S., Duller, G.A.T., Törnqvist, T.E., 2001. Testing optically stimulated luminescence dating of sand-sized quartz and feldspar from fluvial deposits. *Earth and Planetary Science Letters* 193, 617-630.
- Winsemann, J., Lang, J., Böhner, U, Polom, U., Brandes, C., Roskosch, J., Glotzbach, C., Frechen, M., submitted to *Quaternary Science Reviews*. Terrace styles and timing of terrace formation in the Weser and Leine Valley, northern Germany: response of a fluvial system to climate change and glaciation.

Zieliński, P., Sokolowski, R.J., Fedorowicz, S., Jankowski, M., 2011. Stratigraphic position of fluvial and aeolian deposits in the Żabinko site (W Poland) based on TL dating. *Geochronometria* 38, 64-71.

Chapter 7

Acknowledgements/Danksagung

Curriculum vitae

List of publications

Acknowledgements/Danksagung

Auf dem langen Weg der Dissertation wurde ich von zahlreichen Menschen in unterschiedlichster Weise begleitet. Bei ihnen möchte ich mich im Folgenden herzlich bedanken.

Prof. Dr. Jutta Winsemann und Prof. Dr. Manfred Frechen danke ich für ihre Betreuung, fachliche Unterstützung und Ermutigung während aller Phasen meiner Dissertation. Sie wurde vom Niedersächsischen Ministerium für Wissenschaft und Kultur (MWK; Pro* Niedersachsen Projekt Nr. No. 11.2-76202-17-7/08) finanziell unterstützt und in Kooperation mit dem Leibniz-Institut für Angewandte Geophysik (LIAG, Sektion 3 „Geochronologie und Isotopenhydrologie“) durchgeführt.

Mein besonderer Dank gilt Dr. Sumiko Tsukamoto (LIAG), die mir die Methodik der Lumineszenzdatierung im Detail beigebracht hat und für ein oder zwei fachliche Fragen immer parat stand – auch und gerade neben ihrer eigenen Forschung. Okay, es mögen eindeutig mehr als ein oder zwei Fragen gewesen sein. Viele mehr. Habe vielen Dank für deine kollegiale Unterstützung, Sumiko!

Meinen Kollegen sowie früheren und aktuellen Doktoranden der Sektion 3 danke ich für die warmherzige Aufnahme in ihren Kreis, die vielen Hilfestellungen bei technischen oder analytischen Problemen und die interessanten Lumineszenzdiskussionen. Insbesondere Sonja Riemenschneider möchte ich ein großes Dankeschön aussprechen. Sonja, bei dir habe ich die Aufbereitung der Lumineszenzproben von der Pieke auf gelernt. Geduldig hast du mir jede meiner Frage beantwortet. Durch deine herzliche und angenehme Art verflogen die zahlreichen Stunden, Tagen und Wochen im Lumineszenzlabor wie von selbst. Danke, Sonja!

Bei meinen Kollegen und Mitdoktoranden am Institut für Geologie (Leibniz Universität Hannover) Tabea Altenbernd, Meike Bagge, Jean Cors, Maurits Horikx, Dr. Jörg Lang, Dr. Tao „Jet“ Li, Lars Lindner, Dr. Georgios „George“ Maniatis, Janine Meinsen, Lukas Pollok, Lena Rippolz, Dominik Steinmetz, Dr. Heidi Turpeinen, Philipp Uta, Maria Wahle, Cornelia „Conny“ Wangenheim und Axel Weitkamp bedanke ich mich für die geniale Zeit miteinander. Ich erinnere mich so gerne an unsere gemeinsame Zeit „unterm Institutsdach“, an die ausgedehnten Kaffee- und Kuchenpausen, die Feierabendveranstaltungen und Weihnachtsmarktturen. Ihr wart nicht nur Kollegen, ihr wurdet auch Freunde. Habt Dank dafür!

Ein ganz besonderer Dank gilt Dr. Christine Thiel. Christine, du bist eine Person, die ich gefühlt seit Ewigkeiten kenne. Du warst mir nicht nur eine unschlagbare Kollegin, nein, zusammen haben wir bei dem einen oder anderen Kaffee stundenlang über Gott und die (Lumineszenz-)Welt reden können. Ob nah oder fern, deine herzliche und warme Art hat mir den Einstieg in Hannover sehr erleichtert! Danke für all deine Worte und deine Freundschaft!

Meinen Freunden in der Heimat danke ich dafür, dass sie mir immer eine Welt außerhalb der Forschung und Wissenschaft bereitgehalten haben. In diese Welt konnte ich eintauchen, wenn es nötig war – und das war öfter der Fall. Danke!

Mein größter Dank gilt meiner Familie. Es mag nicht immer ein Spaziergang gewesen sein, aber mit dem Wissen, dass ihr hinter mir steht, mich unterstützt und mir Zuversicht gibt, waren die Höhen und Tiefen zu meistern.

Marco und Anja, von eurem durchgängigen Optimismus, dass jedes noch so langwierige Projekt machbar ist, habe ich mich häufig leiten lassen. Zwar hat es meine Dissertation nicht so schnell auf die Welt geschafft wie euer Dezember-Baby, aus dem letztlich die November-Zwillinge Anton und Emil wurden, aber das ist irrelevant. Ich danke euch, ihr 2+2!

Mama, wo fange ich an? Danke für die endlosen Telefonate, in denen du mich aufgebaut oder meine Freuden geteilt hast. Deine Ohren müssen von den Stunden und Tagen am Telefon immer noch glühen! Während dieser Momente habe ich gelernt, Probleme als Herausforderungen anzusehen, die überwindbar sind, wenn man am Ball bleibt. Zu wissen und sich wieder darauf zu konzentrieren, wofür und für wen man diese Herausforderungen meistert, ließ mich durchhalten. Danke für dein Vertrauen in mich und deine Liebe!

Papa, ich weiß, du wärst stolz auf mich. Danke, dass ich deinen Dickkopf und deinen Ehrgeiz geerbt habe.

Curriculum vitae

Name Julia Roskosch
Geburtsdatum 10. März 1983
Geburtsort Datteln

2002 **Abitur**
Clemens-Brentano-Gymnasium Dülmen

2003-2006 **Bachelor of Science (Geowissenschaften)**
Institut für Geologie und Paläontologie
Westfälische Wilhelms-Universität Münster

2006-2009 **Master of Science (Geowissenschaften)**
Institut für Geologie und Paläontologie
Westfälische Wilhelms-Universität Münster

2010-2014 **Wissenschaftliche Mitarbeiterin**
Institut für Geologie
Gottfried Wilhelm Leibniz Universität Hannover

2010-2015 **Promotionsstudium (Geowissenschaften)**
Institut für Geologie
Gottfried Wilhelm Leibniz Universität Hannover

List of publications

Publications in peer-reviewed international journals

Winsemann, J., Lang, J., Böhner, U., Polom, U., Brandes, C., **Roskosch, J.**, Glotzbach, C., Frechen, M., submitted to *Quaternary Science Reviews*. Terrace styles and timing of terrace formation in the Weser and Leine Valley, northern Germany: response of a fluvial system to climate change and glaciation.

Roskosch, J., Tsukamoto, S., Frechen, M., in review. Luminescence dating of fluvial deposits from the Weser valley, Germany: a comparison with independent age control. *Geochronometria*.

Roskosch, J., Winsemann, J., Polom, U., Brandes, C., Tsukamoto, S., Weitkamp, A., Bartholomäus, W., Henningsen, D., Frechen, M., 2015. Luminescence dating of ice-marginal deposits in northern Germany: evidence for repeated glaciations during the Middle Pleistocene (MIS 12 to MIS 6). *Boreas* 44, 103-126.

Meinsen, J., Winsemann, J., **Roskosch, J.**, Brandes, C., Frechen, M., Dultz, S., Böttcher, J., 2014. Climate control on the evolution of Upper Pleistocene alluvial-fan and aeolian sand-sheet systems in NW Germany. *Boreas* 43, 42-66.

Roskosch, J., Tsukamoto, S., Meinsen, J., Frechen, M., Winsemann, J., 2012. Luminescence dating of an Upper Pleistocene alluvial fan and aeolian sand-sheet complex: the Senne in the Münsterland Embayment, NW Germany. *Quaternary Geochronology* 10, 94-101.

Brandes, C., Winsemann, J., **Roskosch, J.**, Meinsen, J., Tanner, D.C., Frechen, M., Steffen, H., Wu, P., 2012. Activity along the Osning Thrust in Central Europe during the Lateglacial: ice-sheet and lithosphere interactions. *Quaternary Science Reviews* 38, 49-62.

Spiske, M., Weiss, R., Bahlburg, H., **Roskosch, J.**, Amijaya, H., 2010. The TsuSedMod inversion model applied to the deposits of the 2004 Sumatra and 2006 Java tsunami and implications for estimating flow parameters of palaeo-tsunami. *Sedimentary Geology* 224, 29-37.

Conference contributions (Abstracts)

Roskosch, J., Weitkamp, A., Rippolz, L., Pollok, L., Polom, U., Brandes, C., Tsukamoto, S., Frechen, M., Winsemann, J., 2012. OSL dating of Middle Pleistocene ice-marginal deposits of the Leinebergland area (Germany). *GeoHannover, Hannover (Germany)*, 01-03 October 2012.

- Roskosch, J.**, Tsukamoto, S., Meinsen, J., Frechen, M., Winsemann, J., 2012. Luminescence dating of the upper Senne complex (NW Germany): a high-resolution chronostratigraphic framework for alluvial fan and aeolian sandsheet systems. GeoHannover, Hannover (Germany), 01-03 October 2012.
- Meinsen, J., Winsemann, J., **Roskosch, J.**, Brandes, C., Frechen, M., 2012. Climate control on the evolution of Upper Pleistocene alluvial fan and aeolian sand sheet systems: the Senne (NW Germany). GeoHannover, Hannover (Germany), 01-03 October 2012.
- Brandes, C., Winsemann, J., **Roskosch, J.**, Meinsen, J., Tanner, D.C., Frechen, M., Steffen, H., Wu, P., 2012. Lateglacial faulting along the Osning Thrust in Central Europe. GeoHannover, Hannover (Germany), 01-03 October 2012.
- Roskosch, J.**, Winsemann, J., Weitkamp, A., Pollok, L., Polom, U., Brandes, C., Tsukamoto, S., Böhner, U., Haßmann, H., Frechen, M., 2012. OSL dating of the Middle Pleistocene Leine valley fill (N Germany): timing Palaeolithic findings. DEUQUA, Bayreuth (Germany), 16-19 September 2012.
- Roskosch, J.**, Tsukamoto, S., Meinsen, J., Frechen, M., Winsemann, J., 2012. Establishment of a high-resolution chronostratigraphic framework for a Late Pleniglacial to Late Glacial alluvial-aeolian complex: the upper Senne (NW Germany). DEUQUA, Bayreuth (Germany), 16-19 September 2012.
- Meinsen, J., Winsemann, J., **Roskosch, J.**, Brandes, C., Frechen, M., 2012. Response of a Late Pleistocene periglacial sedimentary system to climatic change: the Senne (NW Germany). DEUQUA, Bayreuth (Germany), 16-19 September 2012.
- Brandes, C., Winsemann, J., **Roskosch, J.**, Meinsen, J., Tanner, D., Frechen, M., Steffen, H., Wu, P., 2012. Lateglacial neotectonics of the Osning Thrust in northern Germany. DEUQUA, Bayreuth (Germany), 16-19 September 2012.
- Roskosch, J.**, Tsukamoto, S., Meinsen, J., Frechen, M., Winsemann, J., 2011. OSL-Datierung von spätpleistozänen periglazialen Ablagerungen: die obere Senne der Münsterländer Bucht (NW Deutschland). German LED, Köln (Germany), 04-06 November 2011.
- Meinsen, J., **Roskosch, J.**, Brandes, C., Frechen, M., Winsemann, J., 2011. The Senne of the Münsterland Embayment, NW Germany: Saalian meltwater sediments, lake outburst deposits or a Weichselian fluvial-aeolian complex? INQUA, Bern (Switzerland), 21-27 July 2011.

- Roskosch, J.**, Meinsen, J., Brandes, C., Frechen, M., Winsemann, J., 2011. Optically stimulated luminescence dating of the Upper Senne deposits (Münsterland Embayment, NW Germany). INQUA, Bern (Switzerland), 21-27 July 2011.
- Roskosch, J.**, Tsukamoto, S., Meinsen, J., Frechen, M., Winsemann, J., 2011. OSL dating of a late Pleistocene fluvial-aeolian complex: the upper Senne of the Münsterland Embayment, NW Germany. 13th International Conference on Luminescence and Electron Spin Resonance Dating, Toruń (Poland), 10-14 July 2011.
- Brandes, C., **Roskosch, J.**, Meinsen, J., Winsemann, J., Frechen, M., Tanner, D., 2011. Reactivation of the Osning Thrust in Central Europe: ice-sheet and lithosphere interactions during the LGM. EGU General Assembly 2011, Wien (Austria), 03-08 April 2011.
- Spiske, M., Weiss, R., **Roskosch, J.**, Piepenbreier, J., Bahlburg, H., 2010. Inverse modeling of onshore tsunami flow speed and depth – examples from the 2004 Indian Ocean and 2006 Java tsunami. EGU General Assembly 2010, Wien (Austria), 02-07 May 2010.
- Spiske, M., Weiss, R., **Roskosch, J.**, Bahlburg, H., 2008. Inversion of flow depth and speed from tsunami deposits using TsuSedMod.- AGU Fall Meeting, San Francisco (USA), 15-19 December 2008.